Substantial winds from hot accretion flows confining the relativistic jet in M87

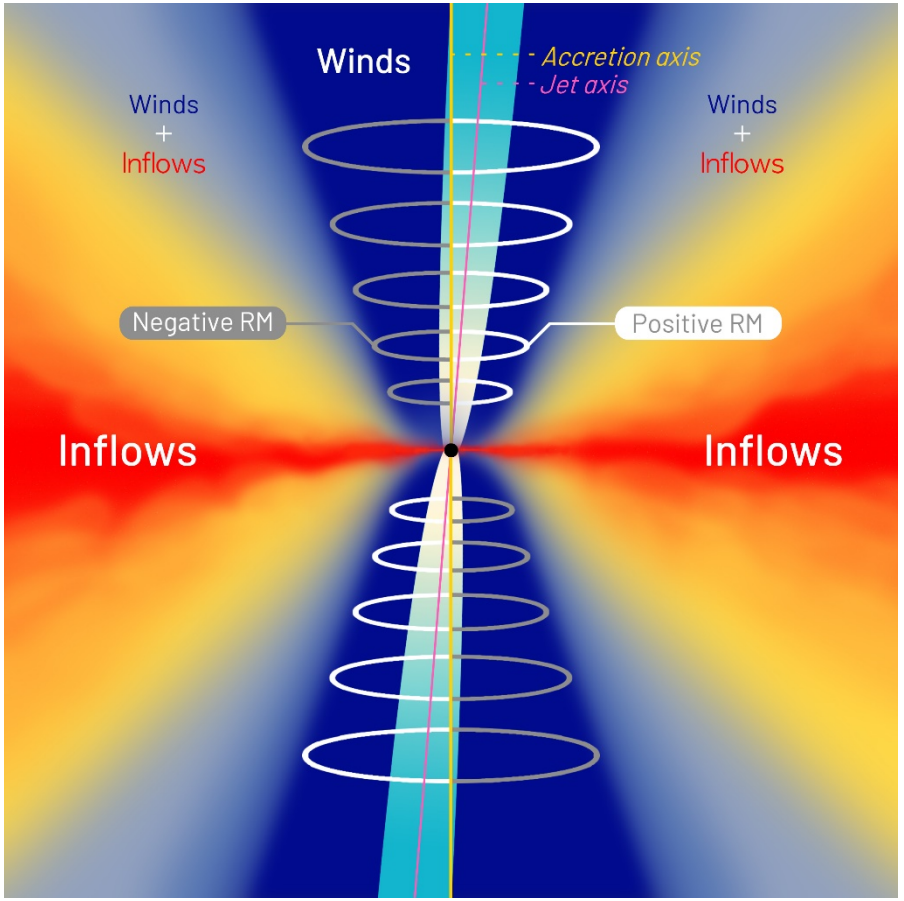

Presenter : Jongho Park (SNU)

Co-I : Kazuhiro Hada (Mizusawa obs), Motoki Kino (Kogakuin Univ. / NAOJ), Masanori Nakamura (ASIAA), Sascha Trippe (SNU)

Hot accretion flows prevalent in low luminosity AGNs (LLAGNs)

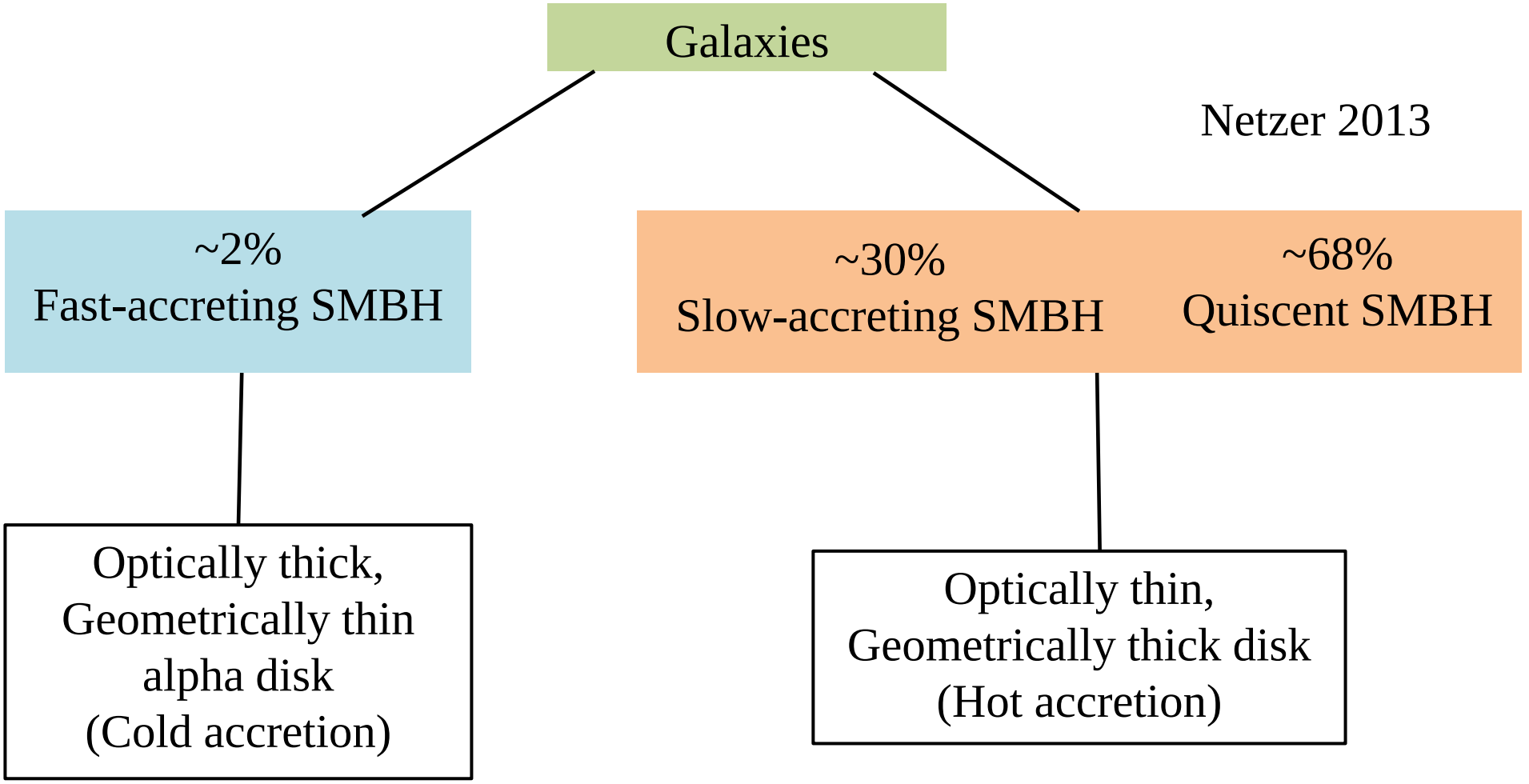

– Understanding hot accretion flows is very important because it might govern evolution of most of the galaxies in the universe.

Properties of hot accretion flows

– Very low luminosity because of advection (instead of being radiated).
→ Advection Dominated Accretion Flows, ADAF.

– Entropy increases with decreasing radius.
→ possibility that the flows are convectively unstable.

– Bernoulli parameter of the flow is positive.
→ indication of strong outflows (winds) and jets.

*Winds : non-relativistic, moderately magnetized gas outflows that occupy a large solid angle ↔ highly collimated relativistic jets

Outflows or convection in hot accretion flows

– Original ADAF self similar solutions (Narayan & Yi 1994):

$$\rho \propto R^{-3/2}, \quad v \propto R^{-1/2}, \quad \Omega \propto R^{-3/2}, \quad c_s^2 \propto R^{-1}$$

→ accretion rate as a function of radius is constant.

– However, a number of simulations of ADAF
→ accretion rate is not constant (decreasing at smaller distance).
because of substantial outflows or convection in hot accretion flows.

Outflows or convection in hot accretion flows

– Original ADAF self similar solutions (Narayan & Yi 1994):

$$\rho \propto R^{-3/2}, \quad v \propto R^{-1/2}, \quad \Omega \propto R^{-3/2}, \quad c_s^2 \propto R^{-1}$$

→ accretion rate as a function of radius is constant.

– However, a number of simulations of ADAF
→ accretion rate is not constant (decreasing at smaller distance).
because of substantial outflows or convection in hot accretion flows.

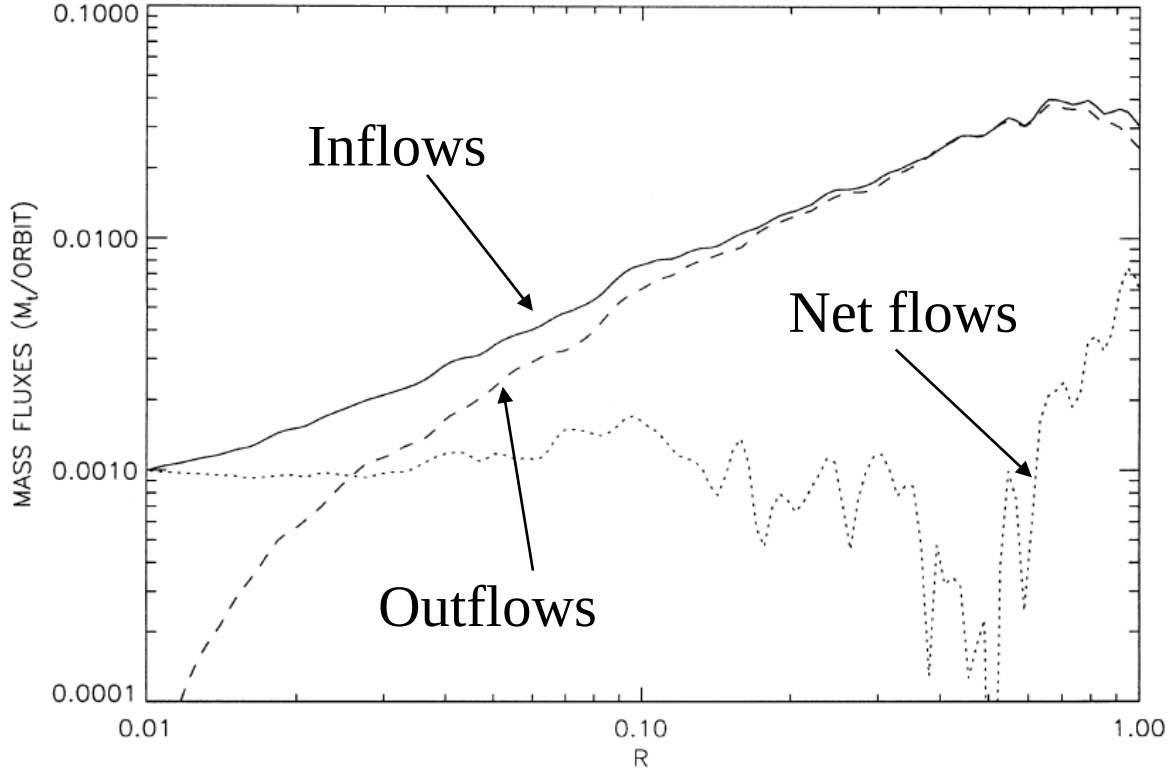

Stone+99

Outflows or convection in hot accretion flows

– Original ADAF self similar solutions (Narayan & Yi 1994):

$$\rho \propto R^{-3/2}, \quad v \propto R^{-1/2}, \quad \Omega \propto R^{-3/2}, \quad c_s^2 \propto R^{-1}$$

→ accretion rate as a function of radius is constant.

– However, a number of simulations of ADAF
→ accretion rate is not constant (decreasing at smaller distance).
because of substantial outflows or convection in hot accretion flows.

$$\dot{M}(r) \propto r^s \qquad \rho(r) \propto r^{-p} \qquad p = 1.5 - s$$

wind parameter

– Variants of ADAF solutions were obtained depending on s values
p = 0.5 → CDAF (Convection Dominated Accretion Flows)
0.5 < p < 1.5 → ADIOS (Adiabatic Inflow Outflow Solution)

The fundamental questions we want to answer are:

1. Which model is valid for LLAGNs? (Inflows)
   → ADAF? CDAF? ADIOS?
   → It is related with how most of SMBHs grow in their quiescent states.

2. Are there really substantial winds from hot accretion flows as seen in numerical simulations? (Outflows)
   → If this is the case, it would be evidence for SMBHs reaction to host galaxy's accretion. → feedback?

Related with how SMBHs and galaxies evolve.

How to study accretion flows or winds?

– We are interested in accretion flows and winds well inside the Bondi radius.
→ VLBI is an ideal tool to study them.
→ M87 is a primary target.

– Accretion flows or Winds are (almost) 'invisible' at radio wavelengths.
We have to observe something behind them and detect their effects.
→ Faraday rotation is an ideal tool.

VLBA archive data analysis

- We analyzed the VLBA archive data at 1.7, 5, 8.3 GHz.
- We obtained EVPA rotation as a function of λ^2 'within the bands' (across different IFs).

Project Code	Epoch	Frequency	D-Term cal.	EVPA cal.
BJ020A	1995 Nov 22	8.11, 8.20, 8.42, 8.59 GHz	OQ 208	OJ 287 (UMRAO)
BJ020B	1995 Dec 09	4.71, 4.76, 4.89, 4.99 GHz	OQ 208	3C 273 (UMRAO)
BC210B	2013 Mar 09	4.85, 4.88, 4.92, 4.95, 4.98, 5.01, 5.04, 5.08 GHz	M87	N/A
BC210C	2014 Jan 29	4.85, 4.88, 4.92, 4.95, 4.98, 5.01, 5.04, 5.08 GHz	M87	N/A
BC210D	2014 Jul 14	4.85, 4.88, 4.92, 4.95, 4.98, 5.01, 5.04, 5.08 GHz	M87	N/A
BH135F	2006 Jun 30	1.65, 1.66, 1.67, 1.68 GHz	M87	3C 286
BC167C	2007 May 28	1.65, 1.66, 1.67, 1.68 GHz	M87	3C 286
BC167E	2007 Aug 20	1.65, 1.66, 1.67, 1.68 GHz	M87	3C 286

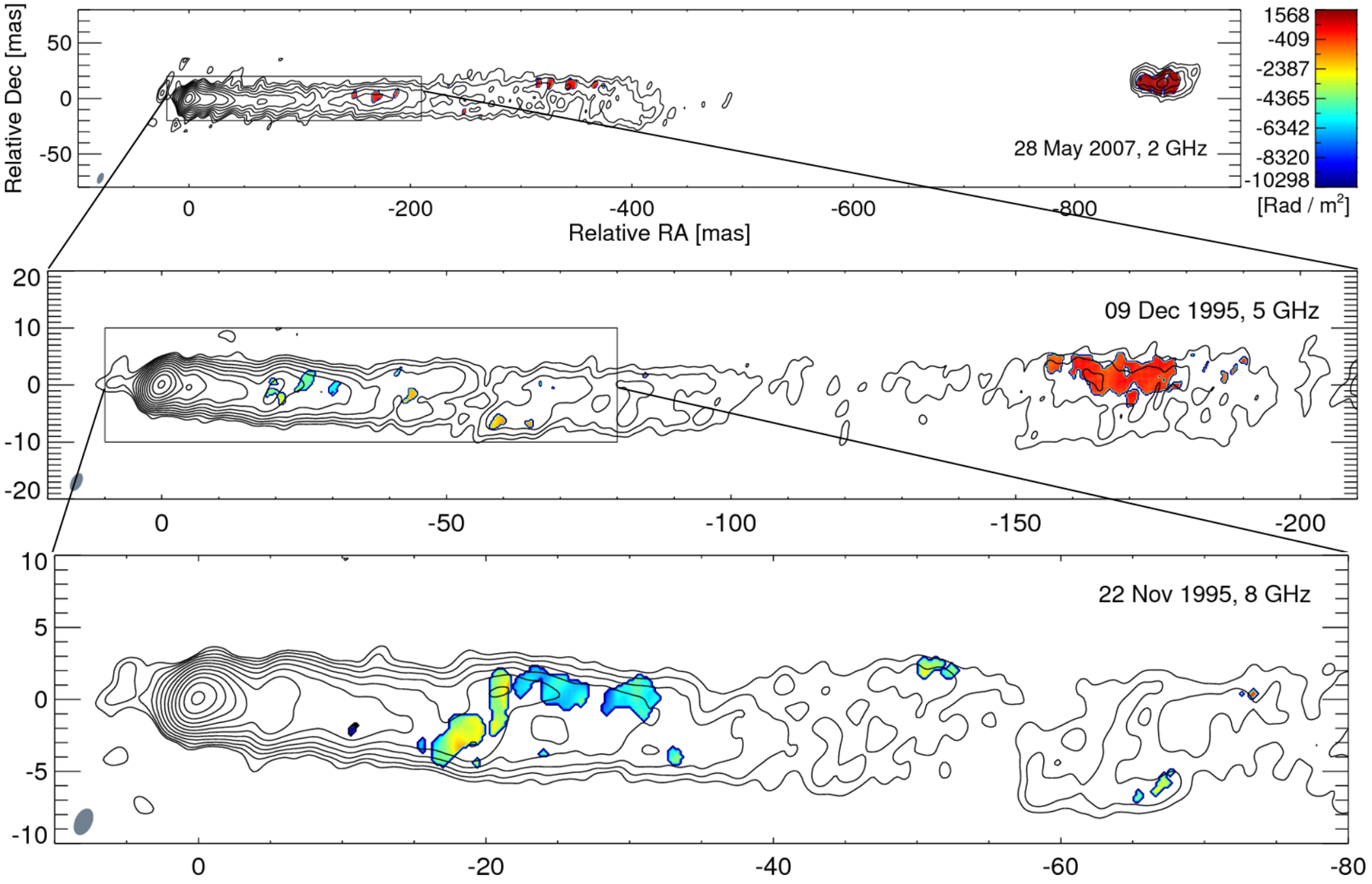
Relative Dec [mas]
50
0
-50
0
-200
-400
-600
-800
Relative RA [mas]
28 May 2007, 2 GHz
1568
-409
-2387
-4365
-6342
-8320
-10298
[Rad / m^2]
20
10
0
-10
-20
0
-50
-100
-150
-200
09 Dec 1995, 5 GHz
10
5
0
-5
-10
0
-20
-40
-60
-80
22 Nov 1995, 8 GHz

RM distribution as a function of distance

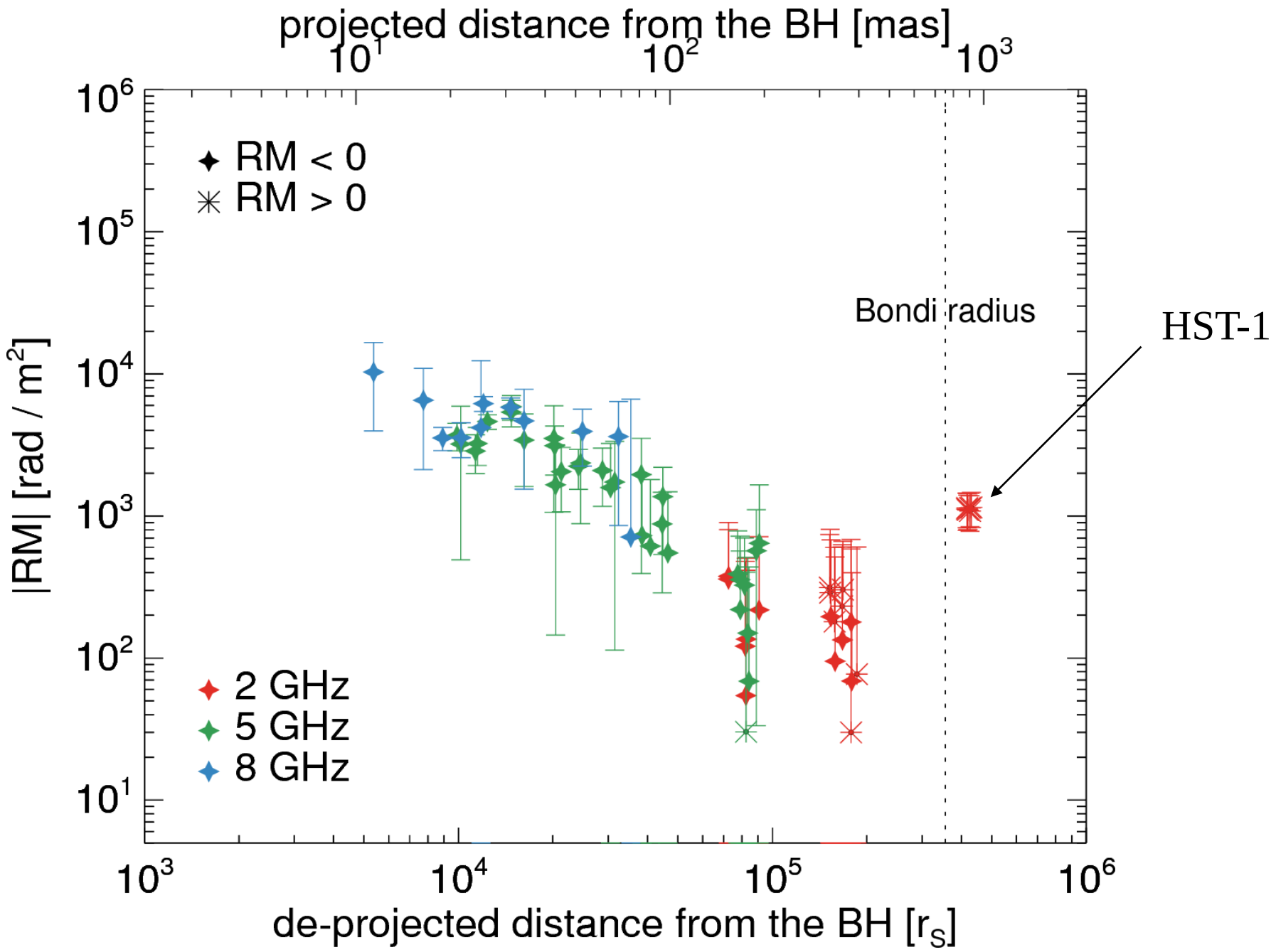

Possibility of internal Faraday rotation?

– Internal Faraday rotation : Faraday rotating electrons are intermixed within the jet.
→ No EVPA rotation larger than 45 deg.

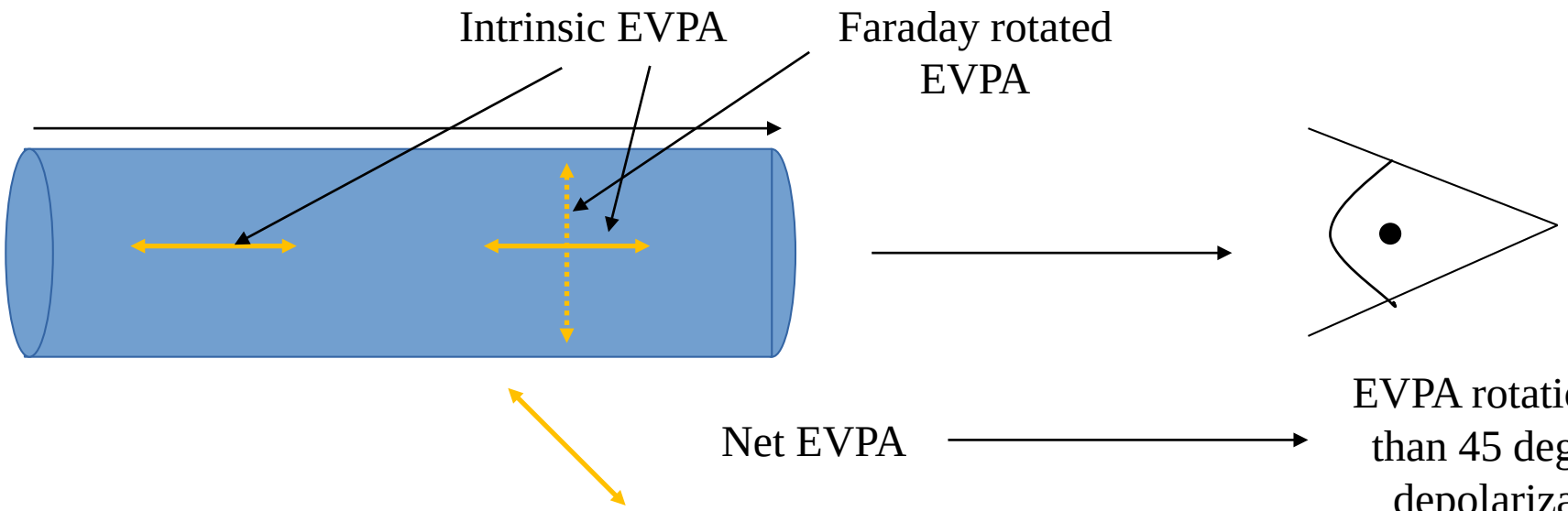

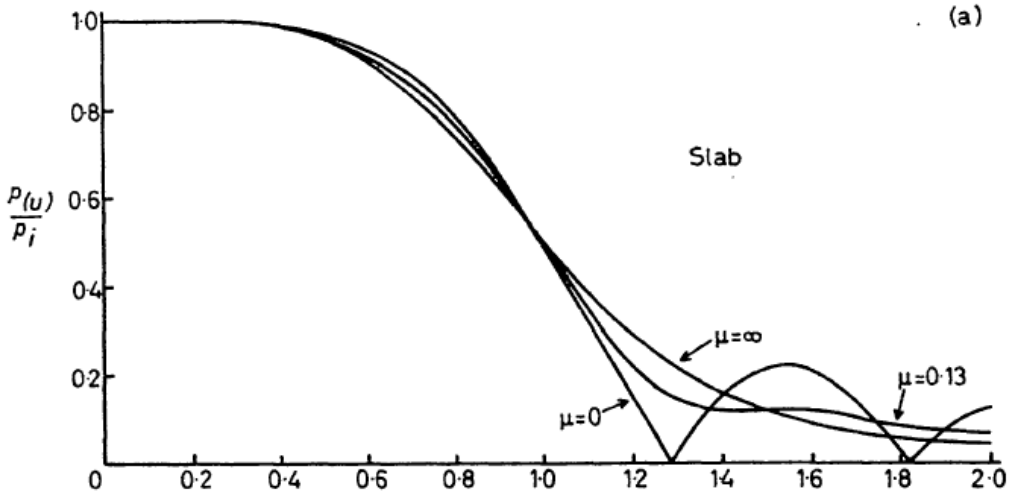

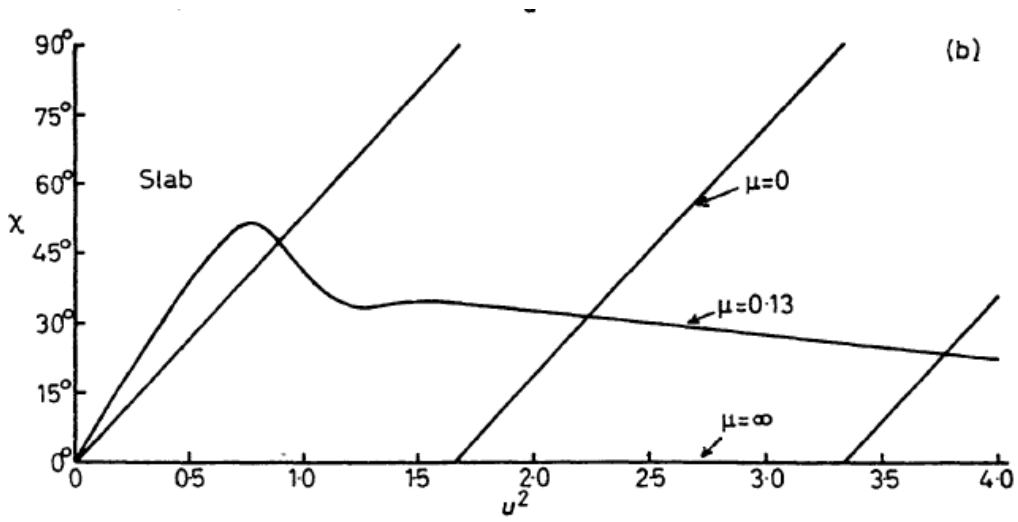

Burn (1966)

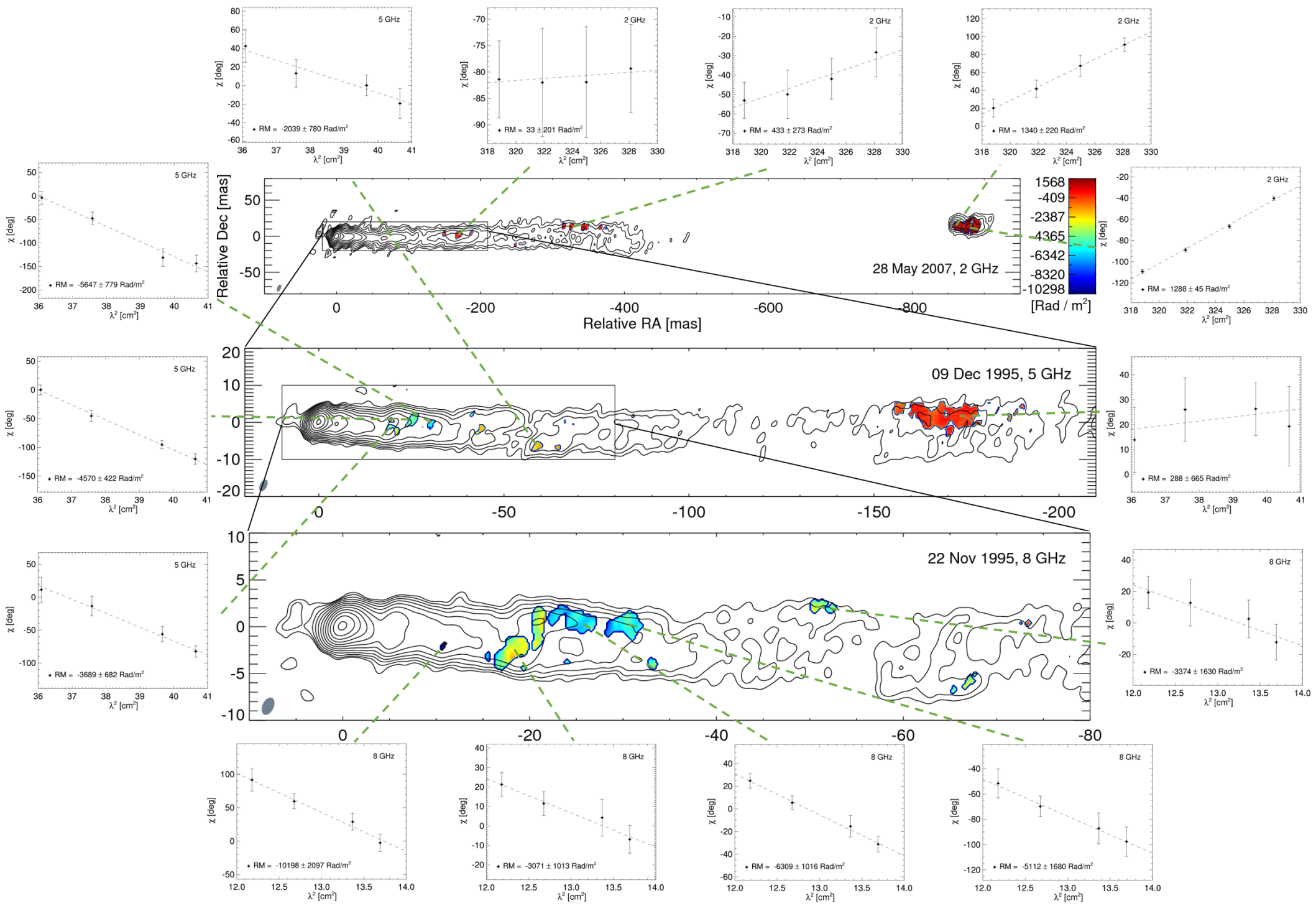
5 GHz
RM = -2039 ± 780 Rad/m²
2 GHz
RM = 33 ± 201 Rad/m²
2 GHz
RM = 433 ± 273 Rad/m²
2 GHz
RM = 1340 ± 220 Rad/m²
5 GHz
RM = -5647 ± 779 Rad/m²
28 May 2007, 2 GHz
Relative Dec [mas]
Relative RA [mas]
1568
-409
-2387
-4365
-6342
-8320
-10298
[Rad / m²]
2 GHz
RM = 1288 ± 45 Rad/m²
5 GHz
RM = -4570 ± 422 Rad/m²
09 Dec 1995, 5 GHz
RM = 288 ± 665 Rad/m²
5 GHz
RM = -3689 ± 682 Rad/m²
22 Nov 1995, 8 GHz
8 GHz
RM = -3374 ± 1630 Rad/m²
8 GHz
RM = -10198 ± 2097 Rad/m²
8 GHz
RM = -3071 ± 1013 Rad/m²
8 GHz
RM = -6309 ± 1016 Rad/m²
8 GHz
RM = -5112 ± 1680 Rad/m²
χ [deg]
λ² [cm²]

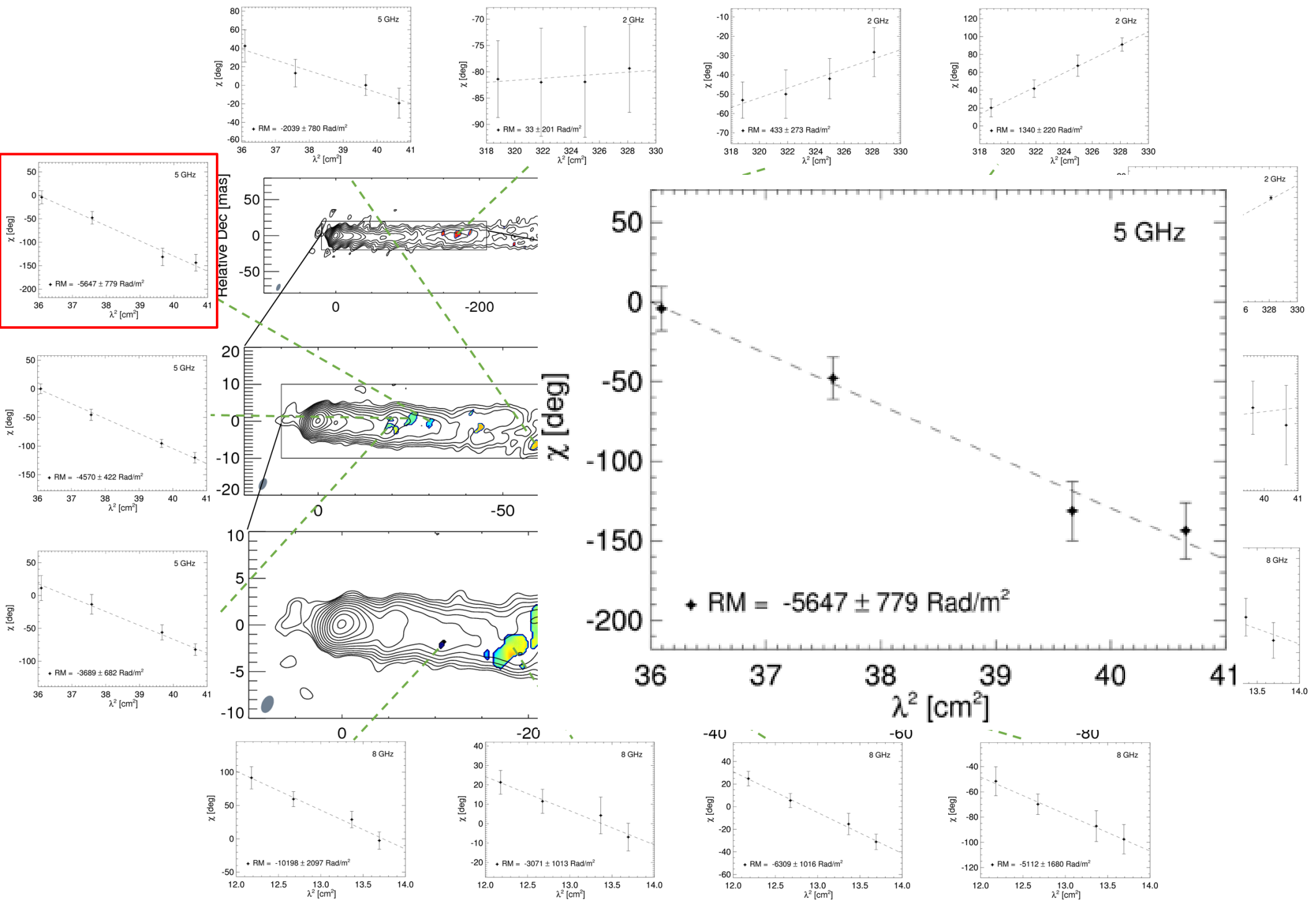
5 GHz
RM = -5647 ± 779 Rad/m²
χ [deg]
λ² [cm²]
Relative Dec [mas]
Relative RA [mas]
2 GHz
RM = 433 ± 273 Rad/m²
RM = 1340 ± 220 Rad/m²
RM = 33 ± 201 Rad/m²
RM = -2039 ± 780 Rad/m²
RM = -4570 ± 422 Rad/m²
RM = -3689 ± 682 Rad/m²
8 GHz
RM = -10198 ± 2097 Rad/m²
RM = -3071 ± 1013 Rad/m²
RM = -6309 ± 1016 Rad/m²
RM = -5112 ± 1680 Rad/m²

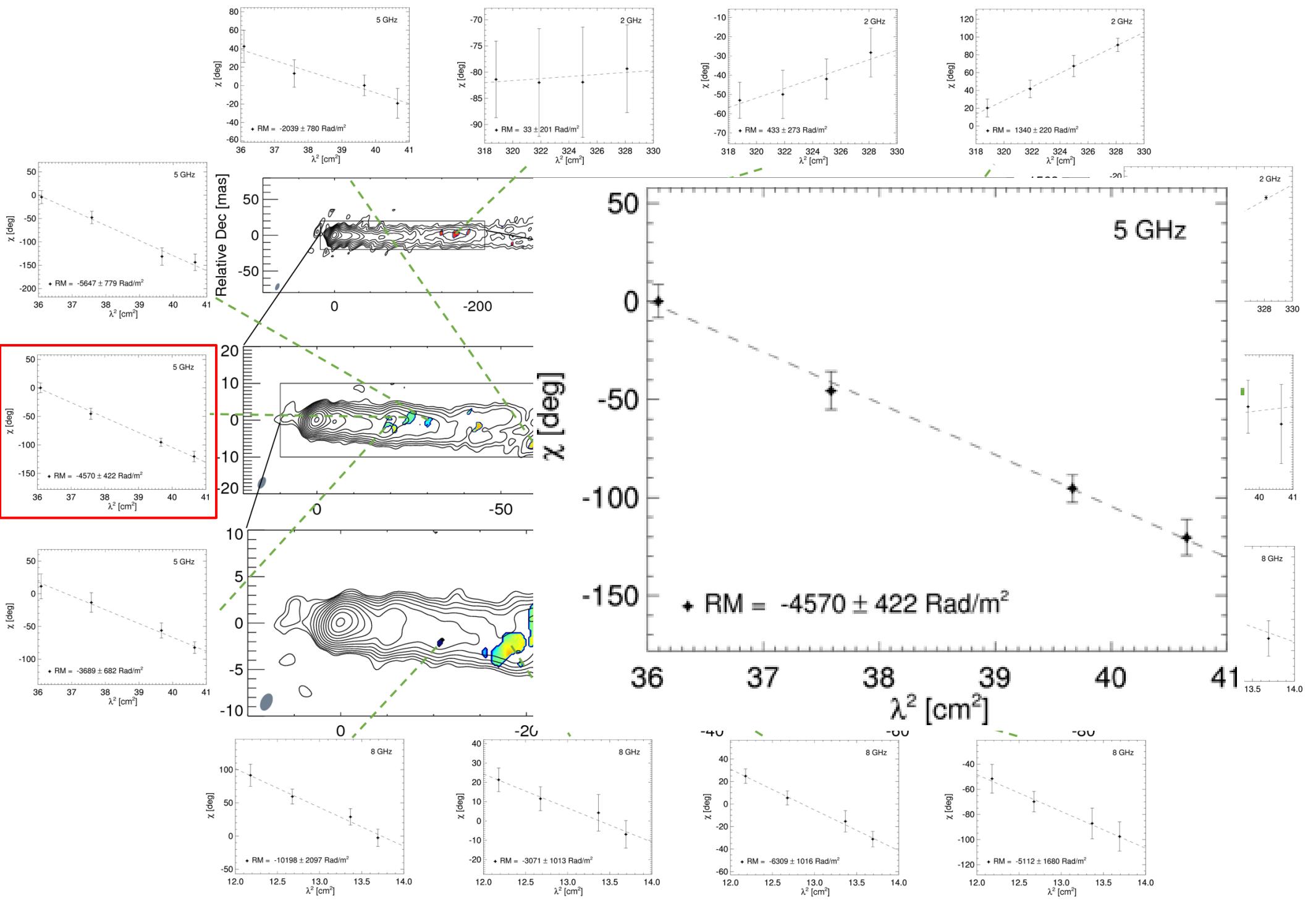
5 GHz
RM = -2039 ± 780 Rad/m²
2 GHz
RM = 33 ± 201 Rad/m²
2 GHz
RM = 433 ± 273 Rad/m²
2 GHz
RM = 1340 ± 220 Rad/m²
5 GHz
RM = -5647 ± 779 Rad/m²
Relative Dec [mas]
5 GHz
RM = -4570 ± 422 Rad/m²
χ [deg]
5 GHz
RM = -3689 ± 682 Rad/m²
λ² [cm²]
8 GHz
RM = -10198 ± 2097 Rad/m²
8 GHz
RM = -3071 ± 1013 Rad/m²
8 GHz
RM = -6309 ± 1016 Rad/m²
8 GHz
RM = -5112 ± 1680 Rad/m²

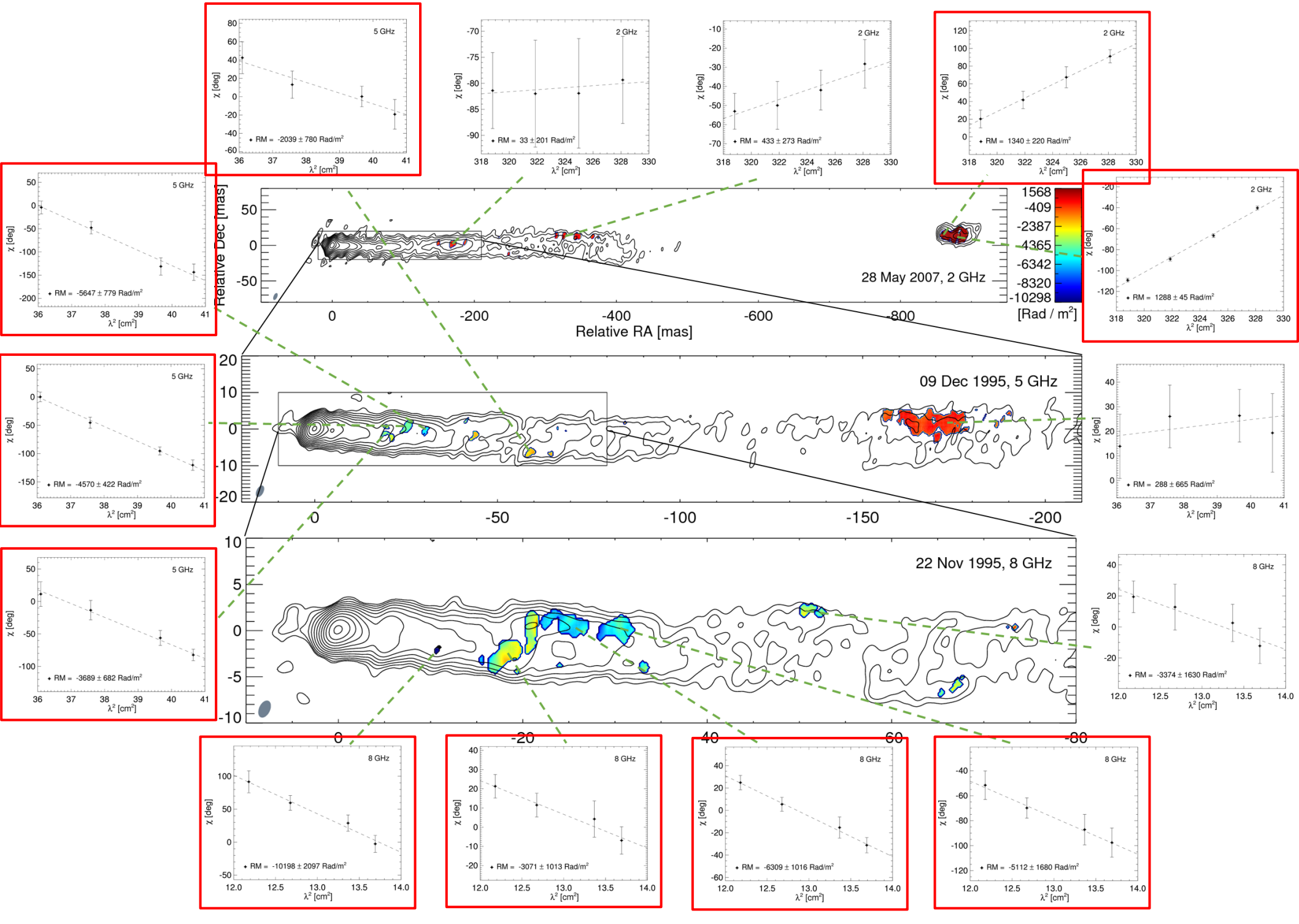
28 May 2007, 2 GHz
09 Dec 1995, 5 GHz
22 Nov 1995, 8 GHz
Relative Dec [mas]
Relative RA [mas]
[Rad / m^2]
χ [deg]
λ^2 [cm^2]
RM = -2039 ± 780 Rad/m^2
RM = 33 ± 201 Rad/m^2
RM = 433 ± 273 Rad/m^2
RM = 1340 ± 220 Rad/m^2
RM = -5647 ± 779 Rad/m^2
RM = 1288 ± 45 Rad/m^2
RM = -4570 ± 422 Rad/m^2
RM = 288 ± 665 Rad/m^2
RM = -3689 ± 682 Rad/m^2
RM = -3374 ± 1630 Rad/m^2
RM = -10198 ± 2097 Rad/m^2
RM = -3071 ± 1013 Rad/m^2
RM = -6309 ± 1016 Rad/m^2
RM = -5112 ± 1680 Rad/m^2

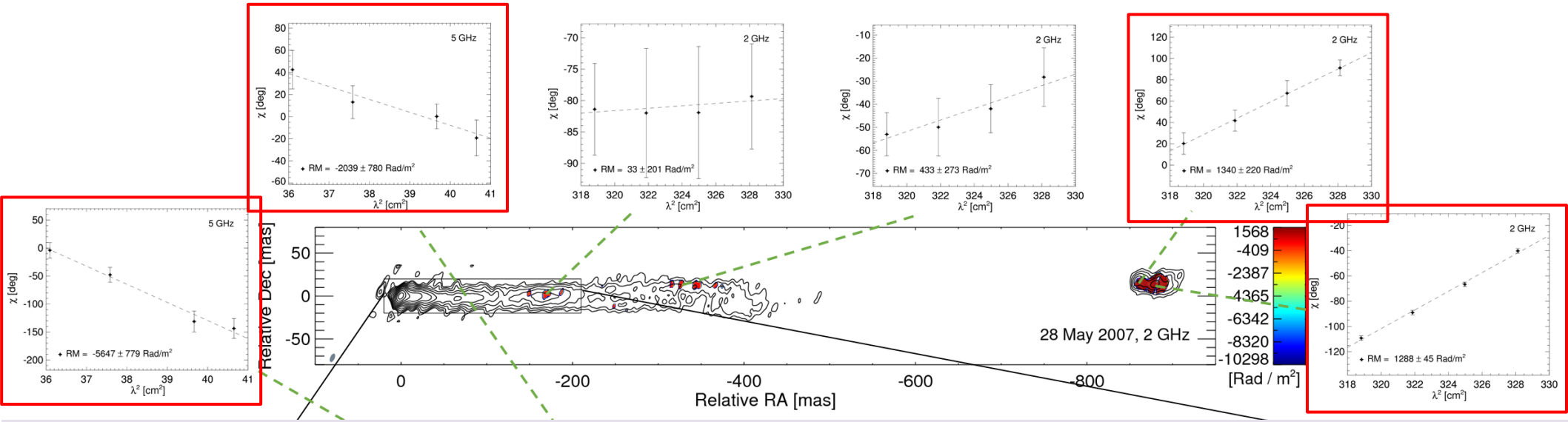

Thermal electrons external to the jet are likely the source of observed Faraday rotation.

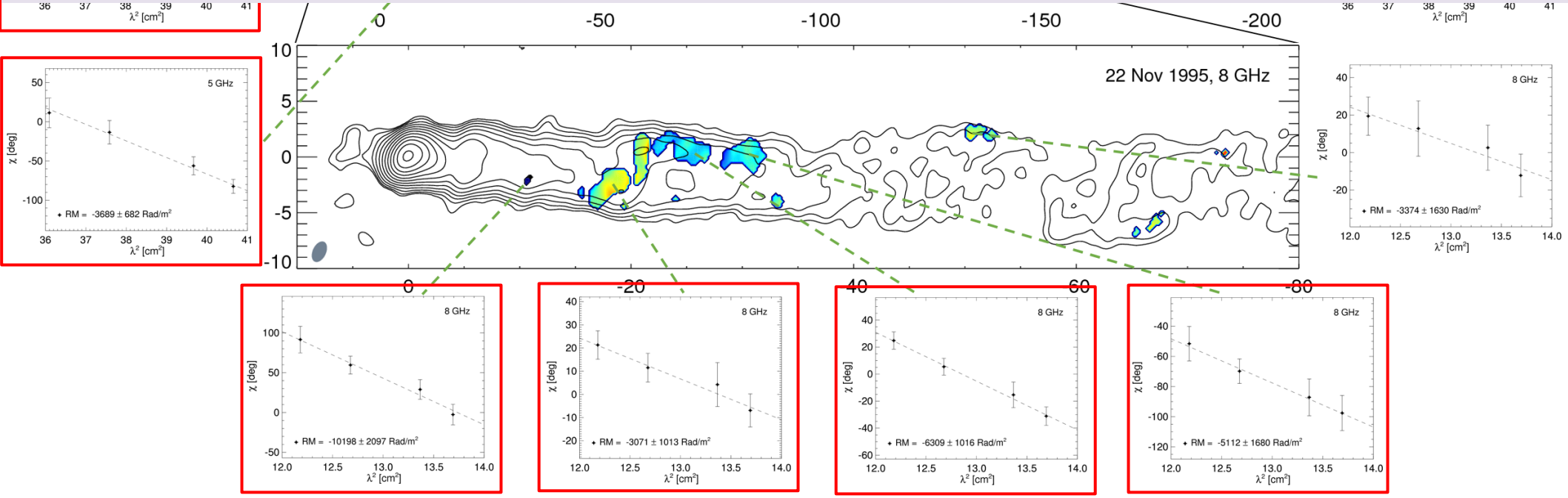

Modelling the external Faraday rotation measures

$$RM = 8.1 \times 10^5 \int n_e B dr$$

$$n_e = n_{\rm out} \left(\frac{r}{r_{\rm out}} \right)^{-p} \qquad B(r) = B_{\rm out} \left(\frac{r}{r_{\rm out}} \right)^{-1}$$

$$RM = 8.1 \times 10^5 n_{\rm out} B_{\rm out} r_{\rm out}^{(p+1)} \int_{r_{\rm in}}^{r_{\rm out}} r^{-(p+1)} dr$$

Modelling the external Faraday rotation measures

$$RM = 8.1 \times 10^5 \int n_e B dr$$

$$n_e = n_{\rm out} \left(\frac{r}{r_{\rm out}} \right)^{-p} \qquad B(r) = B_{\rm out} \left(\frac{r}{r_{\rm out}} \right)^{-1}$$

$$RM = 8.1 \times 10^5 n_{\rm out} B_{\rm out} r_{\rm out}^{(p+1)} \int_{r_{\rm in}}^{r_{\rm out}} r^{-(p+1)} dr$$

from ADAF self-similar solution allowing mass loss

$$\rho(r) \propto r^{-p} \qquad \dot{M}(r) \propto r^{s} \qquad p = 1.5 - s$$

Yuan & Narayan (2014)

Modelling the external Faraday rotation measures

$$RM = 8.1 \times 10^5 \int n_e B dr$$

$$n_e = n_{\rm out} \left(\frac{r}{r_{\rm out}} \right)^{-p}$$

$$B(r) = B_{\rm out} \left(\frac{r}{r_{\rm out}} \right)^{-1}$$

$$RM = 8.1 \times 10^5 n_{\rm out} B_{\rm out} r_{\rm out}^{(p+1)} \int_{r_{\rm in}}^{r_{\rm out}} r^{-(p+1)} dr$$

Modelling the external Faraday rotation measures

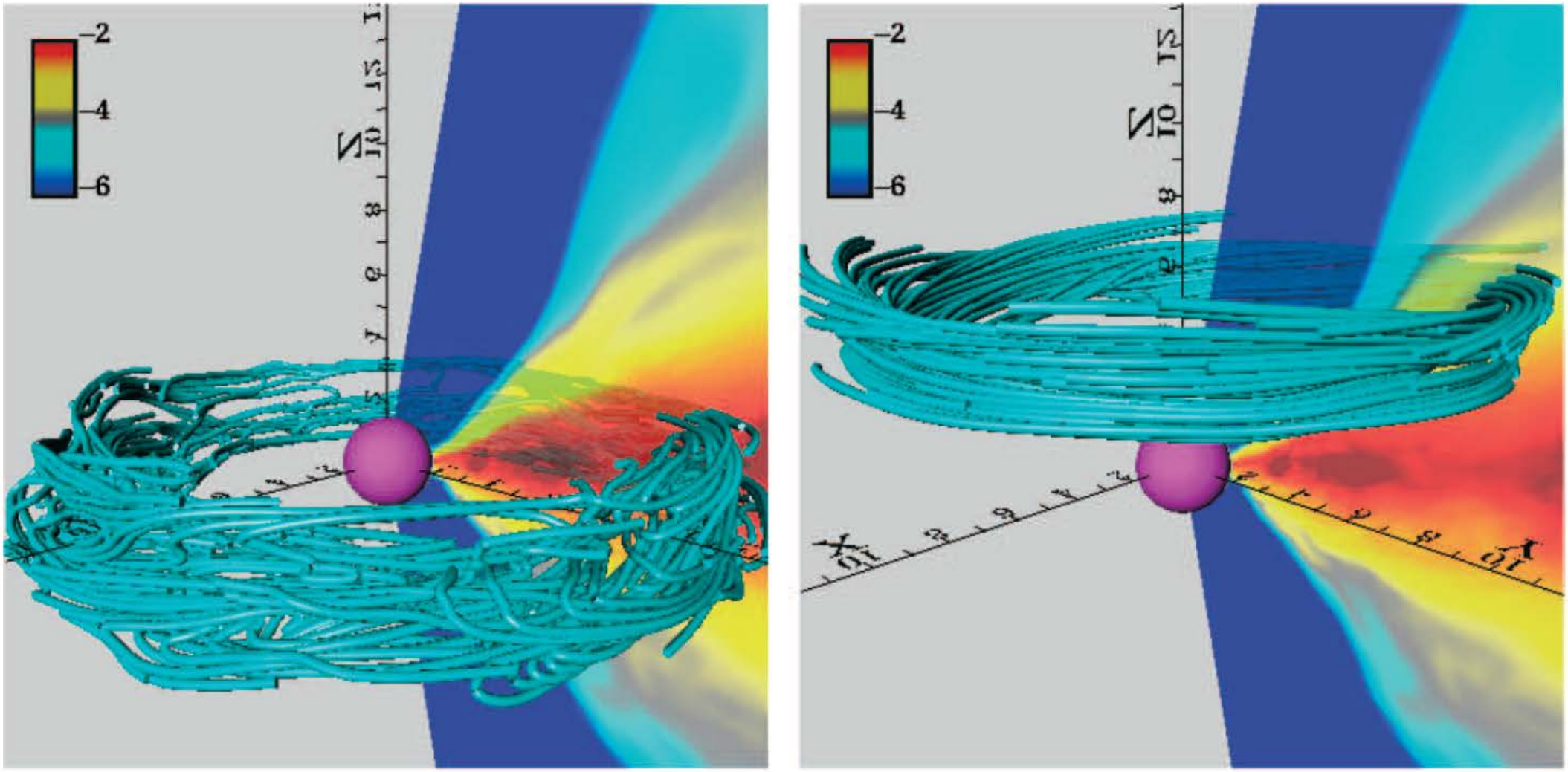

Hirose (2004)

Modelling the external Faraday rotation measures

$$RM = 8.1 \times 10^5 \int n_e B dr$$

$$n_e = n_{\rm out} \left(\frac{r}{r_{\rm out}} \right)^{-p} \qquad B(r) = B_{\rm out} \left(\frac{r}{r_{\rm out}} \right)^{-1}$$

$$RM = 8.1 \times 10^5 n_{\rm out} B_{\rm out} r_{\rm out}^{(p+1)} \int_{r_{\rm in}}^{r_{\rm out}} r^{-(p+1)} dr$$

r_{in} : Jet boundary measured in previous VLBI observations (Asada & Nakamura 2012)
r_{out} : the Bondi radius, $3.6 \times 10^5 r_S$ from previous X-ray observations (Russell+15).
n_{out} : $0.3 \mathrm{cm}^{-3}$ at r_{out} from X-ray observations (Russell+15).

RM distribution as a function of distance

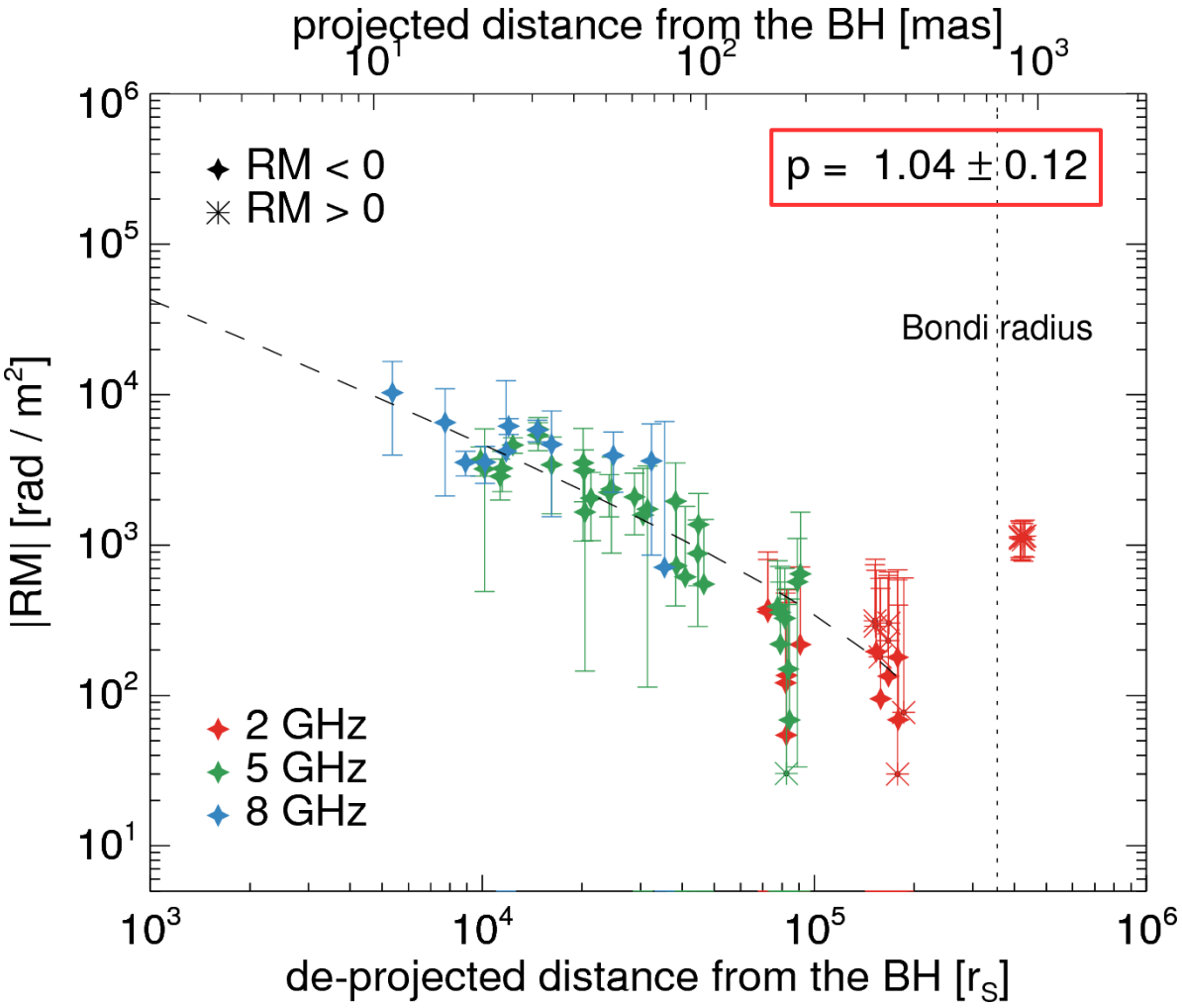

– We obtained p ~ 1. ⟶ $\rho \propto r^{-1}$: Support ADIOS (p ~ 1)

p = 1.5 : classical ADAF (Narayan & Yi 1994)

0.5 < p < 1.5 : ADAF with mass outflows, ADIOS (Blandford & Begelman 1999)

p = 0.5 : convection dominated accretion flows, CDAF (Quataert & Grizunov 00)

→ Cannot explain with spherical inflows such as giant ADAFs.

RM distribution as a function of distance

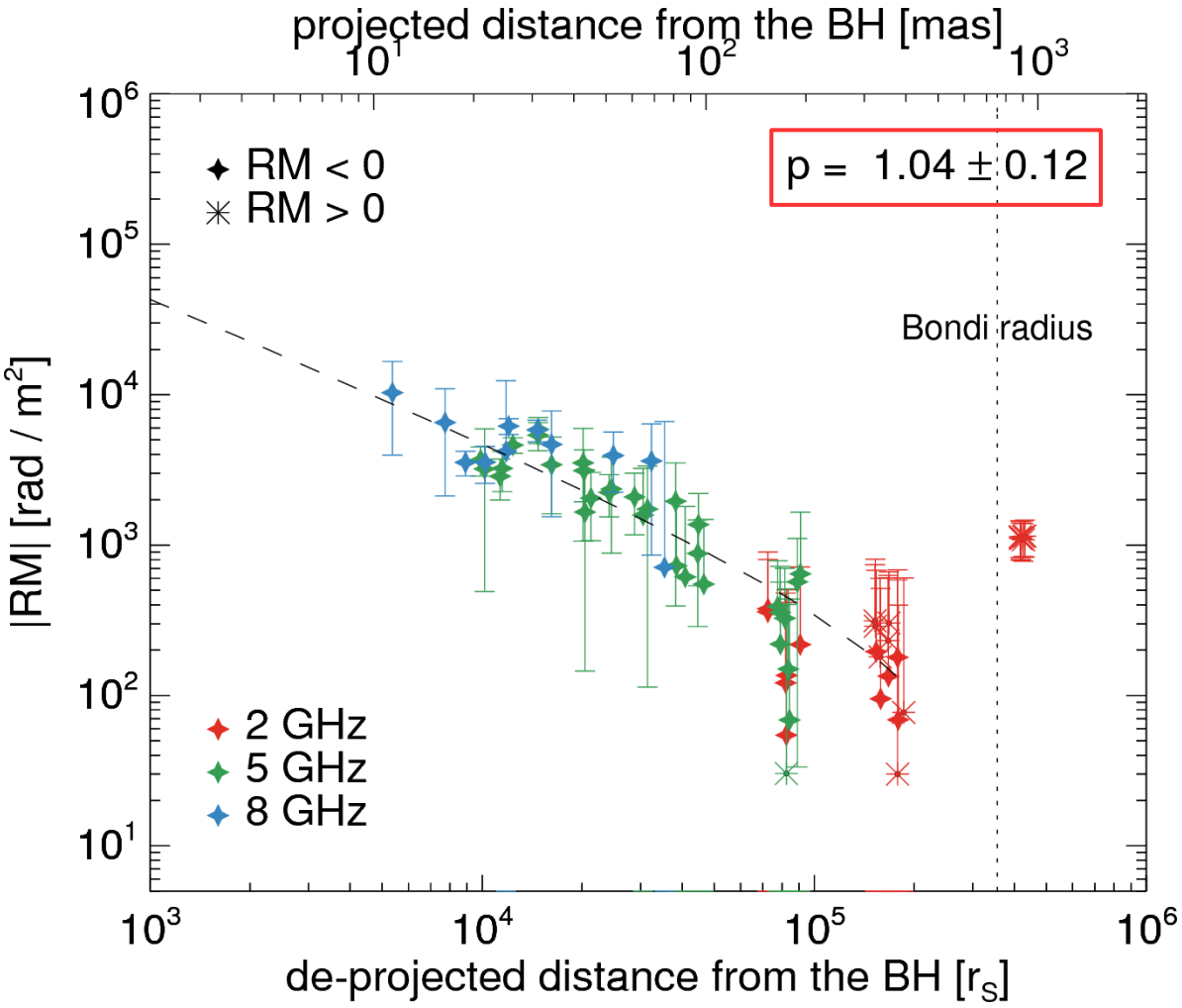

– We obtained p ~ 1. ⟶ $\rho \propto r^{-1}$: Support ADIOS (p ~ 1)

– If the flat density profile is due to decreasing mass accretion rate with distance, then

⟶ $\dot{M}(r) \propto r^{0.5}$

Comparison with Numerical simulations

Yuan et al. (2012)

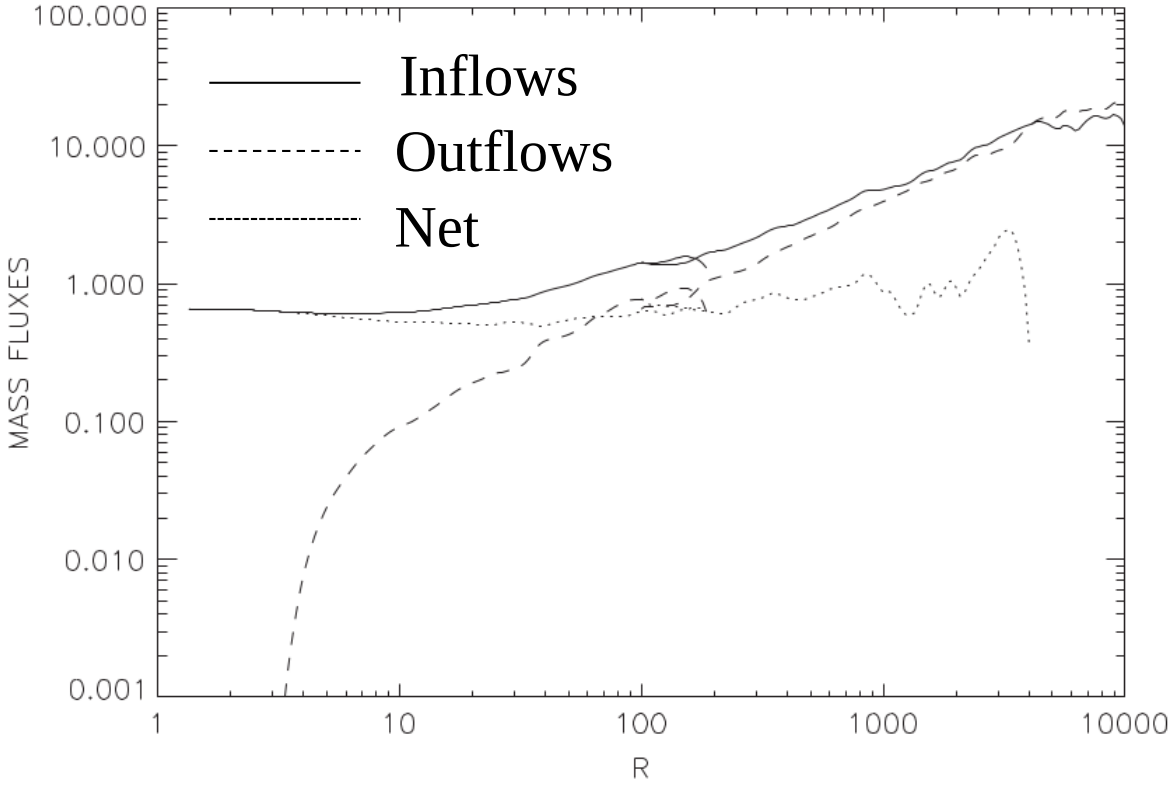

When $\alpha = 0.01$

$$\rho(r) \propto r^{-0.85}, \quad p(r) \propto r^{-1.85}$$

$$\dot{M}_{\rm in}(r) \propto r^{0.54}$$

We have also conducted simulations with $\alpha = 0.05$. We found that convective outflow becomes significantly weaker. The density profile becomes steeper while the accretion rate profiles become flatter.

→ Our results are consistent with the simulations done at relatively large radii.

Comparison with Numerical simulations

Pang et al. (2011)

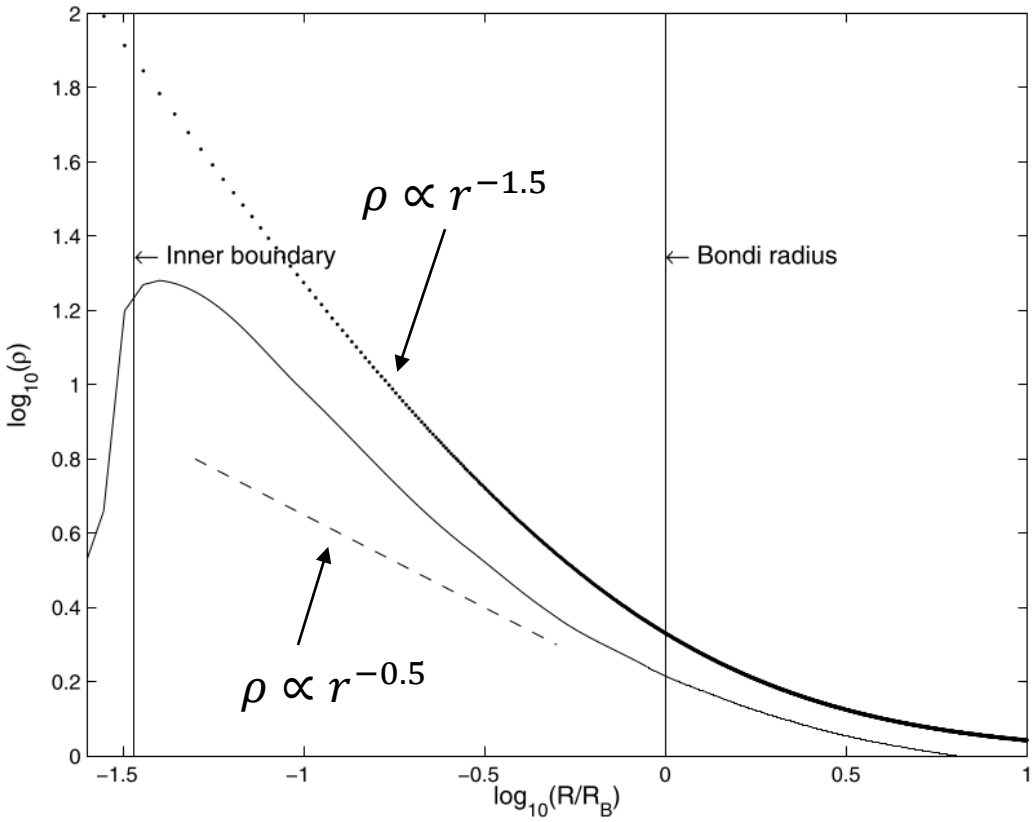

Run	$\frac{R_B}{dx_{min}}$	$\frac{R_B}{R_{in}}$	$1+s_{in}$	$\Re_B$	β_0	$\frac{R_K}{R_B}$	$\frac{t_{sim}}{t_B}$	θ_{Bj}	$\frac{\dot{M}}{\dot{M}_{Bondi}}$	k_{eff} [a]
1	500	67	1.023	40.15	∞	0	8	N/A	1.02	1.5047
2	250	33	1.013	59.29	∞	0	3	N/A	1.10	1.5273
3	125	17	1.013	48.11	100	0	6–20	45°	0.49	1.2482
4	250	33	1.013	59.29	100	0	6–20	45°	0.31	1.1650
5	500	67	1.023	40.15	100	0	6–20	45°	0.22	1.1399
6	1000	133	1.0315	30.82	100	0	6–10	45°	0.16	1.1253
7	250	33	1.013	59.29	1	0	6–20	45°	0.15	0.9574
8	250	33	1.013	59.29	10	0	6–20	45°	0.26	1.1147
9	250	33	1.013	59.29	1000	0	6–20	45°	0.40	1.2379
10	250	33	1.013	59.29	100	0.1	6–20	45°	0.289	1.1450
11	250	33	1.013	59.29	100	0.5	6–20	45°	0.286	1.1420
12	250	33	1.013	59.29	100	1.0	6–20	45°	0.31	1.1650
13[b]	62.5	33	1.06	14.24	100	0	6–20	45°	0.30	1.1557
14[c]	125	33	1.037	28.94	100	0	6–20	45°	0.33	1.1829
15	250	33	1.013	59.29	∞	0.1	6–20	45°	0.615	1.3610
16	250	33	1.013	59.29	∞	0.5	6–20	45°	0.621	1.3637
17	250	33	1.013	59.29	∞	1.0	6–20	45°	0.759	1.4211
18	250	33	1.013	59.29	1000	0.1	6-20	45°	0.400	1.2379
19	250	33	1.013	59.29	1000	0.1	6–20	90°	0.469	1.2835
20	250	33	1.013	59.29	100	0.1	6–20	90°	0.300	1.1557
21	250	33	1.013	59.29	10	0.1	6–20	90°	0.233	1.0834
22	250	33	1.013	59.29	1	0.1	6–20	90°	0.188	1.0220
23	250	33	1.013	59.29	100	0	6–20	90°	0.340	1.1915
24	500	67	1.0315	31.65	100	0.1	6–20	63°	0.18	1.2434
25[d]	1000	58.9	1.015	64	100	0.1	6–20	63°	0.19	1.0925
26[e]	8000	117	1.00185	515	100	0.1	21.1465	63°	0.11	1.0365

(i) In the presence of magnetic fields, the flow develops a superadiabatic temperature gradient and flattens to $k \sim 1$. Gas pressure

The most preferable value of $p \sim 1$ in a numerical survey of parameter space.

→ Our results are consistent with the simulations done at relatively large radii.

Discussion : Accretion rate

Narayan & Fabian 11

$$\dot{M}(r) = \dot{M}_{\rm ADAF}\left(\frac{r}{r_{\rm out}}\right)^{0.5} \qquad \dot{M}_{\rm ADAF} \approx 0.3\dot{M}_{\rm Bondi}$$

When α ~ 0.1,
a reasonable choice for ADAF.

– $\dot{M}_{\rm Bondi} = 0.1 M_\odot {\rm yr}^{-1}$ (Russell+15).
– Accretion rate within $10r_S$ is almost constant (e.g., Yuan et al. 2012).

$$\dot{M} \approx 0.3 \times 0.1 M_\odot {\rm yr}^{-1}\left(\frac{10{\rm r_S}}{3.6\times10^5{\rm r_S}}\right)^{0.5} \approx 1.58\times10^{-4}{\rm M_\odot yr^{-1}}$$

→ accretion rate is smaller than the upper limit, $9.2\times10^{-4}M_\odot{\rm yr}^{-1}$ obtained in Kuo et al. (2014).

– However, this is true only when the gas density profile is similar for equatorial regions, which could not be probed by the current data only.

Discussion : What is the source of Faraday rotating medium?

– We conclude that external Faraday rotation is dominant over all radial ranges of significant RM detection.

→ What is the ‘external medium’?

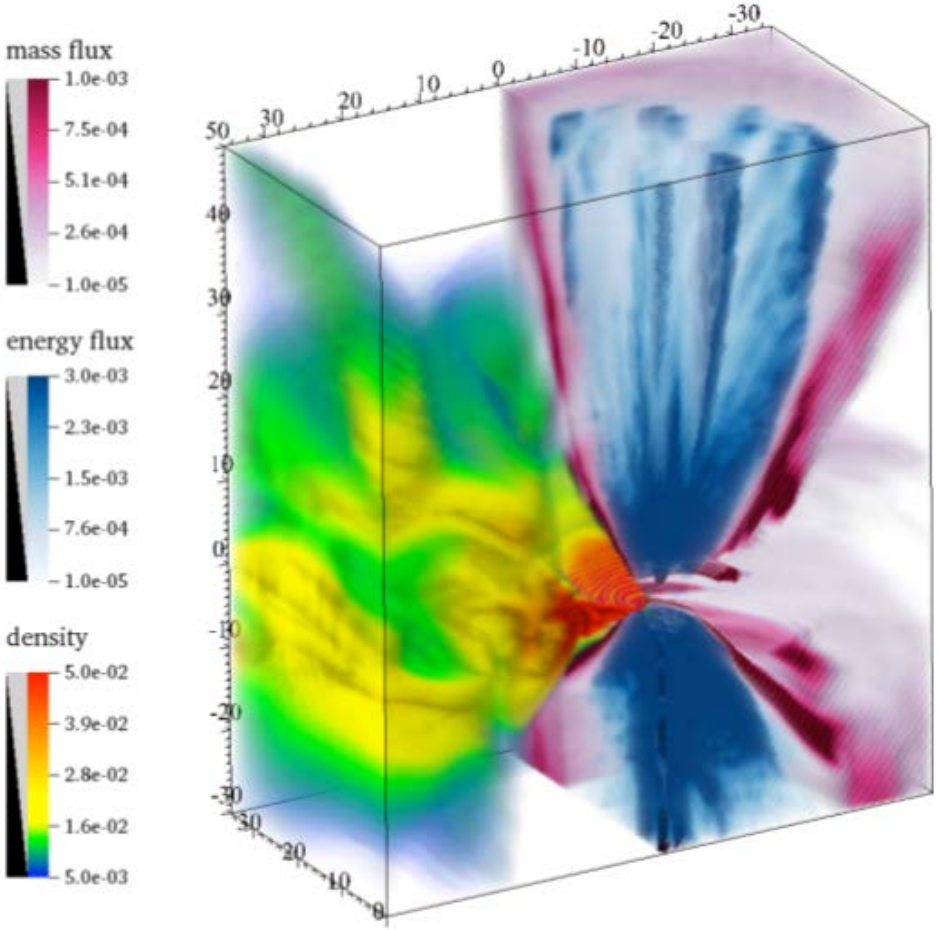

$a_* = 0.7$ SANE

Sadowski+13

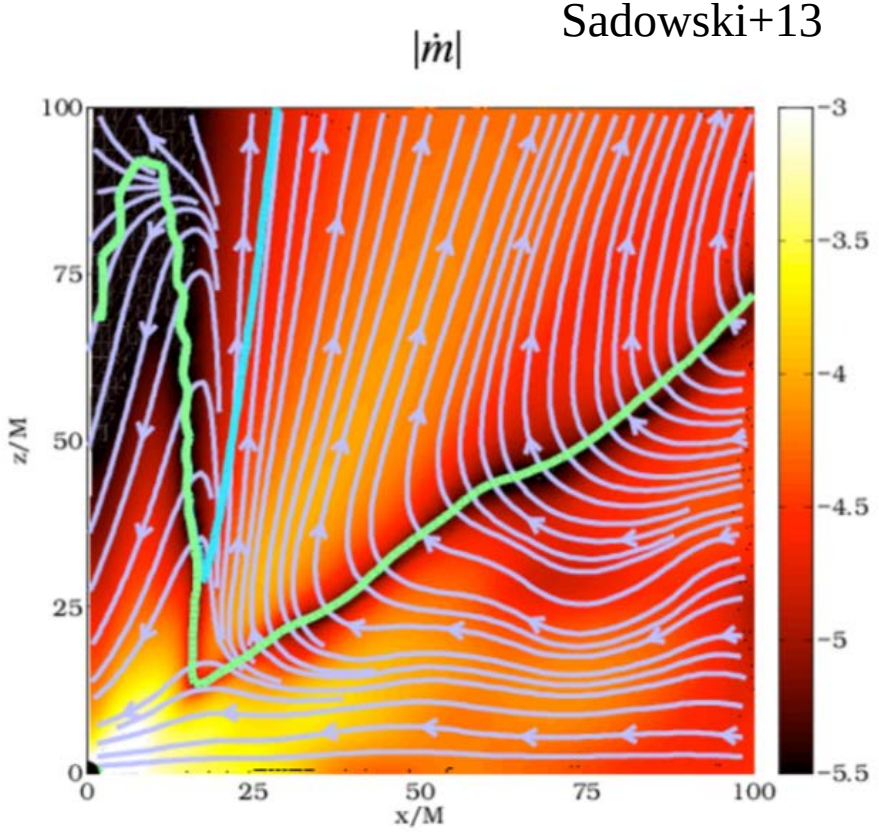

Blue line : dividing line between jet/wind
Green line : dividing line between wind/inflow

– “It is clear that the strong energy flux region is surrounded by the region where the mass-loss is most efficient.” (Sadowski+ 2013)

Discussion : What is the source of Faraday rotating medium?

– We conclude that external Faraday rotation is dominant over all radial ranges of significant RM detection.

→ What is the ‘external medium’?

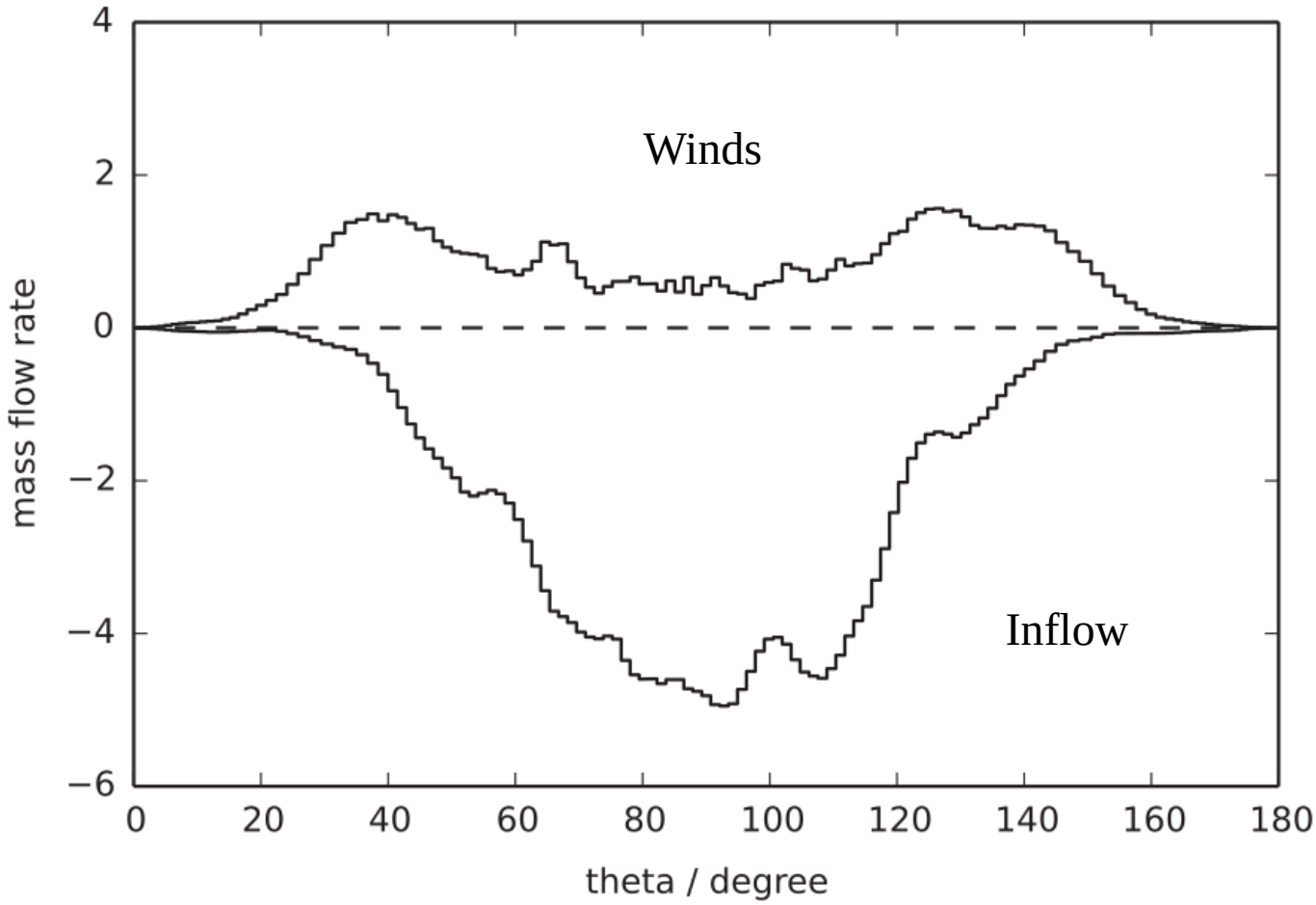

– Small jet viewing angle (~17 deg), winds are likely the source of Faraday rotation.

Discussion : Jet collimation & acceleration

☞ component of the momentum equation

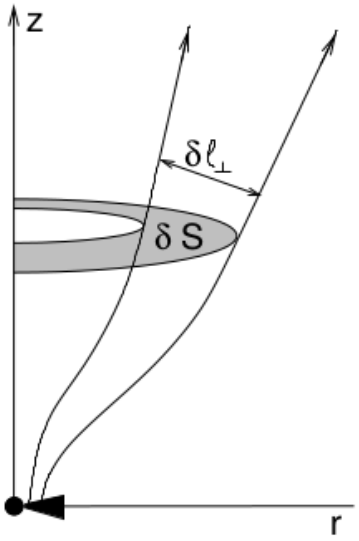

$$\gamma\rho_0(\boldsymbol{V}\cdot\nabla)(\gamma\xi\boldsymbol{V}) = -\nabla p + J^0\boldsymbol{E} + \boldsymbol{J}\times\boldsymbol{B}$$

along the flow (wind equation): $\gamma \approx \mu - \mathcal{F}$

where $\mathcal{F} \propto \varpi^2 B_p$

Lorentz factor

Total energy (conserved)

since $B_p \delta S = \text{const}$,

$\mathcal{F} \propto \varpi^2/\delta S \propto \varpi/\delta\ell_\perp$

acceleration requires the separation between streamlines to increase faster than the cylindrical radius

the collimation-acceleration paradigm:

$\mathcal{F}\downarrow$ through stronger collimation of the inner streamlines relative to the outer ones (differential collimation)

– Jet collimation and acceleration are intimately related.

Taken from Vlahakis' lecture note

Discussion : Jet collimation & acceleration

– AGN jets cannot be self confined → must be confined by an external medium.

(Winds)

Komissarov+ (2009)

$$\frac{1}{a}\left(\frac{1}{a}-1\right)+CZ^{2-\alpha}-K^4Z^{2-4/a}=0$$

$$p_{\rm ext}=p_{\rm ext,lc}(z/z_{\rm lc})^{-\alpha}$$

$$z\propto r^a$$

(i) $\alpha<2\Leftrightarrow a=4/\alpha>2$,
(ii) $\alpha=2\Leftrightarrow 1<a\leq 2$,] → Parabolic jet shape (collimation)

(iii) $\alpha>2\Leftrightarrow a=1$. → Conical jet shape (free expansion)

– To have a parabolic jet shape, $\boxed{\alpha\leq 2}$ is needed (external-confinement).

$$\rho\propto r^{-1}\qquad P_{\rm gas}\propto\rho^{\gamma}\propto r^{-1.67}$$

$$\gamma=5/3$$

$$\boxed{P_{\rm gas}\propto r^{-1.67}}$$

Discussion : Jet collimation & acceleration

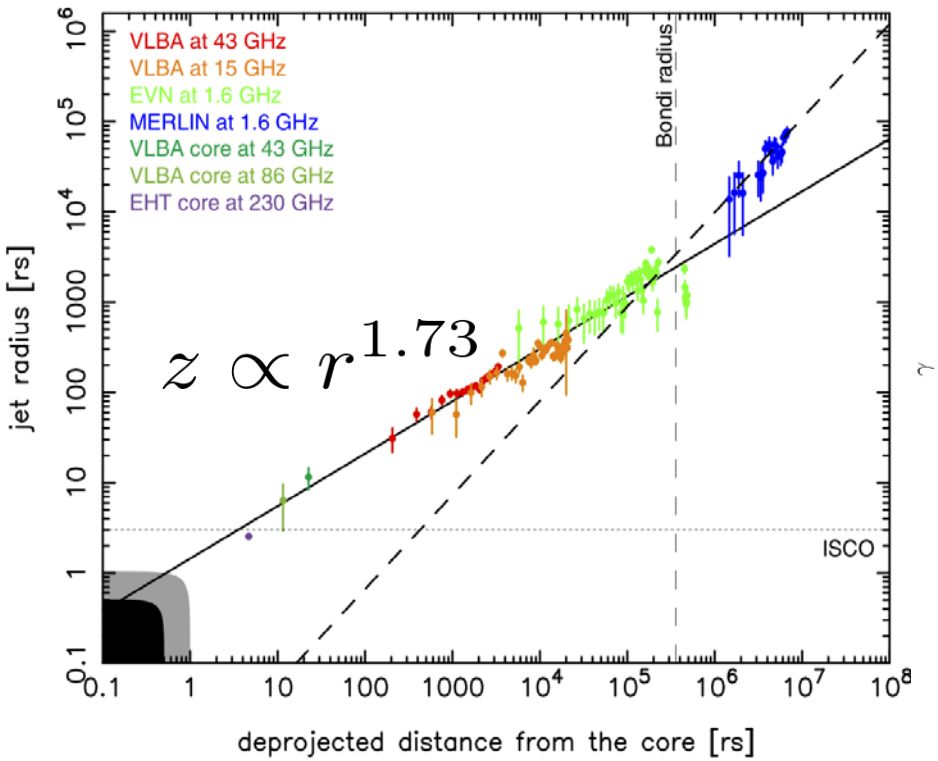

Nakamura & Asada (2013)

Jet collimation

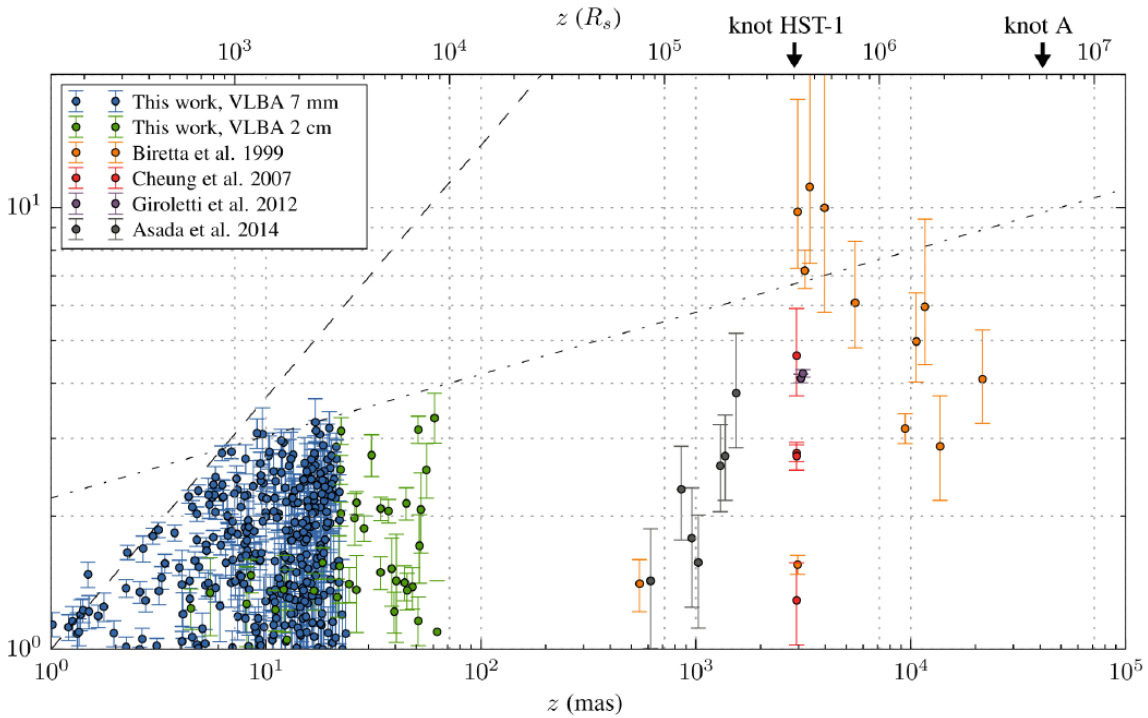

Mertens+ (2016)

Jet acceleration

Confinement of the jet by winds ⟶ collimation ⟶ acceleration

Discussion : mis-alignment between the jet axis and the accretion axis

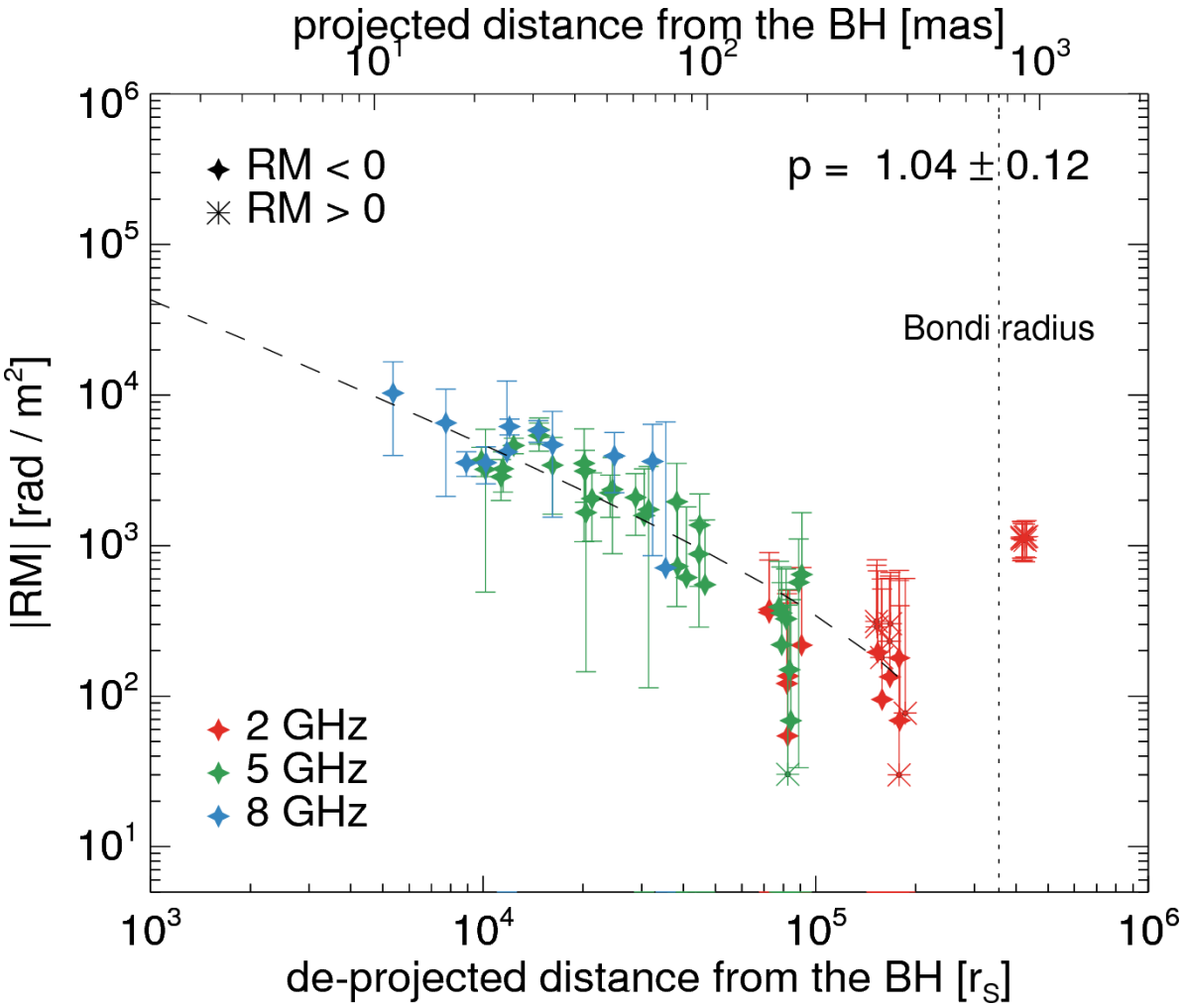

– RM sign is negative in almost all distance ranges.

Discussion : mis-alignment between the jet axis and the accretion axis

Broderick & McKinney (2010)

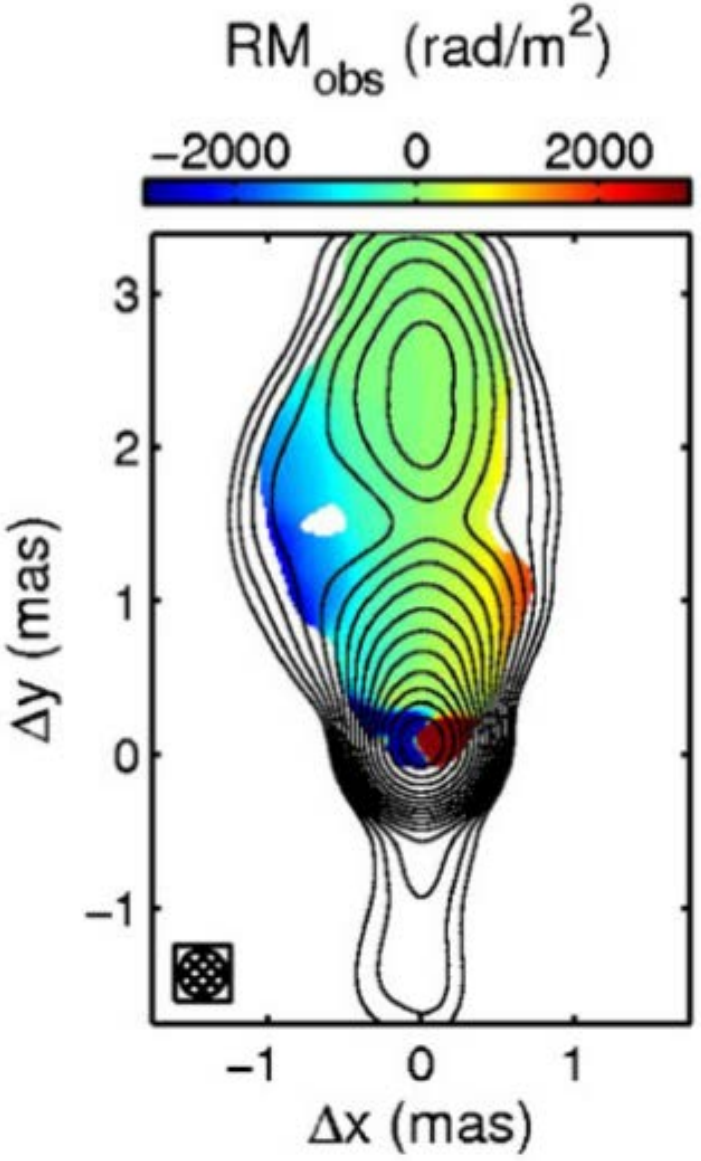

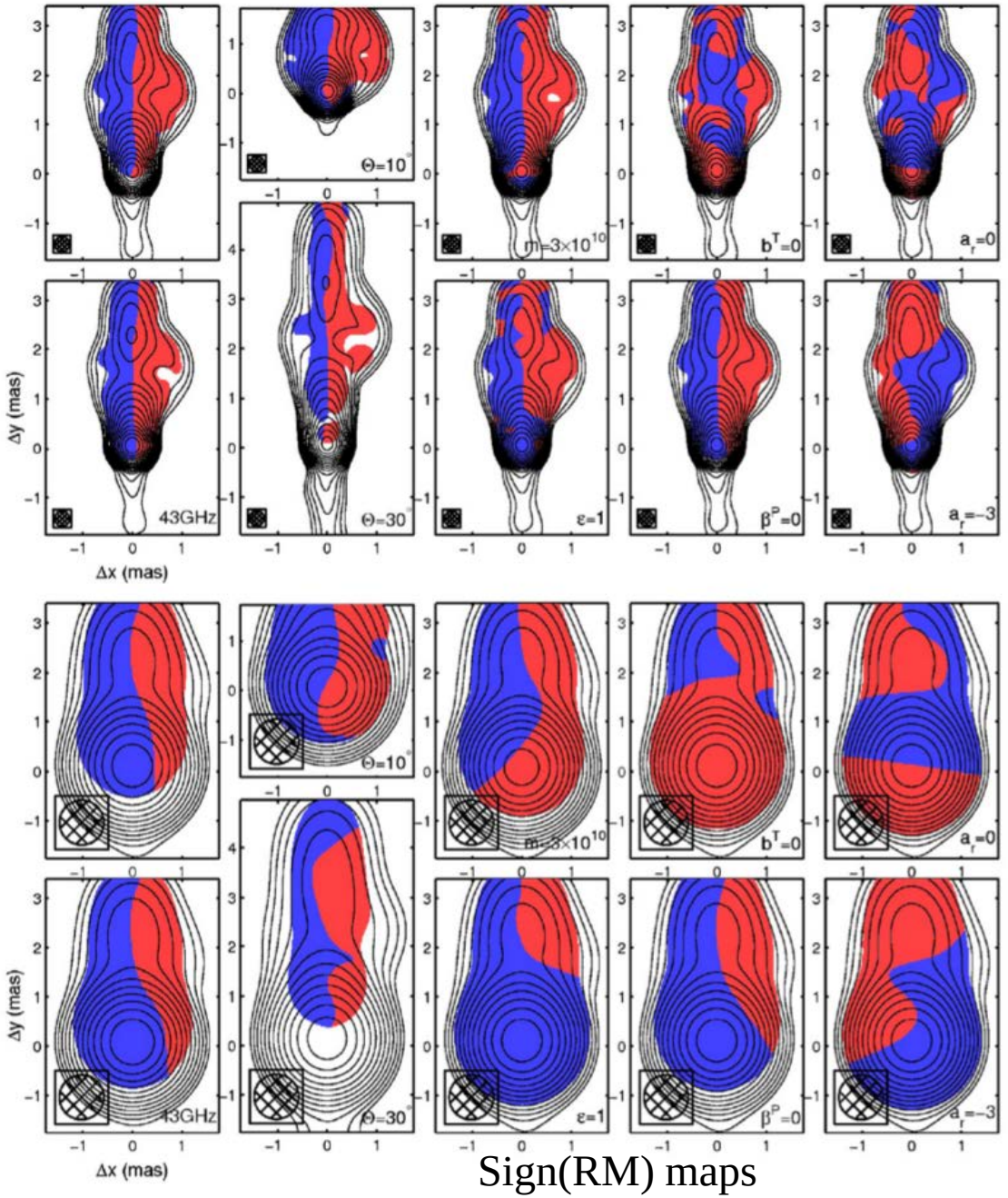

Sign(RM) maps

If the Faraday screen is very close to the jet, e.g., a jet sheath, then

→ Different RM signs on different jet sides with respect to the axis.

Discussion : mis-alignment between the jet axis and the accretion axis

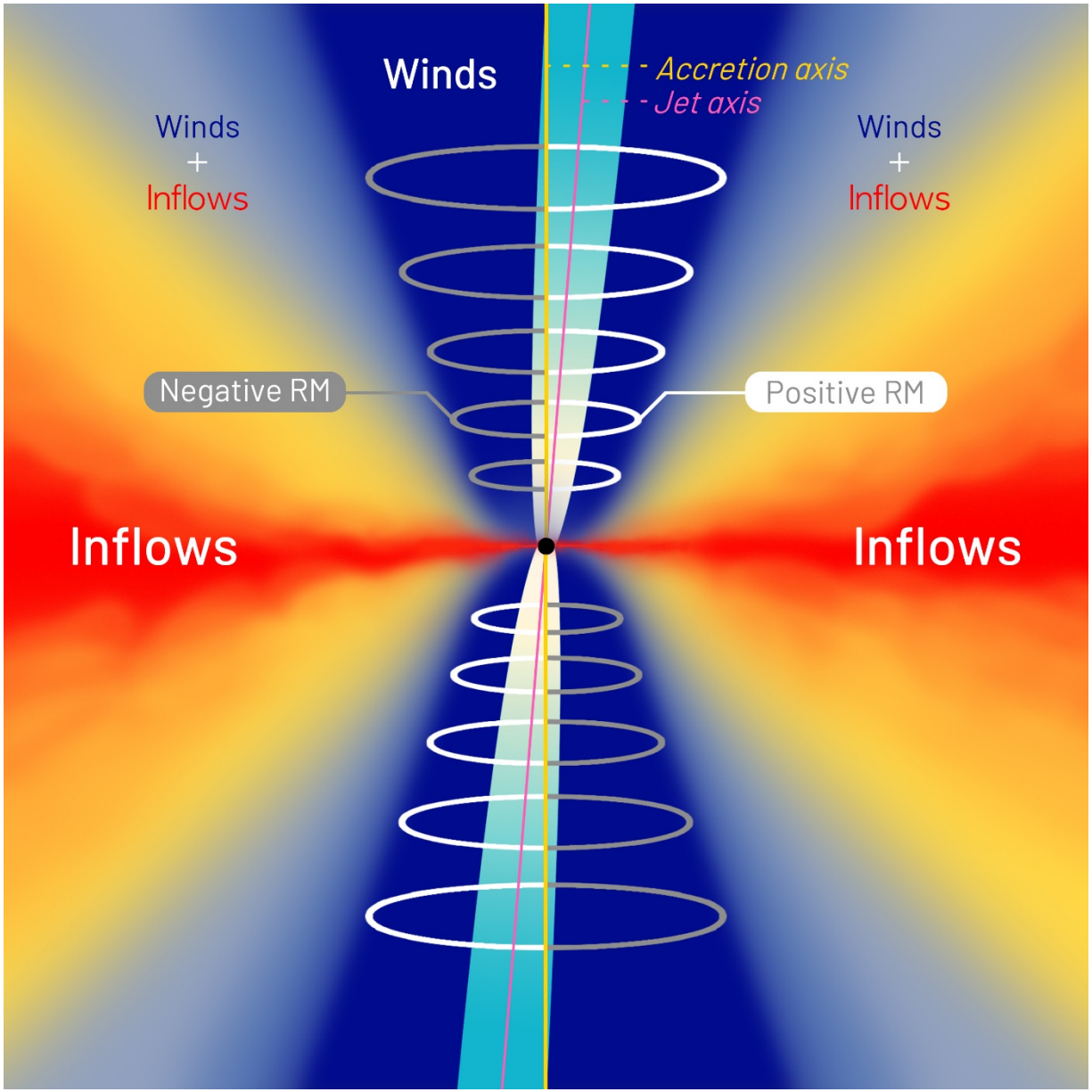

The background light source exposes only one side of the toroidal magnetic loops.

→ A mis-alignment between the jet axis and the accretion axis.

Summary

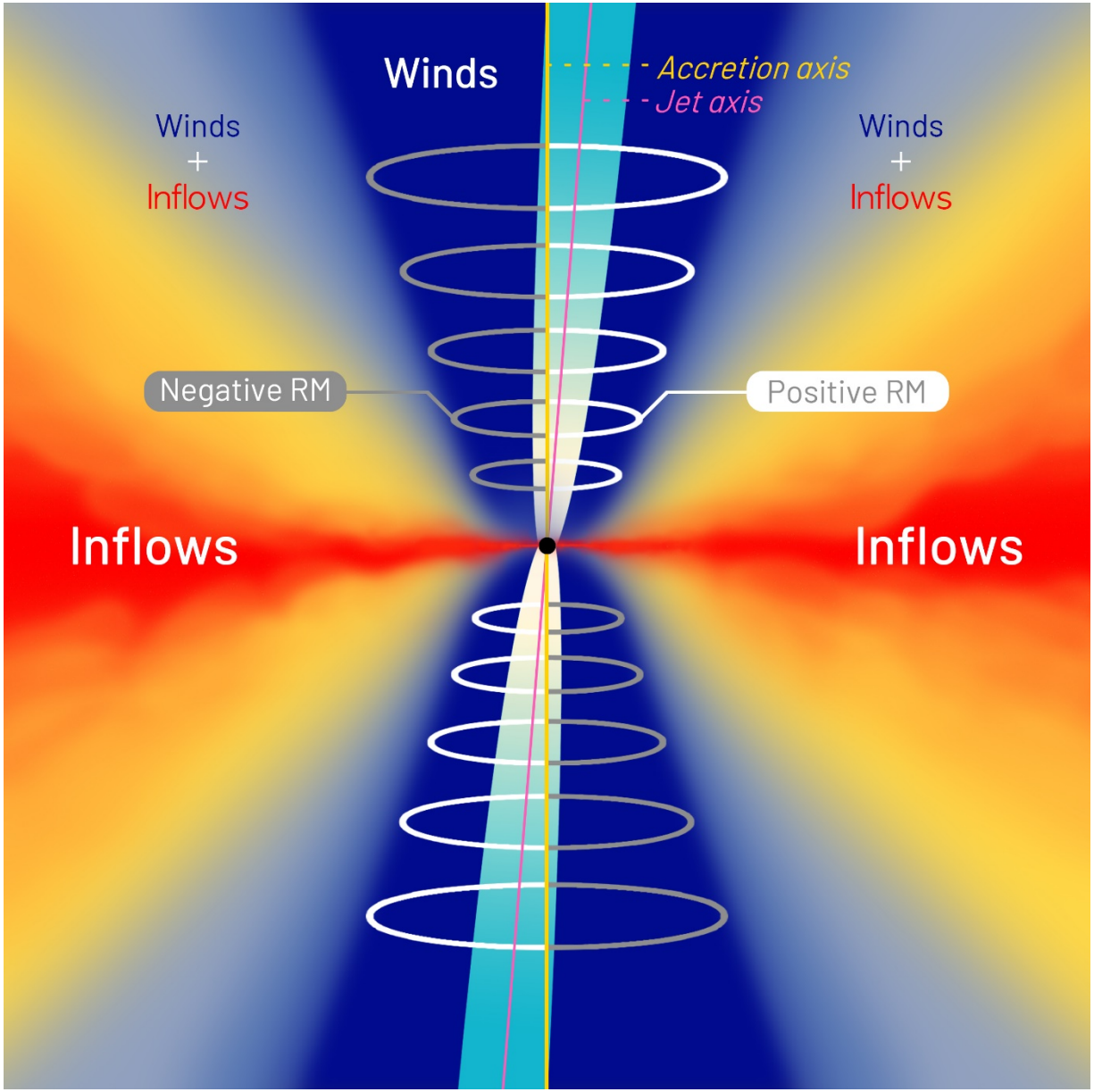
Winds
Accretion axis
Jet axis
Winds
+
Inflows
Winds
+
Inflows
Negative RM
Positive RM
Inflows
Inflows

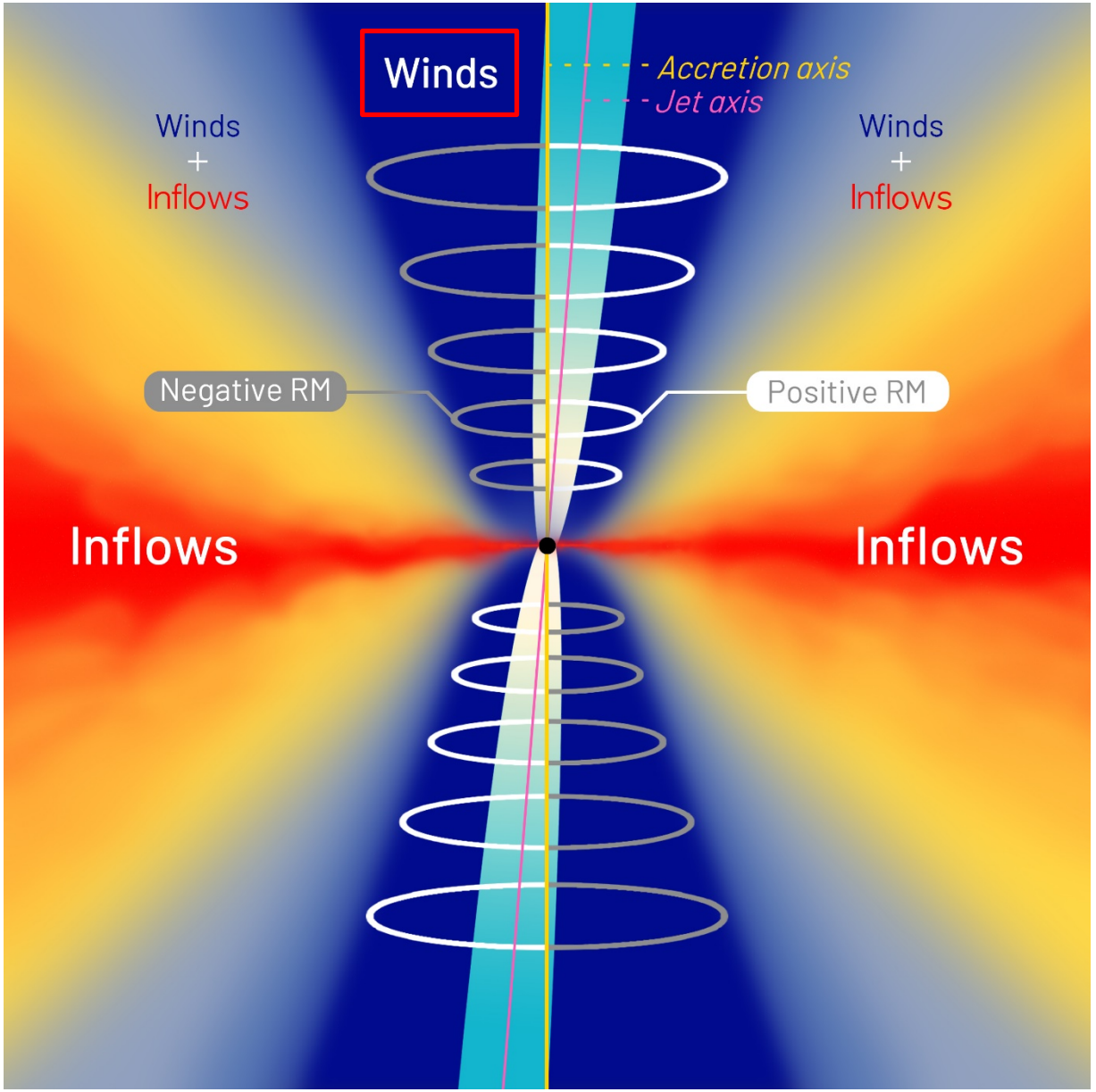
Winds
Accretion axis
Jet axis
Winds
+
Inflows
Winds
+
Inflows
Negative RM
Positive RM
Inflows
Inflows

A significant fraction of gas in the accretion flows might be lost

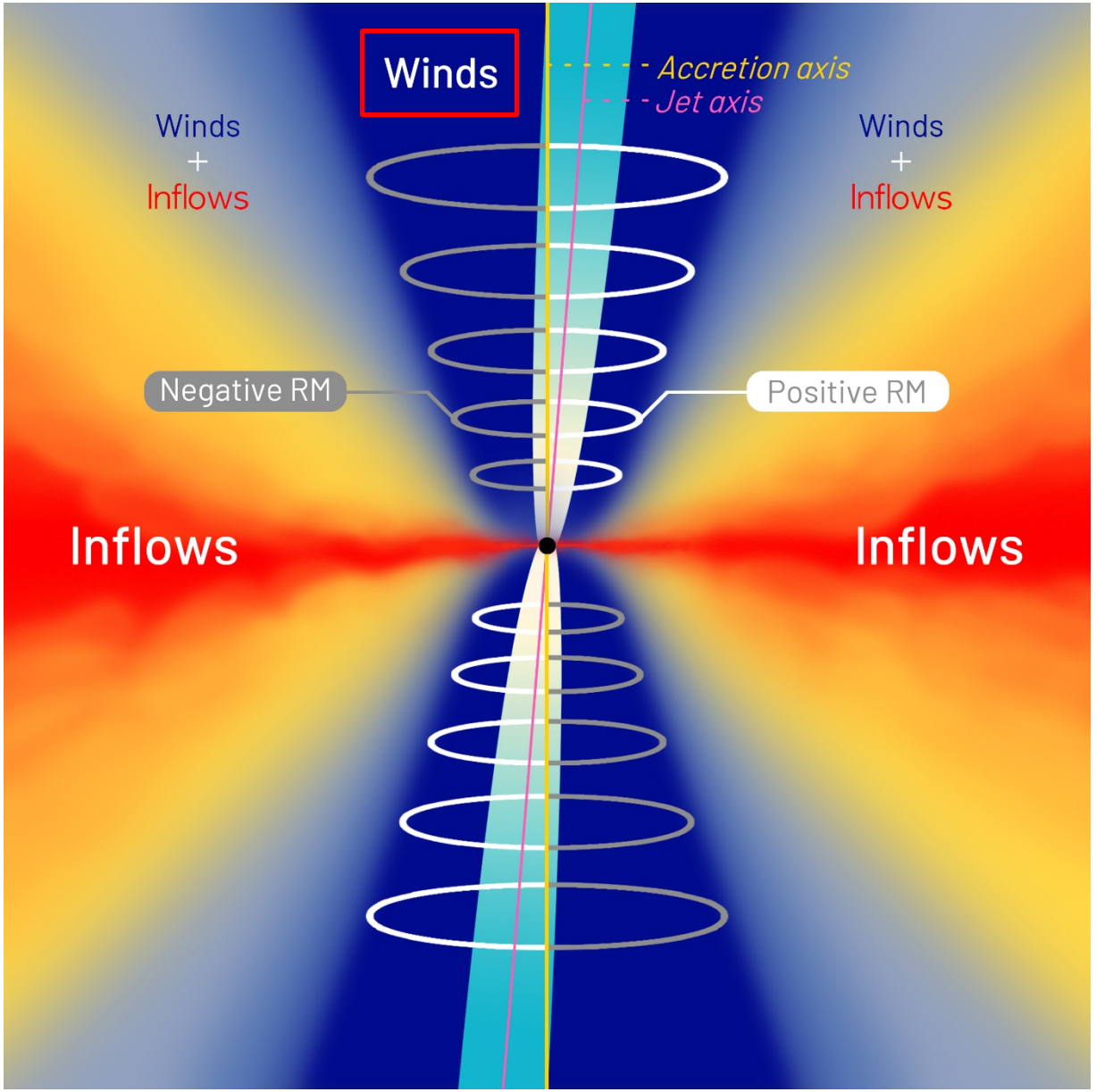

Jets confined by winds

→ collimation → acceleration (MHD)

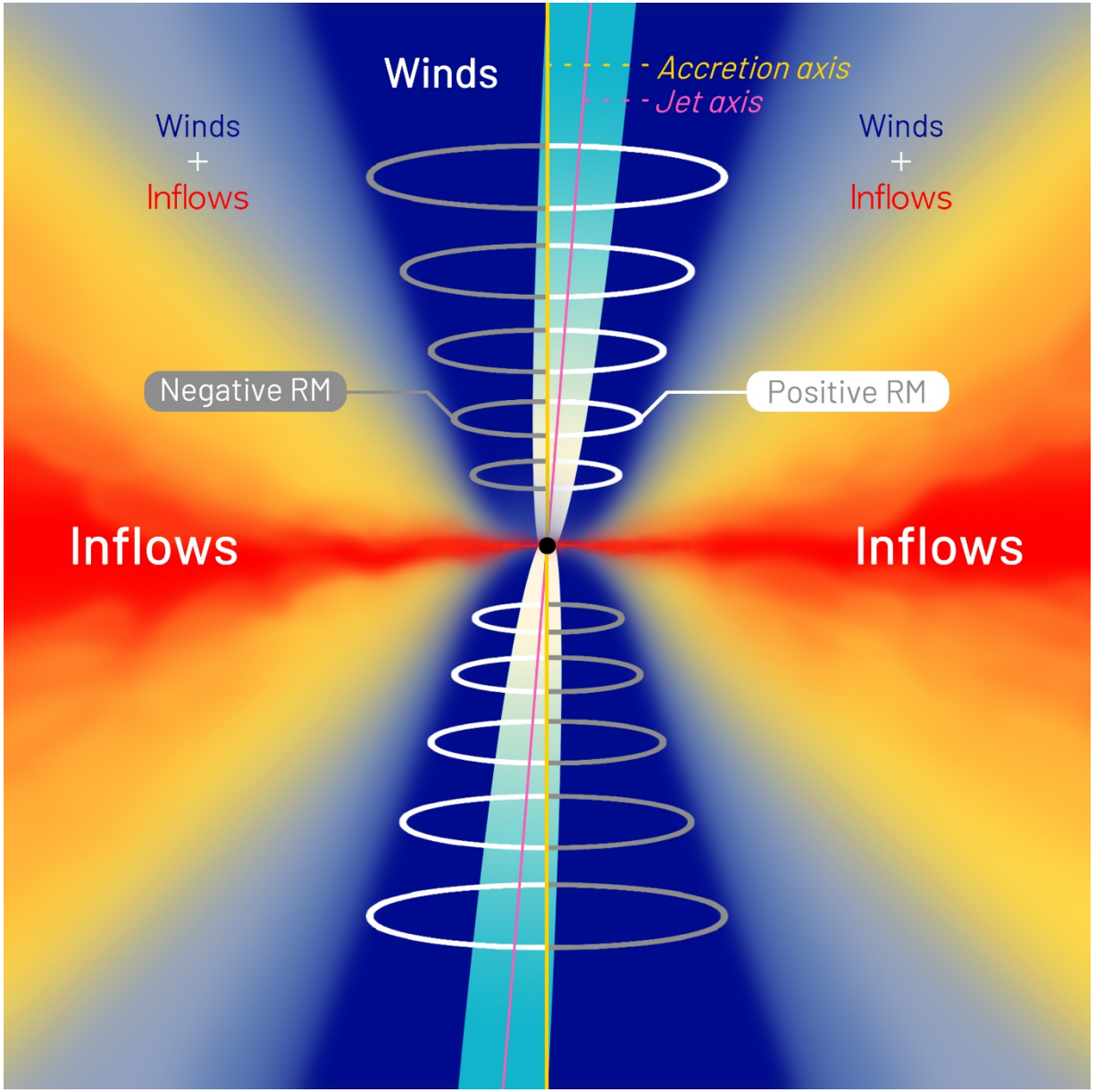

A mis-alignment between
the jet axis and the accretion axis

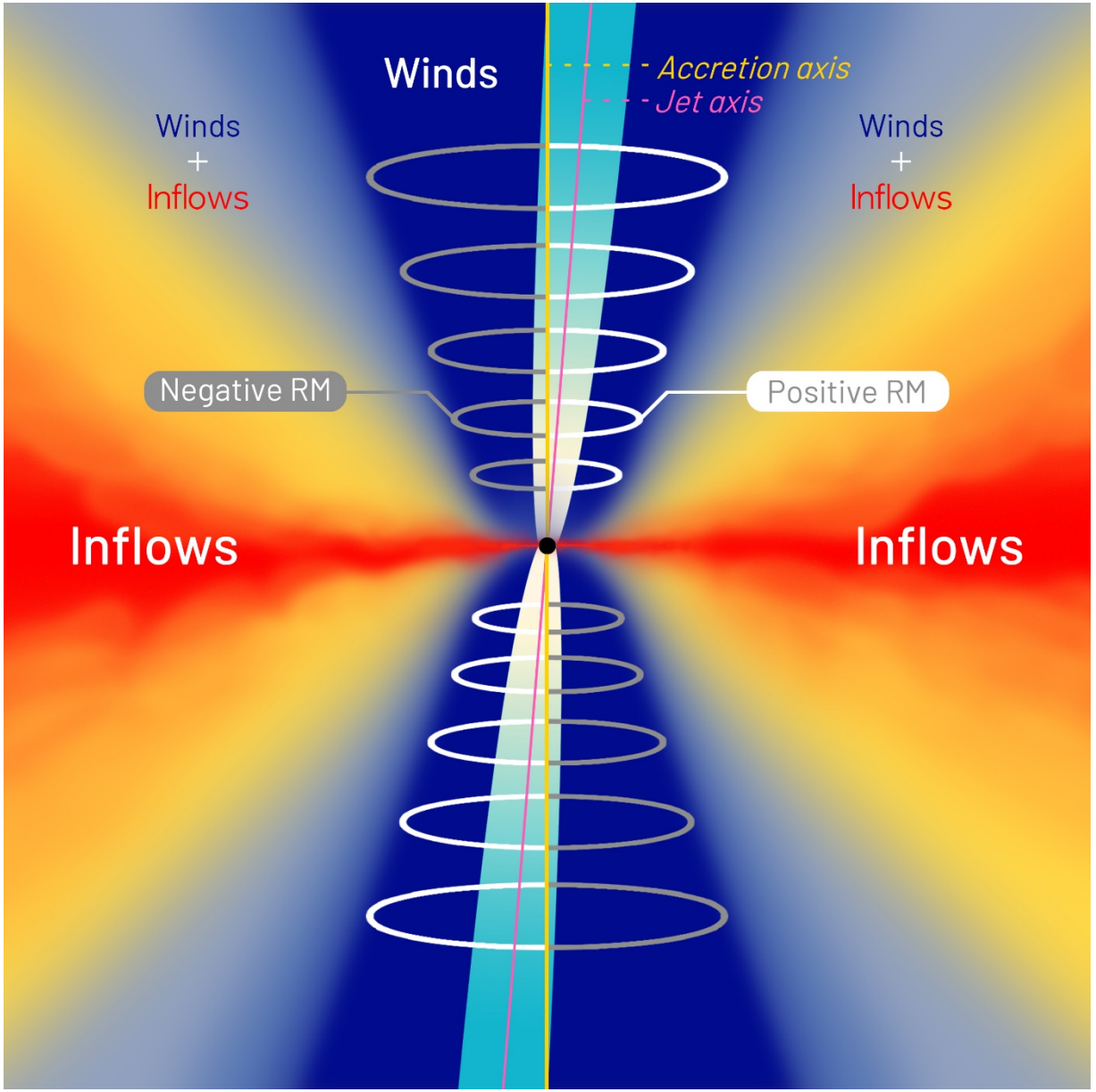

Backup Slides

$$
\begin{aligned}
\dot{M}(R) &= 4\pi\rho RH|v| \\
\dot{M}_o(R) &= 4\pi\rho_o RH|v| = \text{const.} \\
\dot{M}_{\text{in}}(R) &= 4\pi\rho RH|v| \propto R^s \\
\rho &= \rho_o R^s \propto R^{-1.5+s}
\end{aligned}
$$

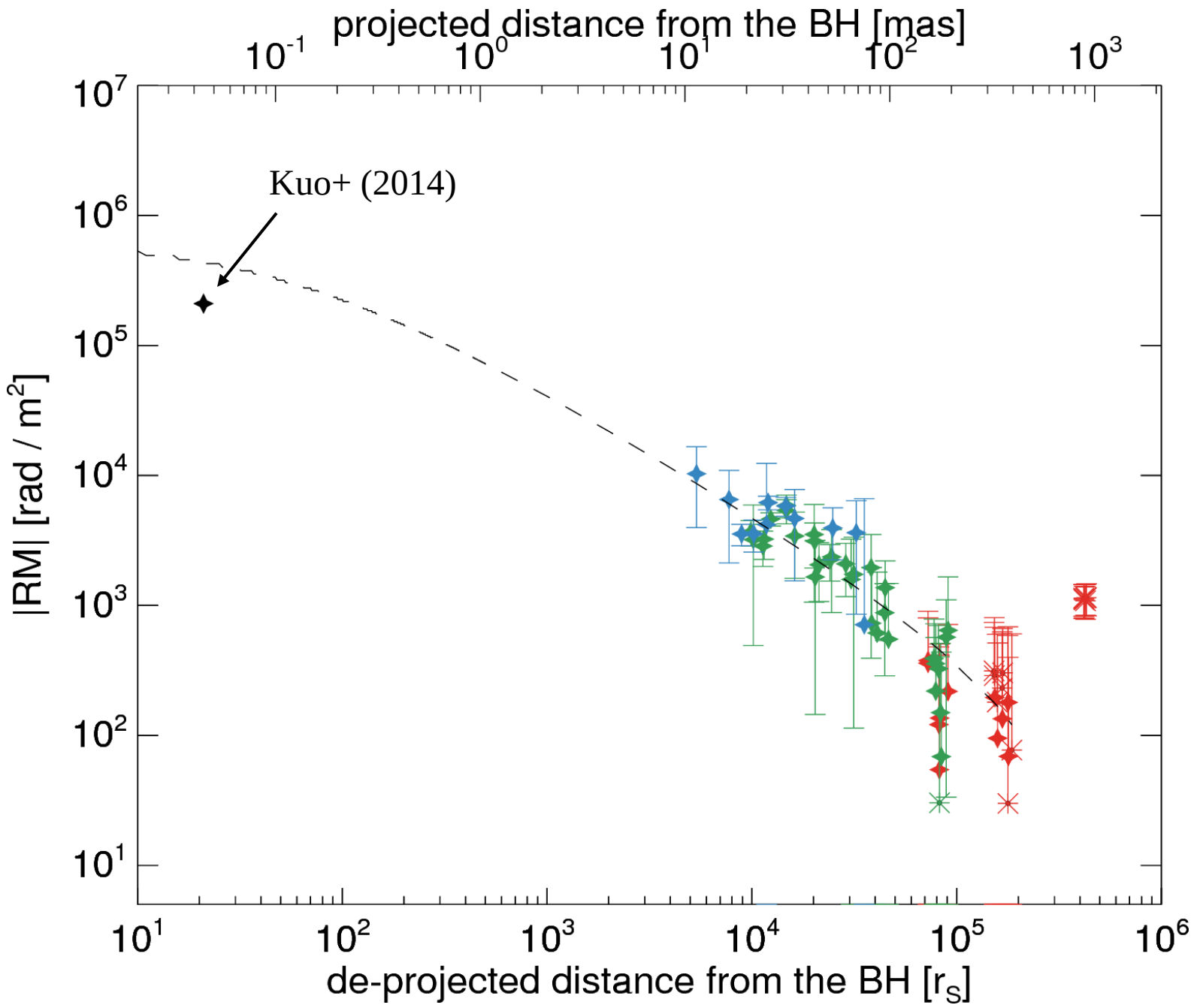
projected distance from the BH [mas]
10^-1
10^0
10^1
10^2
10^3
Kuo+ (2014)
|RM| [rad / m^2]
10^7
10^6
10^5
10^4
10^3
10^2
10^1
10^1
10^2
10^3
10^4
10^5
10^6
de-projected distance from the BH [r_S]

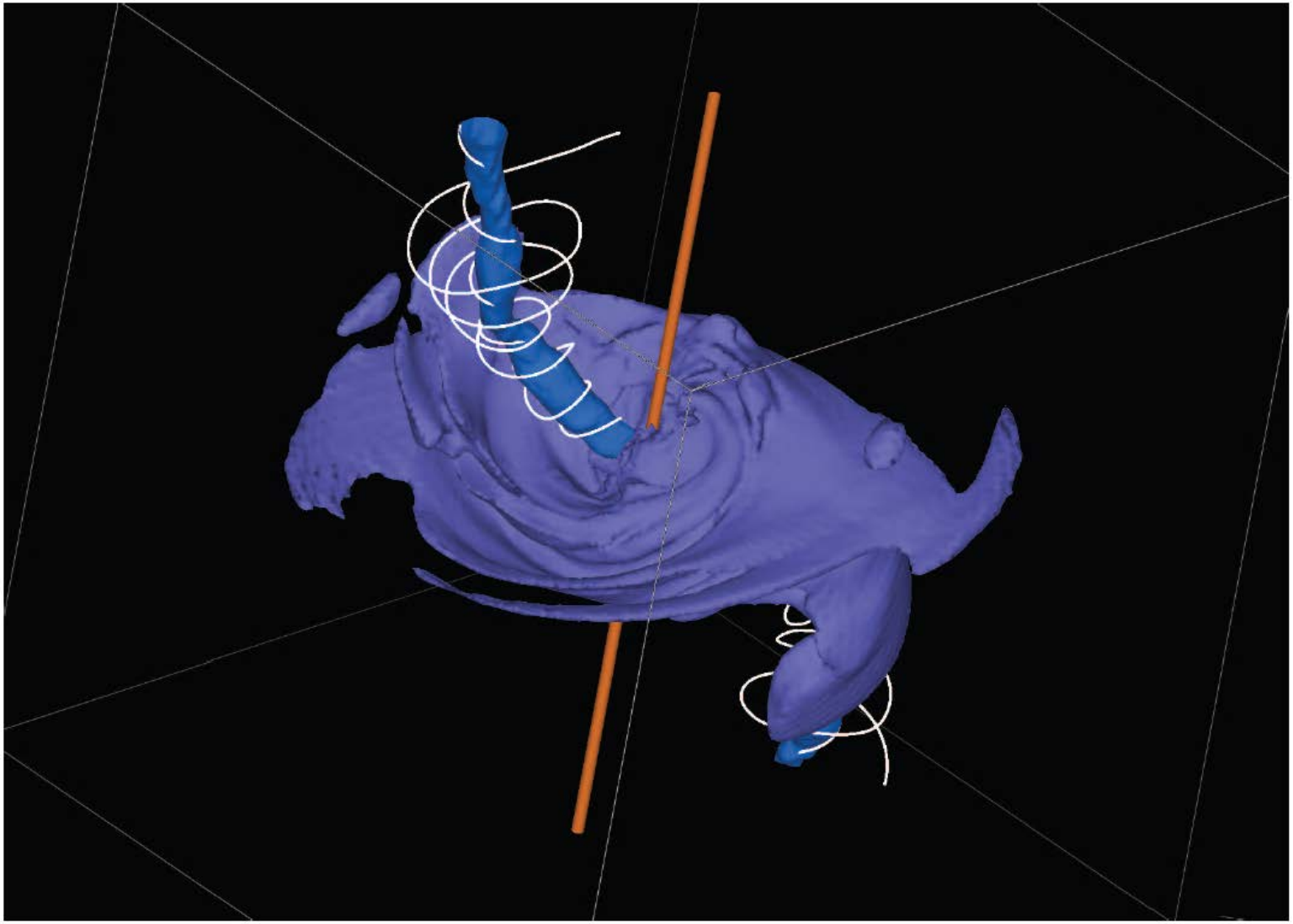

McKinney et al. (2013)

Although the BH's present angular momentum axis is set by the history of plasma accretion and mergers with other BHs, the gas being currently supplied to the BH can have an arbitrarily different angular momentum axis.
→ 'magneto-spin alignment' of the jet axis and the accretion axis with the BH spin axis by strong magnetic fields near the BH.

Model name	BH j	Disk H/R	Initial tilt	Disk tilt $r = 4r_g$	Jet tilt $r = 4r_g$	Disk tilt $r = 30r_g$	Jet tilt $r = 30r_g$
A0.94BfN40	0.9375	0.6	0	0	0	0	0
A0.94BfN40T0.35	0.9375	0.6	0.35	0.0	0.0	0.2	0.2
A0.94BfN40T0.7	0.9375	0.6	0.70	0.0	0.0	0.4	0.3
A0.94BfN40T1.5708	0.9375	0.6	1.5708	0.0	0.1	0.5	0.7
A-0.9N100	−0.9	0.3	0	0	0	0	0
A-0.9N100T0.15	−0.9	0.3	0.15	0.1	0.1	0.1	0.2
A-0.9N100T0.3	−0.9	0.3	0.30	0.2	0.2	0.2	0.2
A-0.9N100T0.6	−0.9	0.3	0.60	0.2	0.3	0.4	0.3
A-0.9N100T1.5708	−0.9	0.3	1.5708	0.2	0.4	0.9	0.8
A0.9N100	0.9	0.3	0	0	0	0	0
A0.9N100T0.15	0.9	0.3	0.15	0.0	0.0	0.1	0.1
A0.9N100T0.3	0.9	0.3	0.30	0.1	0.1	0.2	0.2
A0.9N100T0.6	0.9	0.3	0.60	0.1	0.1	0.3	0.3
A0.9N100T1.5708	0.9	0.3	1.5708	0.2	0.3	0.7	0.6
A0.9N100	0.99	0.3	0	0	0	0	0
A0.99N100T0.15	0.99	0.3	0.15	0.0	0.1	0.1	0.1
A0.99N100T0.3	0.99	0.3	0.30	0.1	0.1	0.2	0.2
A0.99N100T0.6	0.99	0.3	0.60	0.1	0.1	0.3	0.4
A0.99N100T1.5708	0.99	0.3	1.5708	0.1	0.1	0.6	0.6

A mis-alignment between the jet and the accretion axis by ~0.1 rad (~6 deg) is very common even when the ‘magneto-spin alignment’ takes place.

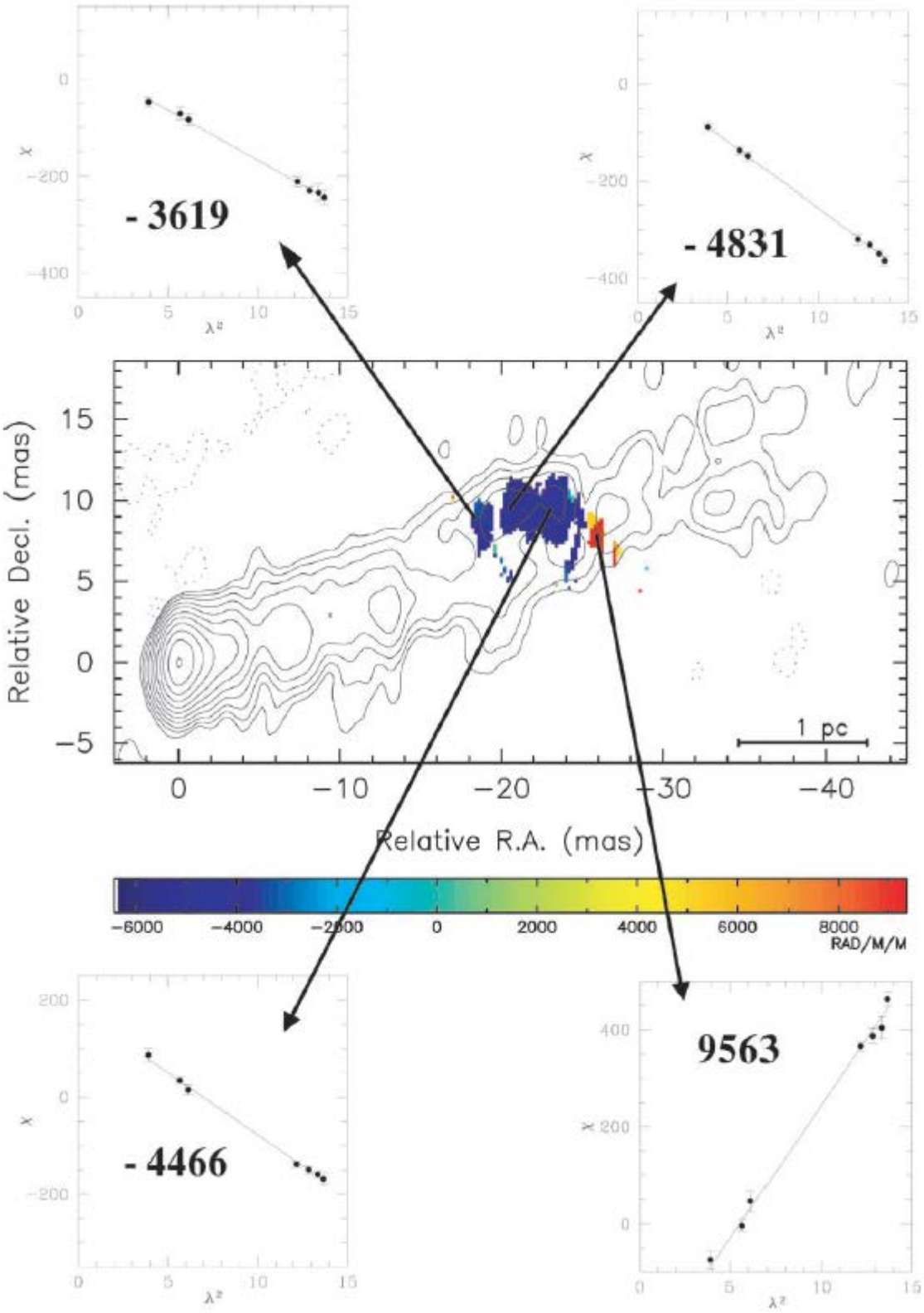

The positive RM patch is a transient? Very small area and not detected in other epochs.

Zavala & Taylor (2002)

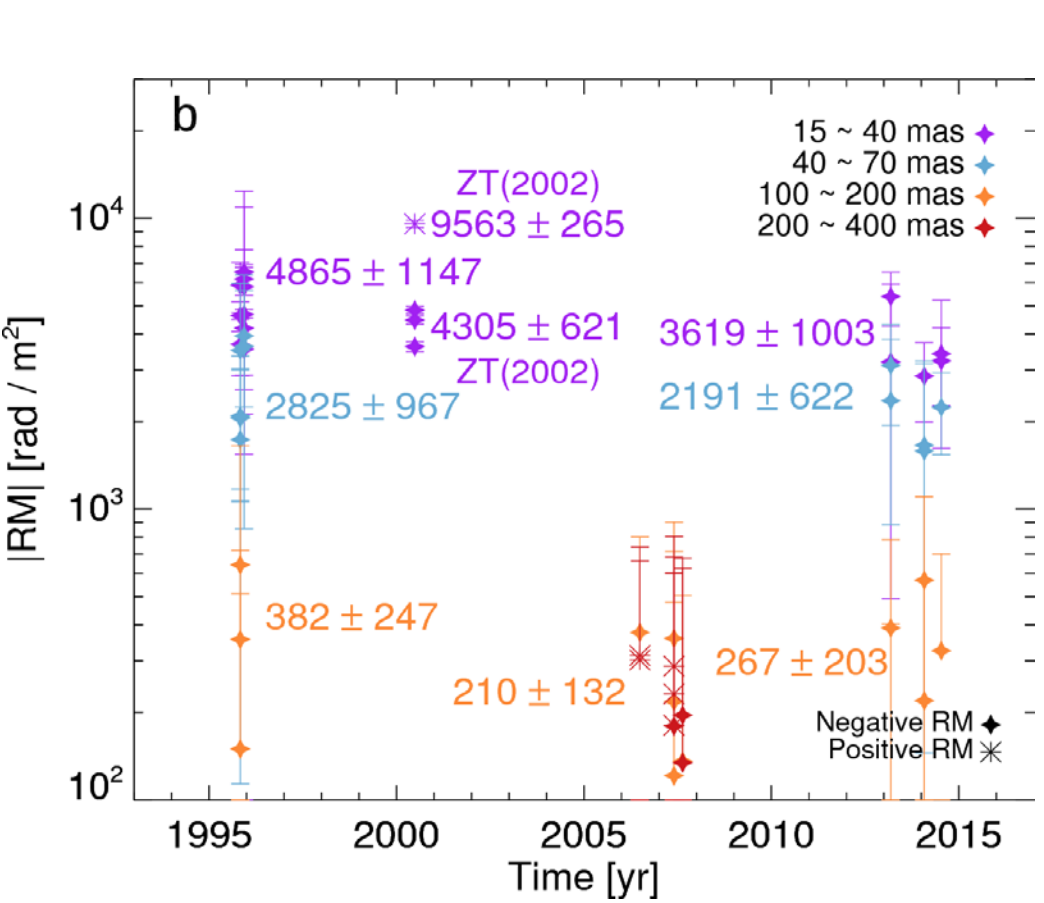
b
15 ~ 40 mas
40 ~ 70 mas
100 ~ 200 mas
200 ~ 400 mas
ZT(2002)
9563 ± 265
4865 ± 1147
4305 ± 621
ZT(2002)
2825 ± 967
3619 ± 1003
2191 ± 622
382 ± 247
210 ± 132
267 ± 203
Negative RM
Positive RM
|RM| [rad / m²]
Time [yr]

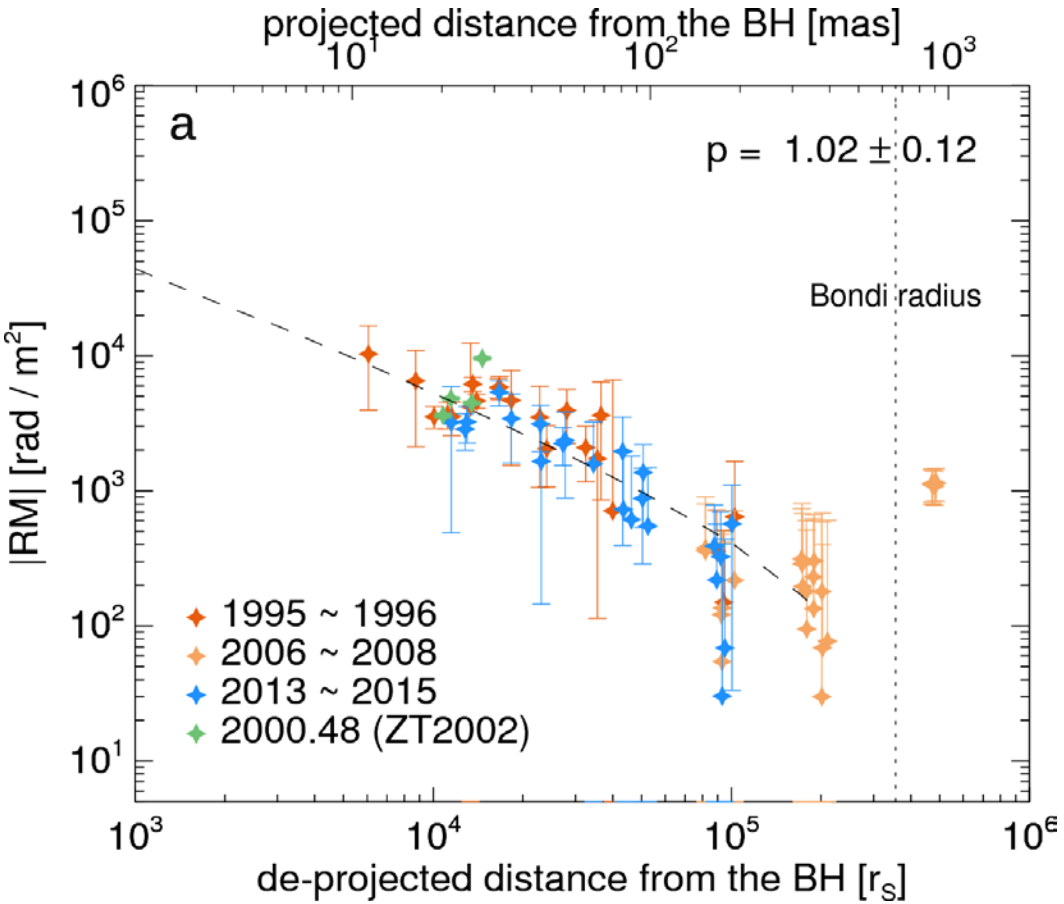
projected distance from the BH [mas]
a
p = 1.02 ± 0.12
Bondi radius
1995 ~ 1996
2006 ~ 2008
2013 ~ 2015
2000.48 (ZT2002)
|RM| [rad / m²]
de-projected distance from the BH [r_S]

Observations of density profile of LLAGNs within Bondi radius

$$\dot{M}(r) \propto r^{s} \qquad \rho(r) \propto r^{-p} \qquad p = 1.5 - s$$

Sgr A*

– $p \sim 0.9$ and $s \sim 0.6$
from X-ray spectrum modeling, albeit with large uncertainty
(Baganoff et al. 2003)

– $p \sim 1$ and $s \sim 0.3$
from SED modeling with ADAF model
(Yuan et al. 2003)

– $p \sim 0.5$ and $s \sim 1$
from fitting of Iron $K\alpha$ line
(Wang et al. 2013)

NGC 3115

– $p \sim 1$
from 'spatially resolved' Chandra observation near the Bondi radius but flattens to $p \sim 0.62$ more inside (down to ~ 0.1 Bondi radius.
(Wong et al. 2011, 2014)

Our result is in good agreement with observations of other LLAGNs.

Density profile near the Bondi radius from X-ray observations

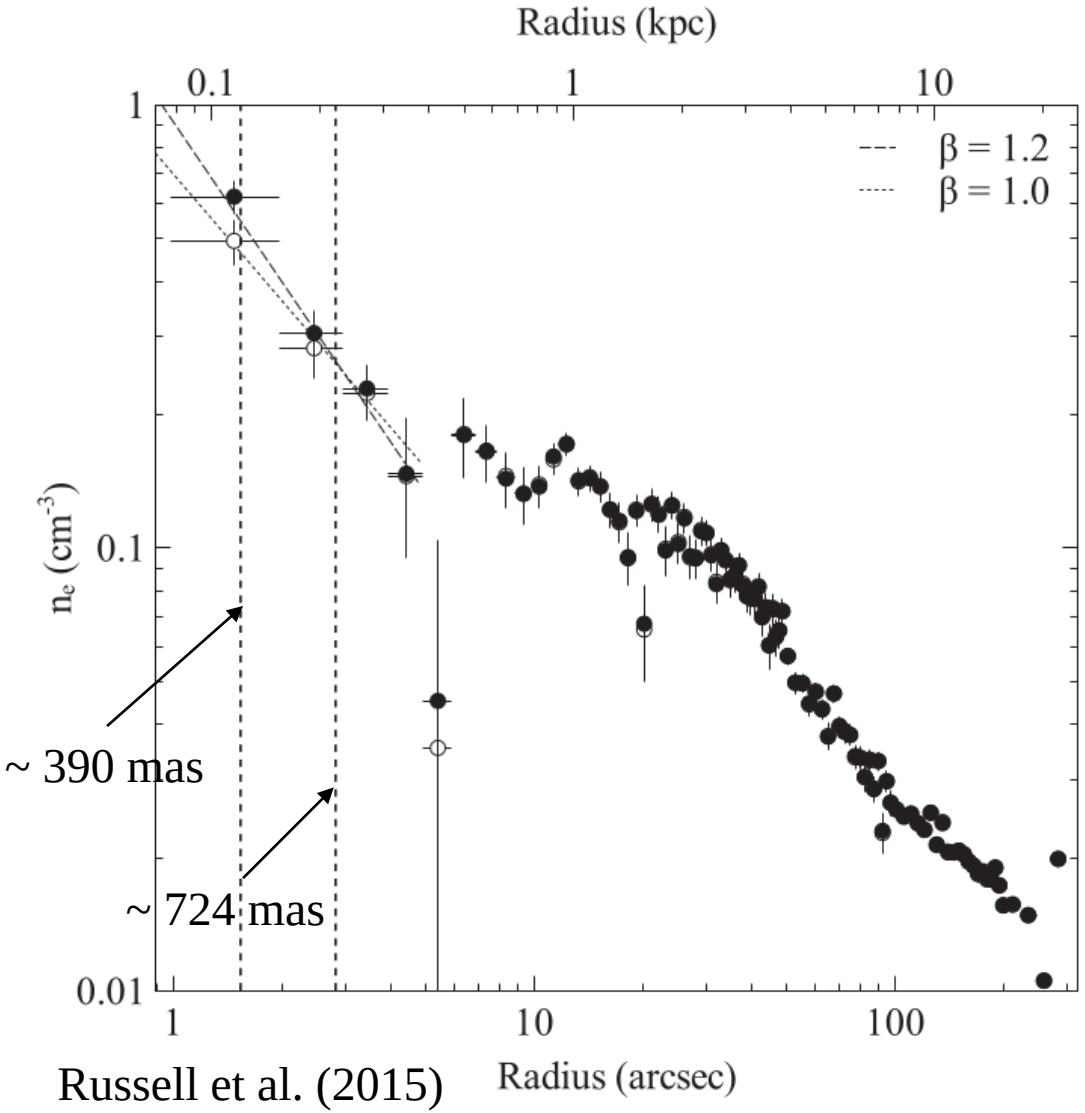

Russell et al. (2015)

$p \sim 1$ is observed inside the Bondi radius from Chandra X-ray observation
→ consistent with our results at smaller radius

X-ray observations of LLAGNs could resolve ~0.1 Bondi radius scale. However, we were able to constrain the density profile down to ~0.01 Bondi radius with VLBI for the first time.

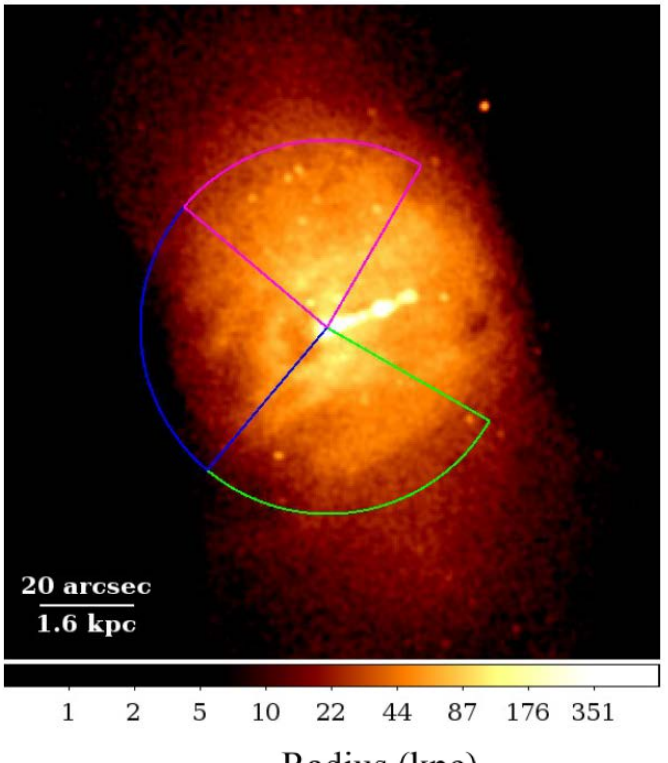

Russell et al. (2018)

External jet confinement

Porth & Komissarov (2015)

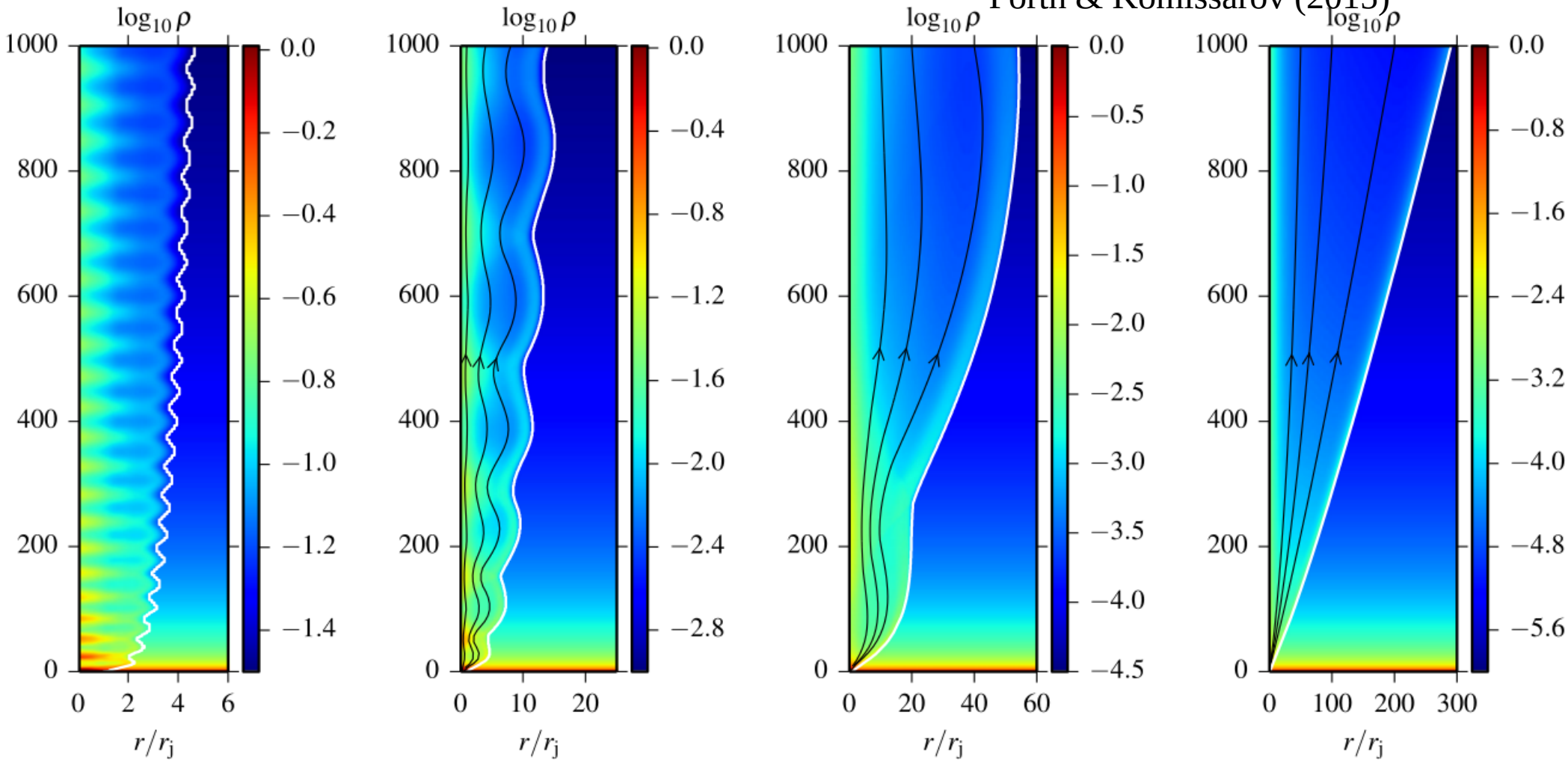

parabolic

quasi-conical

It looks okay for \kappa = 1.5 to have a parabolic jet shape.

Plasma \beta

$n_{\rm out} = 0.3{\rm cm}^{-3}$ $T_{\rm out} = 0.9{\rm KeV}$ (when M = 6.6e9 Msun, Russell et al. 2015).

$\rightarrow P_{\rm gas,out} = 4.32 \times 10^{-10}{\rm dyn/cm}^2$ (at the Bondi radius)

$B_{\rm out} = 2.6\mu{\rm G}$ (we estimated)

$\rightarrow P_{\rm mag,out} = B^2/8\pi = 2.7 \times 10^{-13}{\rm dyn/cm}^2$

$\rightarrow \beta_{\rm out} = P_{\rm gas,out}/P_{\rm mag,out} = 1631$

$P_{\rm gas} \propto \rho^{\gamma} \propto \rho^{5/3} \propto r^{-1.67}$ (when $\rho \propto r^{-1}$)

$P_{\rm mag} \propto r^{-2}$ (assuming toroidal-dominated)

$\beta = P_{\rm gas}/P_{\rm mag} \propto r^{-0.33}$

$\beta_{\rm out} \approx 68$ (when $\beta_{r=1r_s} \approx 1$)

→ seems to be much smaller than the estimated \beta_out.

→ There is an indication that we are looking at the mixture of inflows (high \beta) and outflows (low \beta).

Discussion : Sudden increase of RM at HST-1

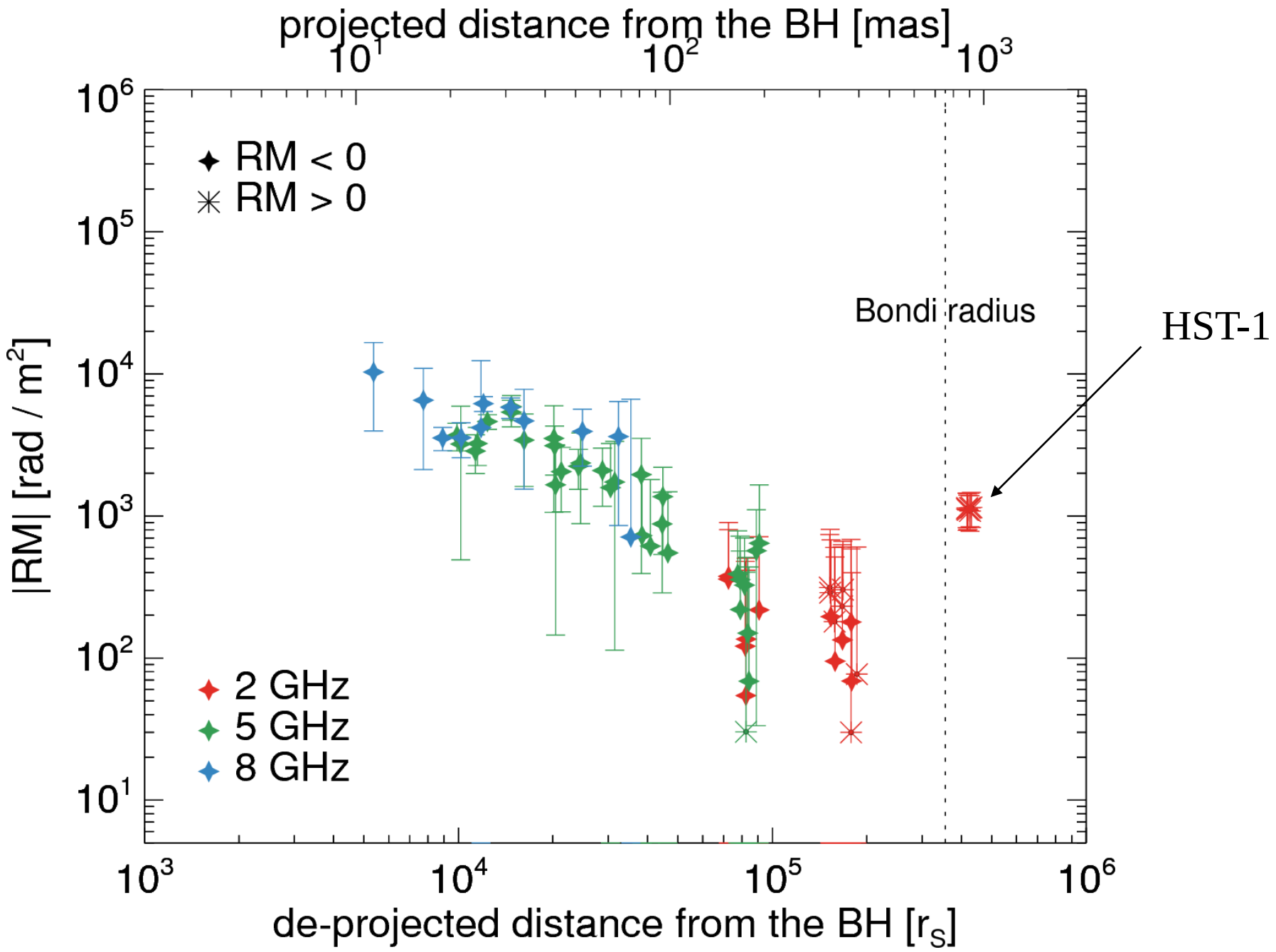

Discussion : Sudden increase of RM at HST-1

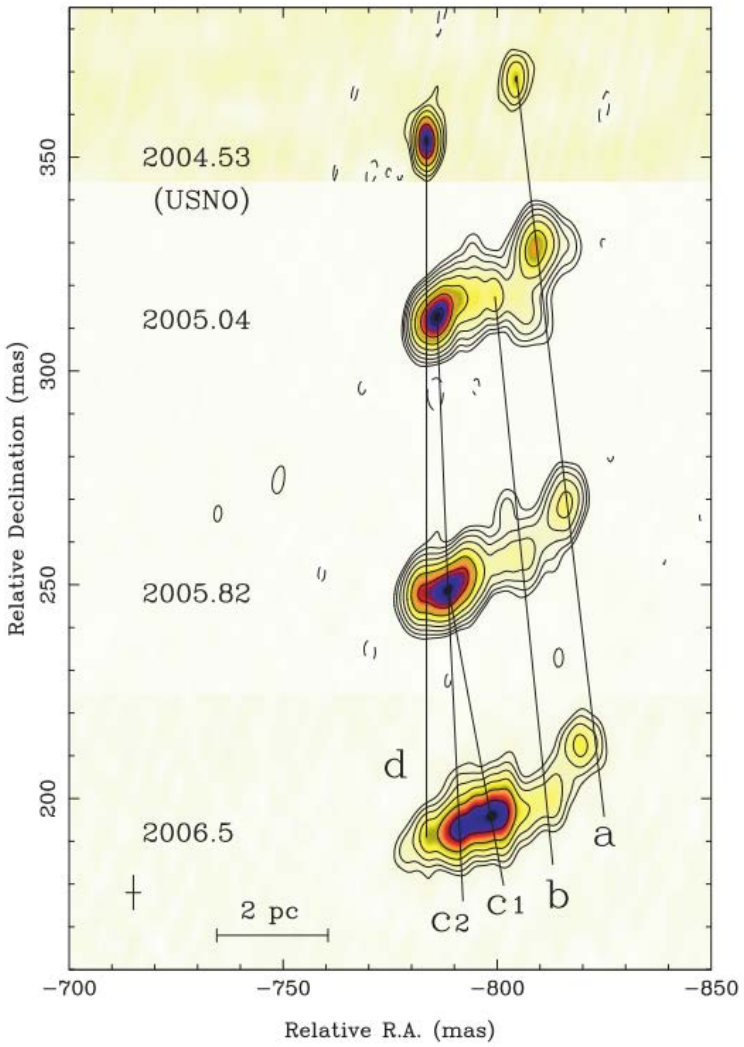

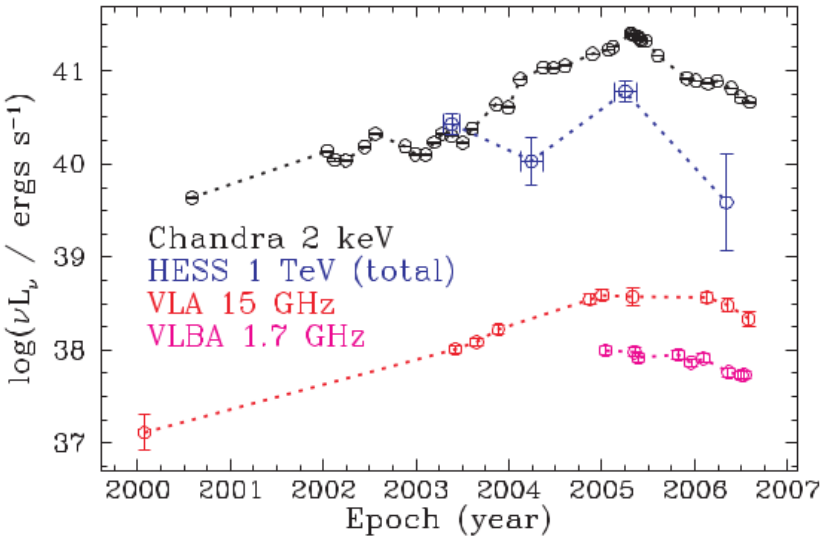

Cheung+ 07

Levinson & Globus 2017

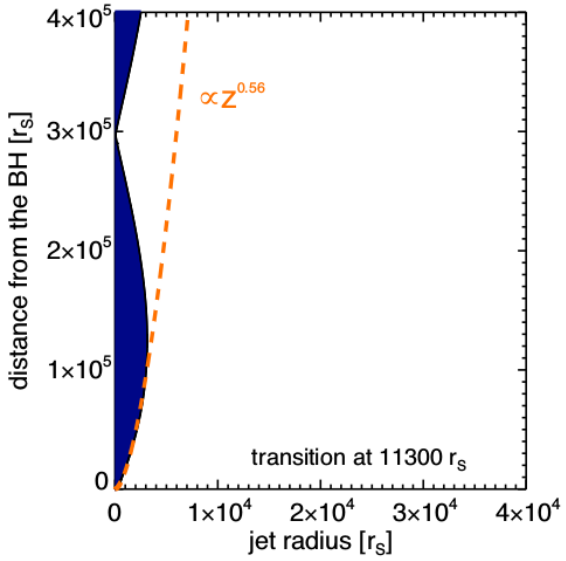

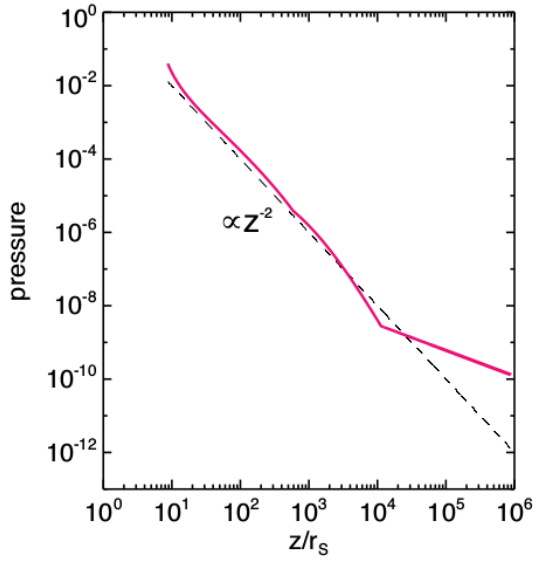

− HST-1 has shown a quasi-stationary component from which superluminal components are emerging and was identified as the site of high-energy flare.

− It has been modeled with a recollimation shock or jet focusing due to the change in pressure profile of external medium.

An enhancement of RM at HST-1 due to a recollimation shock?

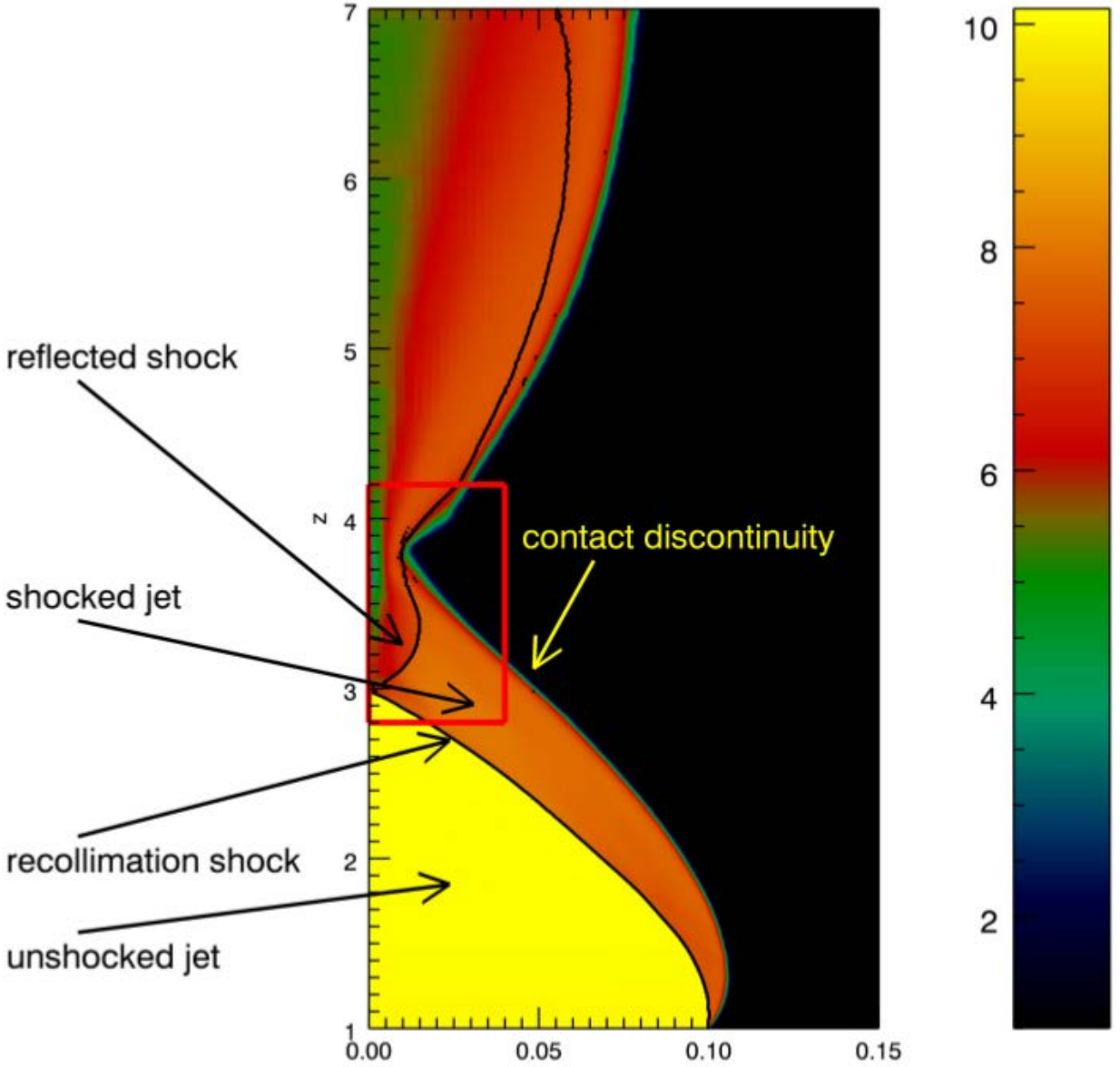

Bodo & Tavecchio (2018)

An enhancement of RM at HST-1 due to a recollimation shock?

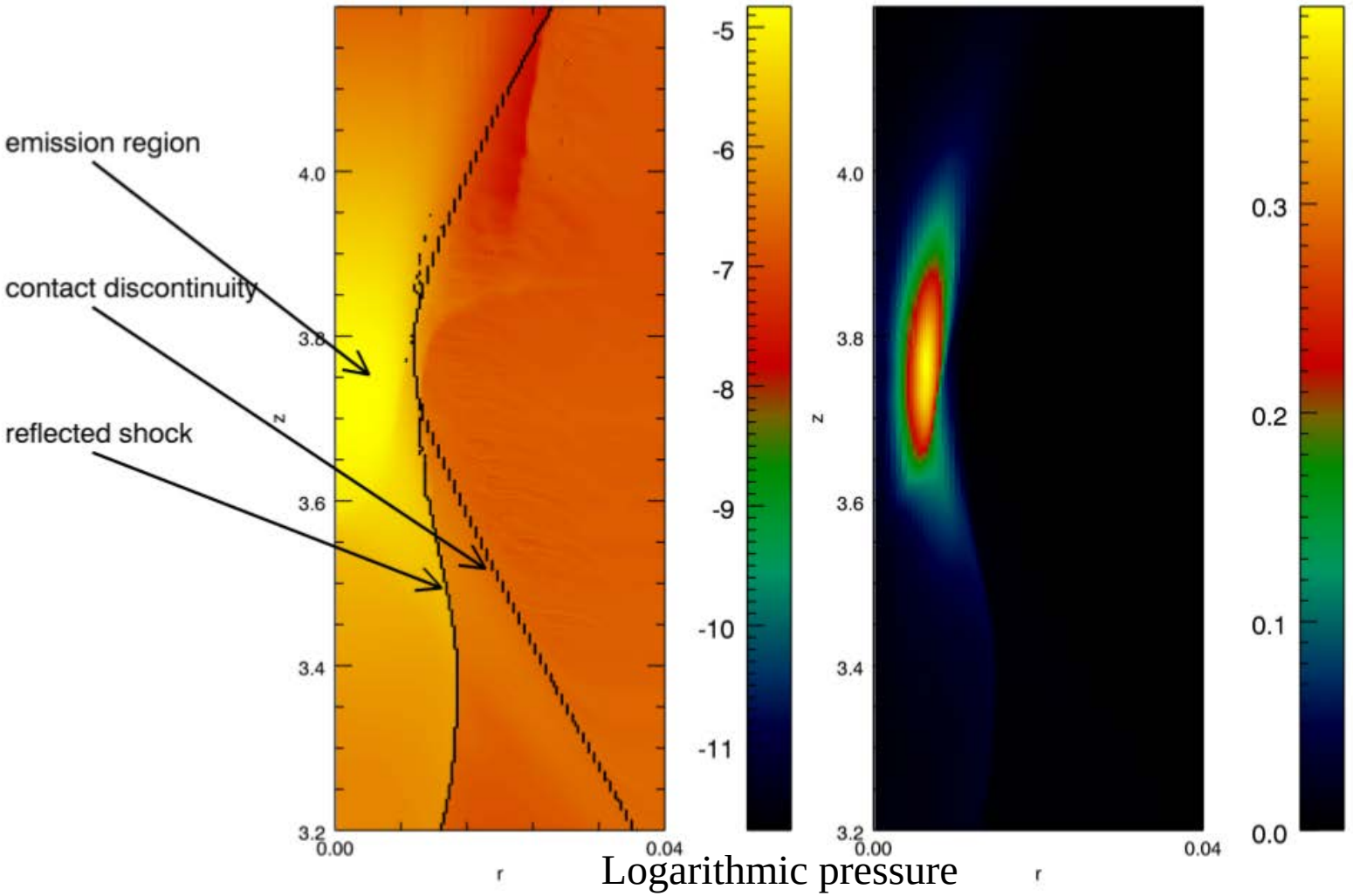

(IC) Emissivity distribution

Logarithmic pressure distribution

Bodo & Tavecchio (2018)

Emission region is concentrated near the jet axis where the pressure is highest. The emission would pass through the ‘shocked region’ surrounding the emission region.
→ enhanced electron density & strong magnetic fields (order of mG).
→ enhanced RM

Equilibrium
(un-perturbed)

t = 0.9

t = 5.0

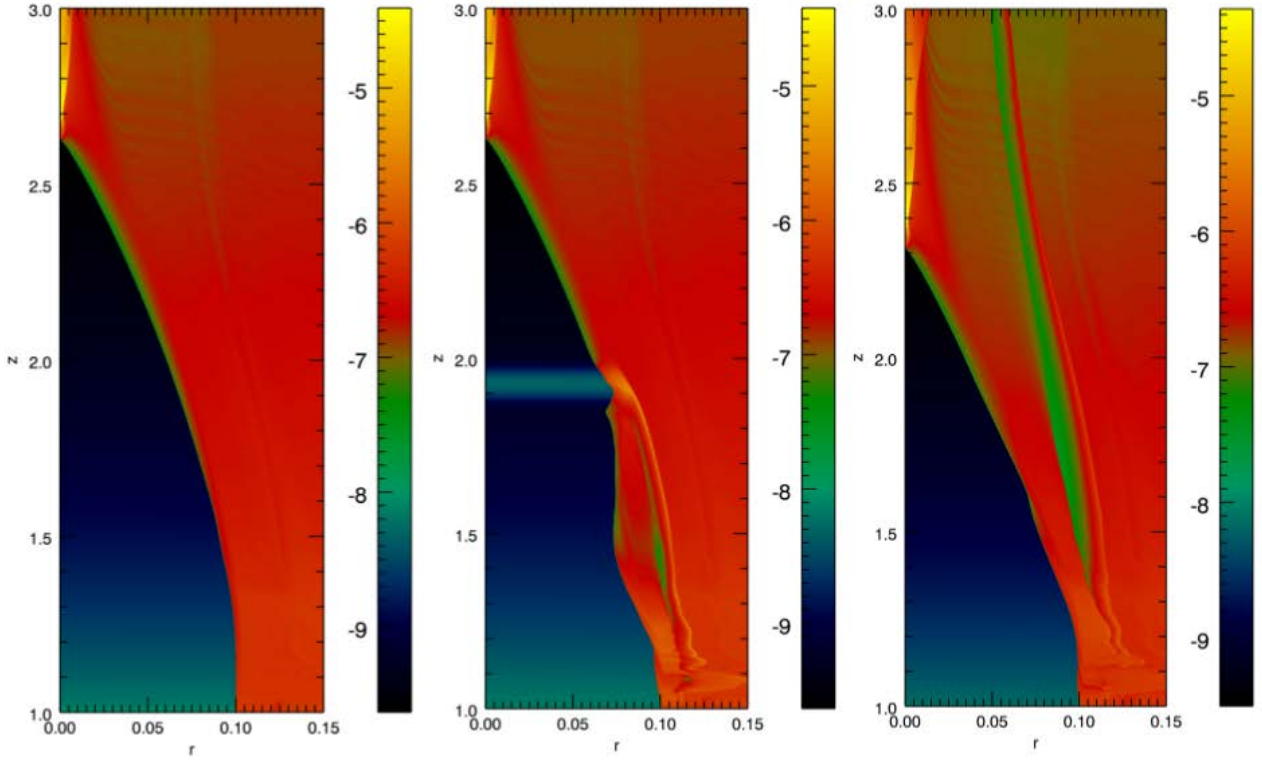

Logarithmic
pressure distribution

Bodo & Tavecchio (2018)

Density perturbatio
n injection

Emissivity as a fun
ction of z

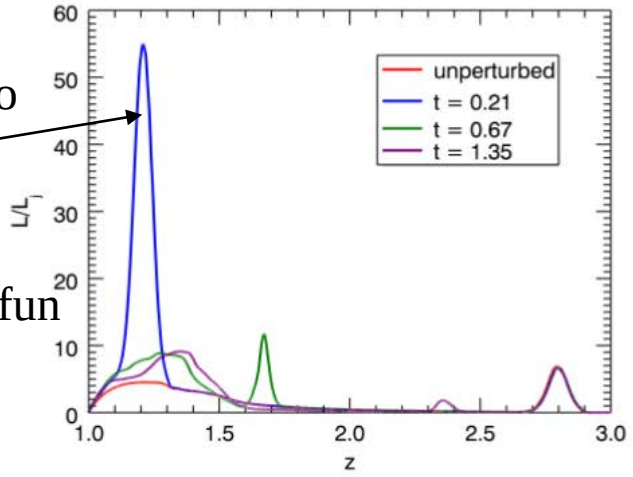

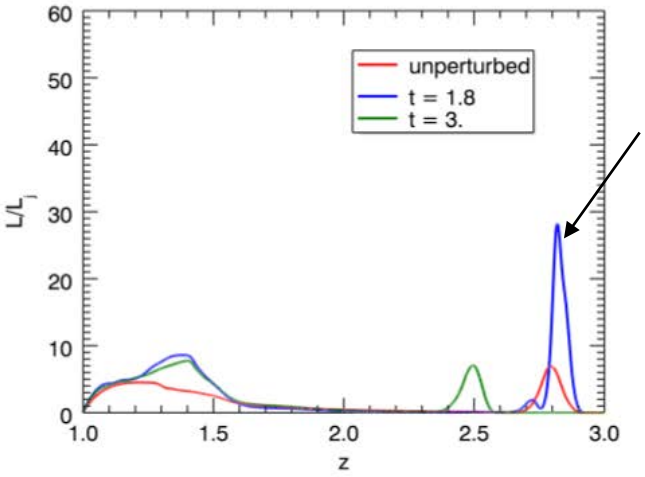

Arrived at the recol
limation nozzle at t
= 1.8
→ substantial lumi
nosity increase

But, a global structure of the recollimation shock seems to be intact. → stable RM while there is a flare in HST-1?

Discussion : Accretion rate

$$\dot{M}(r) = \dot{M}_{\rm ADAF}\left(\frac{r}{r_{\rm out}}\right)^{0.5}$$

Narayan & Fabian 11

$$\dot{M}_{\rm ADAF} \approx 0.3\dot{M}_{\rm Bondi}$$

When α ~ 0.1,
a reasonable choice for ADAF.

– Bondi accretion rate of M87 is ~ 0.1 $M_{\odot}{\rm yr}^{-1}$ for M = $6.6 \times 10^{9} M_{\odot}$ (Russell+15).
– Accretion rate within $10r_S$ is almost constant according to numerical simulations (e.g., Yuan et al. 2012).

$$\dot{M} \approx 0.3 \times 0.1 M_{\odot}{\rm yr}^{-1}\left(\frac{10{\rm r_S}}{3.6\times10^{5}{\rm r_S}}\right)^{0.5} \approx 1.58\times10^{-4}{\rm M_{\odot}yr^{-1}}$$

→ accretion rate is smaller than the upper limit, $9.2 \times 10^{-4} M_{\odot}{\rm yr}^{-1}$ obtained in Kuo et al. (2014).

– Accretion rest mass energy is

$$\dot{M}_{\rm acc}c^2 = 8.97\times10^{42}{\rm erg/s}$$

Discussion : Accretion rate and Jet production efficiency

$$\dot{M}_{\rm acc}c^2 = 8.97 \times 10^{42}{\rm erg/s}$$

– Jet power of M87 estimated from X-ray cavity observations is

$$P_{\rm Jet} \approx 8 \times 10^{42}{\rm erg/s}$$ Russell+ 15

– The jet production efficiency is defined as

$$\eta \equiv P_{\rm Jet}/\dot{M}_{\rm acc}c^2$$

$$\boxed{\approx 89\%}$$

– The obtained jet production efficiency is 89 %, which indicates that almost all the rest mass energy of inflows are converted into the jet power. Remind that the maximum gravitational binding energy released for the standard thin disk is around 40 %.

→ There is additional source of energy : Spin energy of the SMBH!
(The Blandford - Znajek process)

Discussion : Accretion rate and Jet production efficiency

– Such a high jet production efficiency can be achieved only when
(i) accretion disk of M87 is in MAD (Magnetically Arrested Disk) state.
(ii) the jet is launched by BZ process.

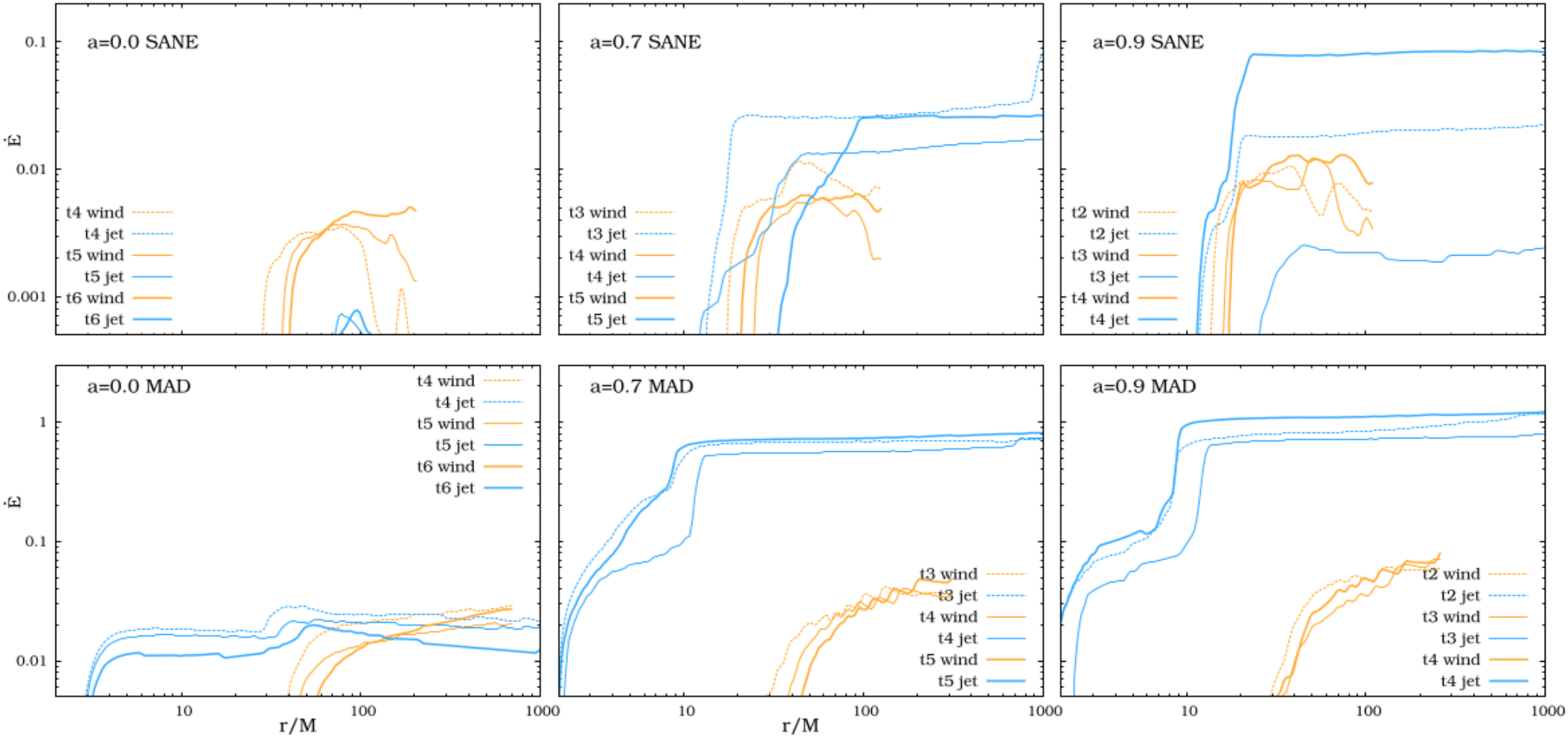

Sadowski+ 13

– If no MAD → efficiency at most 10%.
– If no BZ → efficiency at most 1% even in the MAD state.

Discussion : Accretion rate and Jet production efficiency

– Such a high jet production efficiency can be achieved only when
(i) accretion disk of M87 is in MAD (Magnetically Arrested Disk) state.
(ii) the jet is launched by BZ process.

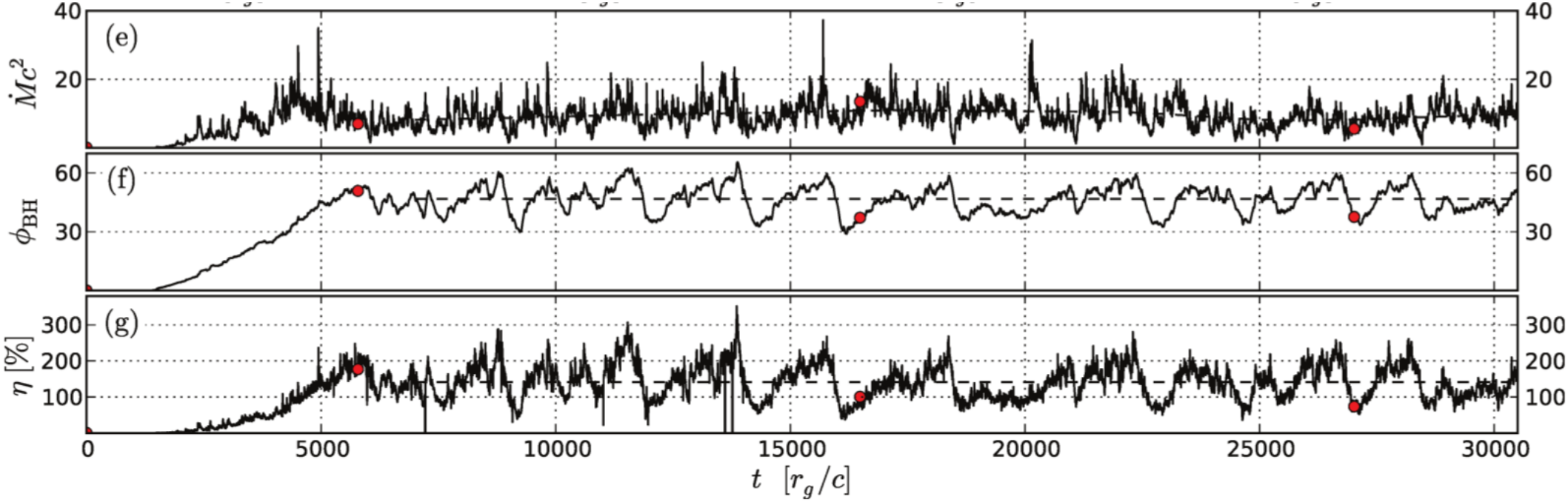

Tchekhovskoy+ 11

– With the BZ process in the MAD state, the jet production efficiency can go up to ~300 % and the observed very high jet production efficiency can be well explained.

Discussion : Accretion rate and Jet production efficiency

– We used the jet power estimated from X-ray cavity observation but this is in general regarded as a lower limit on the total mechanical energy because (i) it is likely that the lack of exposure time easily leads to miss other cavities and (ii) weak shocks and sound waves also contribute a lot.

– Other independent measurements of jet power:

1. the energy required to grow the radio halo and dividing it by the buoyancy timescale → few $\times 10^{44} \sim 10^{45}$ erg/s (Owen+. 2000, de Gasperin+12).
→ average jet power over ~10 Myr.
2. Interpreting knot A as an oblique shock within the jet → $(1\sim3) \times 10^{44}$ erg/s (Bicknell & Begelman 1996)
→ time delay between BH and knot A is $\sim 2 \times 10^3$ yr.
3. Identifying HST-1 with a recollimation shock → $\sim 10^{44}$ erg/s (Stawarz+06, Bromberg & Levinson 09).
→ time delay is ~30 years : the smallest time delay between jet power & accretion

– In general, the jet power of M87 is potentially higher than what we used for jet production efficiency estimation and $\eta \sim 89\%$ is likely lower limit.

→ How could it be possible?

Discussion : Inferred B field strength near the horizon

$$\Phi_{\rm MAD} \approx 50\, \dot{M}_{\rm BH}^{1/2} R_g c^{1/2} \qquad B_{\rm MAD} \approx \frac{\Phi_{\rm MAD}}{2\pi R_g^2} = 10^{10}\, m^{-1/2} \dot{m}_{\rm BH}^{1/2}\ {\rm G}$$

Yuan and Narayan 2014

$$m \equiv \frac{M}{{\rm M}_\odot}, \quad \dot{m} \equiv \frac{\dot{M}}{\dot{M}_{\rm Edd}} \qquad \dot{M}_{\rm Edd} \equiv 10 L_{\rm Edd}/c^2 = 1.39 \times 10^{18} (M/{\rm M}_\odot)\ {\rm g\ s^{-1}}$$

- BH mass ~ $6 \times 10^9 M_\odot$
- Eddington mass accretion rate ~ 132 $M_\odot {\rm yr}^{-1}$
- Mass accretion rate at $10 r_S$ ~ $1.6 \times 10^{-4} M_\odot {\rm yr}^{-1}$

→ $B_{\rm MAD}$ ~ 142 G

→ roughly consistent with Kino+15 limit

Table 1
Results When the EHT Region Contains the SSA-thick Region

L_j (erg s^{-1})	Allowed $B_{\rm tot}$ (G)	Allowed $\theta_{\rm thick}$ (μas)	Allowed $U_\pm/U_B$
5×10^{44}	$50 \leqslant B_{\rm tot} \leqslant 124$	$21 \leqslant \theta_{\rm thick} \leqslant 26.3$	$7.9 \times 10^{-7} \leqslant \frac{U_\pm}{U_B} \leqslant 2.3 \times 10^{-3}$

Kino+ 15

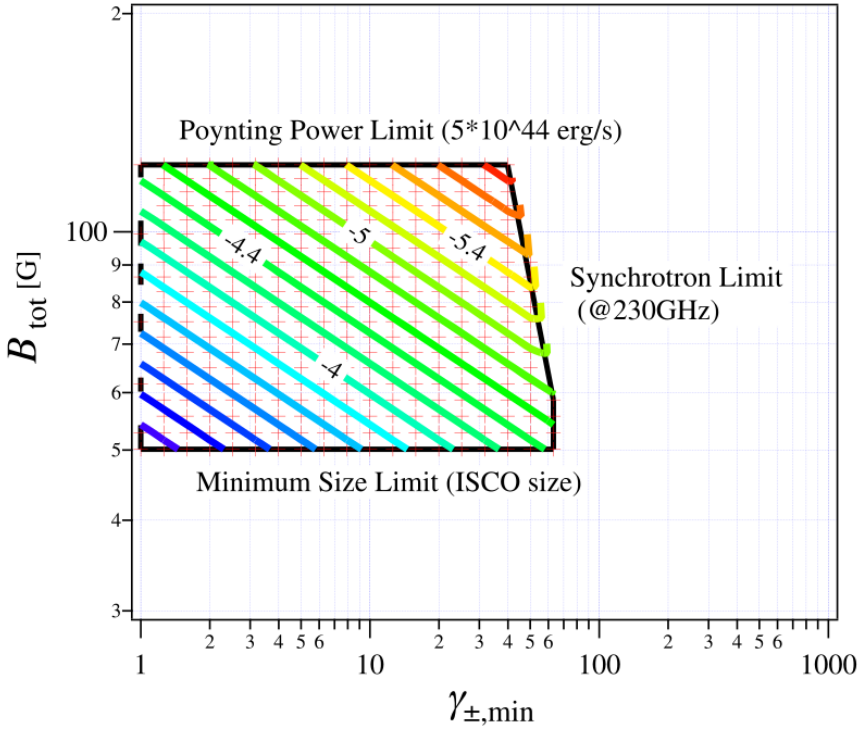

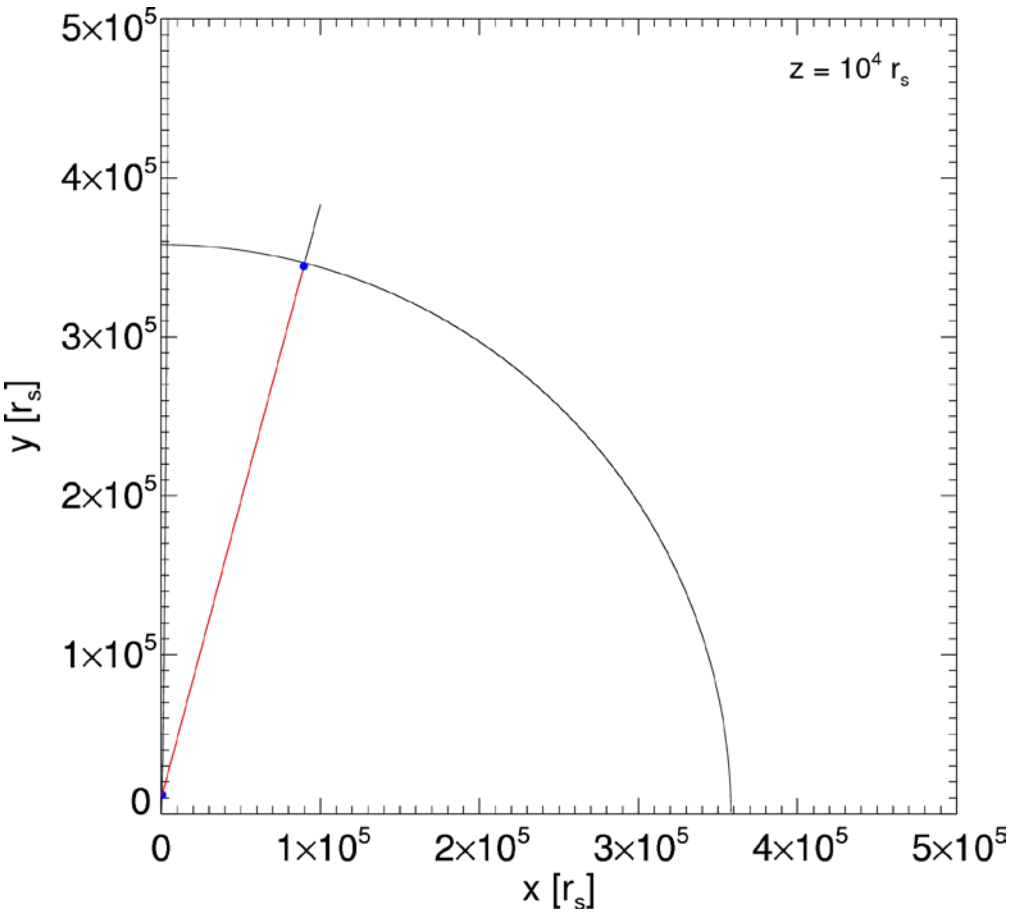

When z = 10^4 r_s

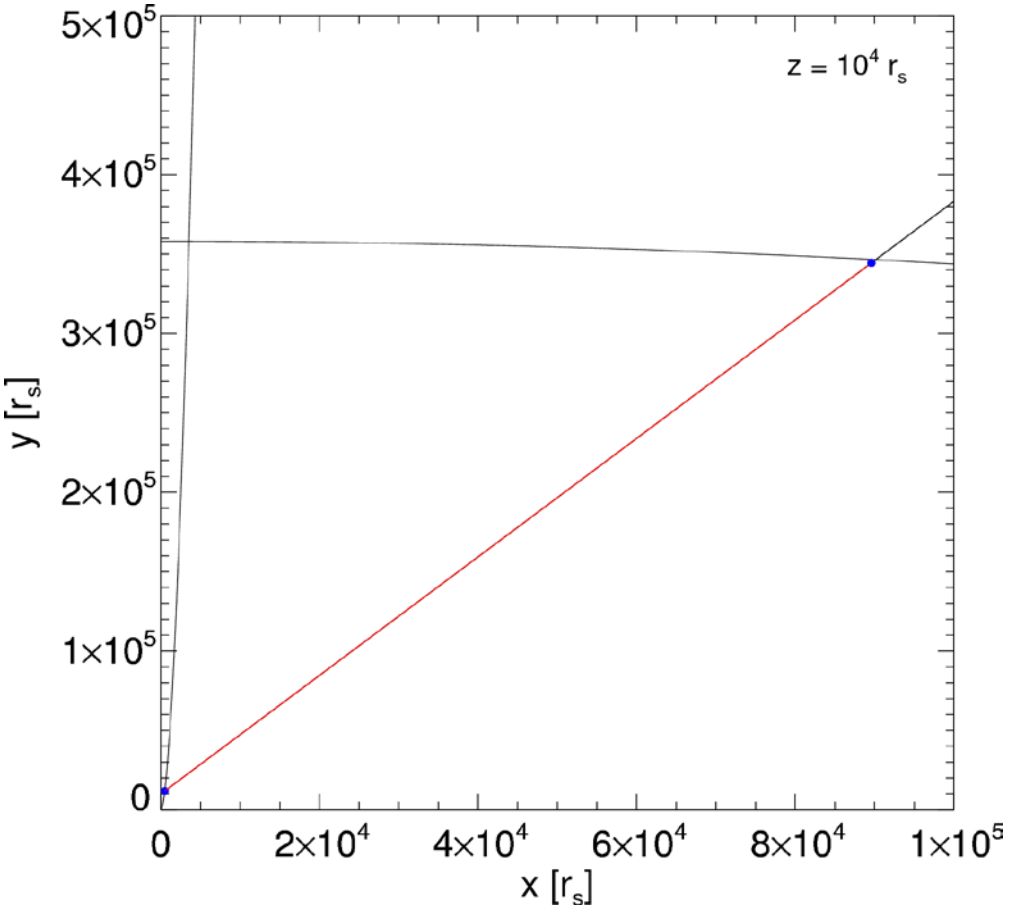

Zoom-in version

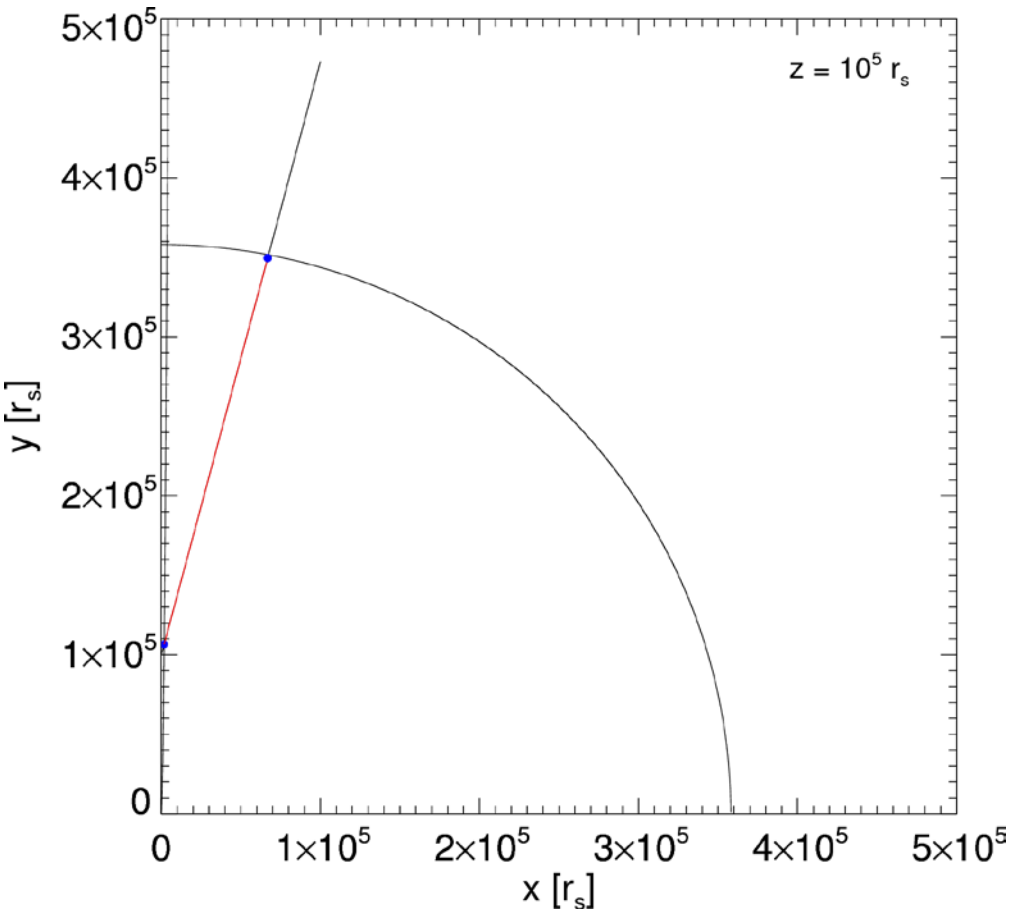

When z = 10^5 r_s

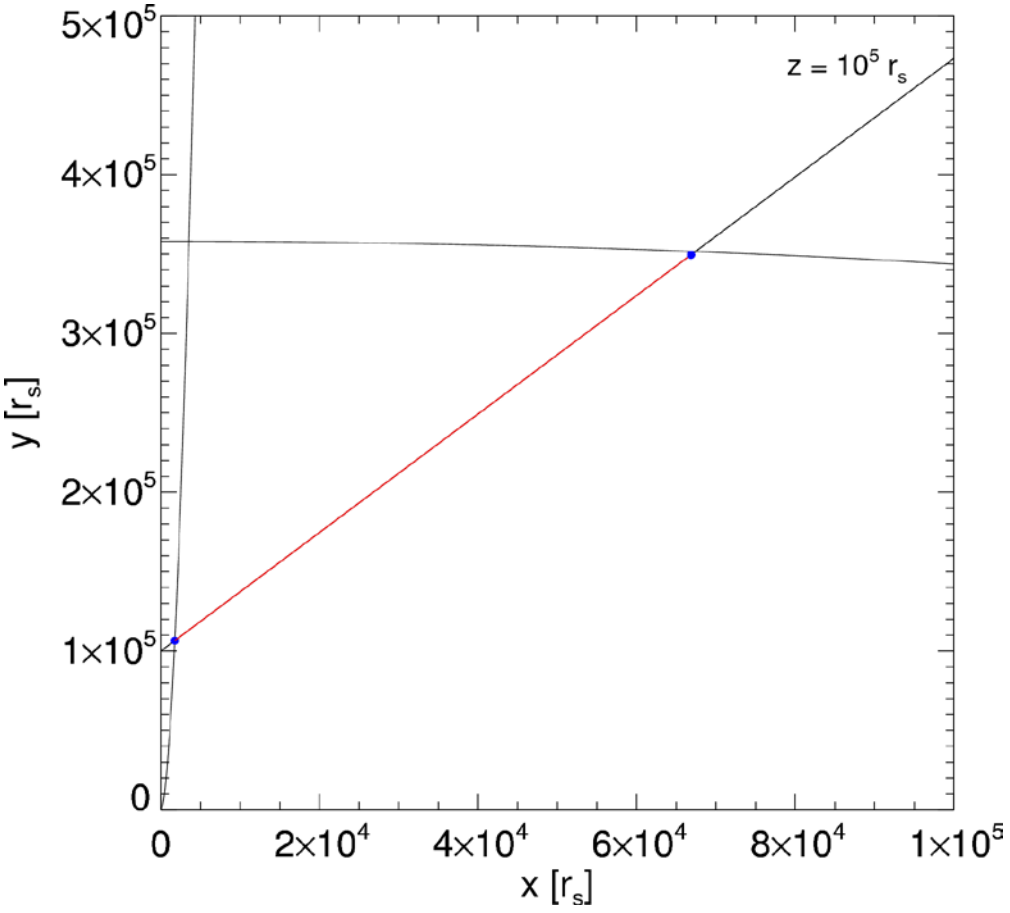

Zoom-in version

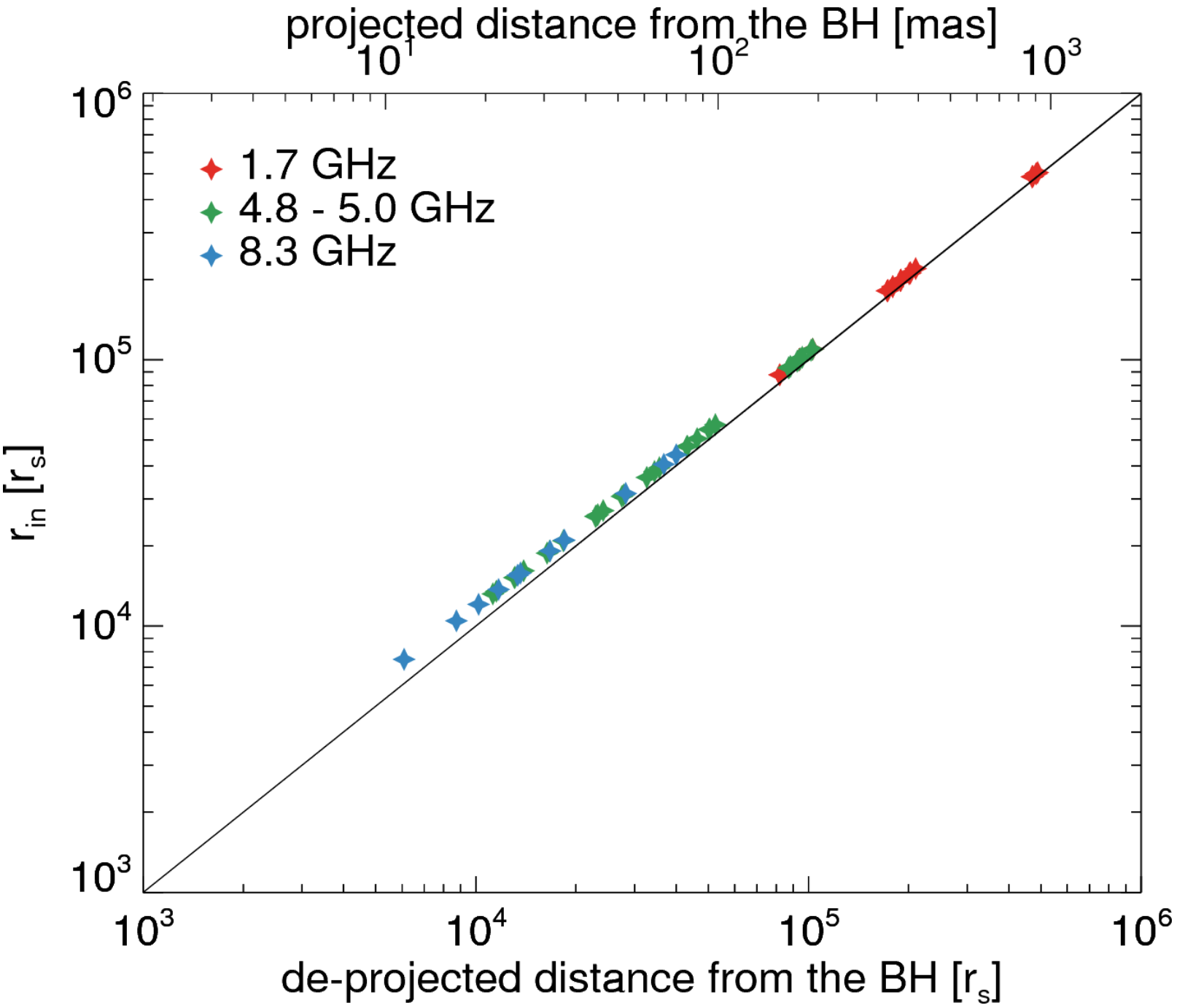

r_in versus distance

How much contribution of ‘foreground’ Faraday rotating medium?

– Negligible contribution of the ISM in our Galaxy due to the large galactic latitude b = 74.5 deg (less than ~20 rad / m^2, e.g., Taylor et al. 2009)

– Small contribution of the IGM in the Virgo Cluster (less than 30 rad / m^2, e.g., Wezgowiec et al. 2012)

– Contribution of the diffuse gas along the line of sight to the jet, e.g., backflow of the jet or extended lobe, which is different from inflows or outflows governed by the central SMBH is unclear.

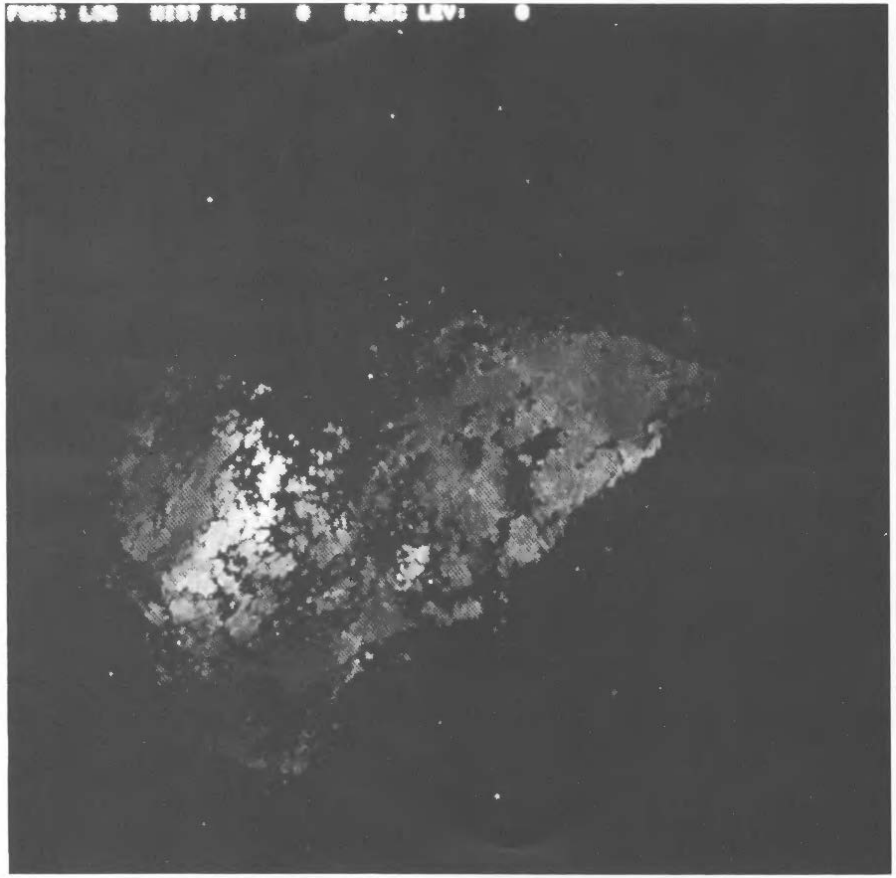

Owen et al. (1990)

FIG. 1.—Gray scale of the rotation measure map of M87. The brightest areas show rotation measure ~6000–8000 rad m^{-2}; the typical rotation measure for the western lobe, away from the jet, is ~750–1000 rad m^{-2}. The inner jet has RM ~ 200 rad m^{-2}.

How much contribution of ‘foreground’ Faraday rotating medium?

– Negligible contribution of the ISM in our Galaxy due to the large galactic latitude b = 74.5 deg (less than ~20 rad / m^2, e.g., Taylor et al. 2009)

– Small contribution of the IGM in the Virgo Cluster (less than 30 rad / m^2, e.g., Wezgowiec et al. 2012)

– Contribution of the diffuse gas along the line of sight to the jet, e.g., backflow of the jet or extended lobe, which is different from inflows or outflows governed by the central SMBH is unclear. But it seems that ~130 rad / m^2 is typical for the jet region.

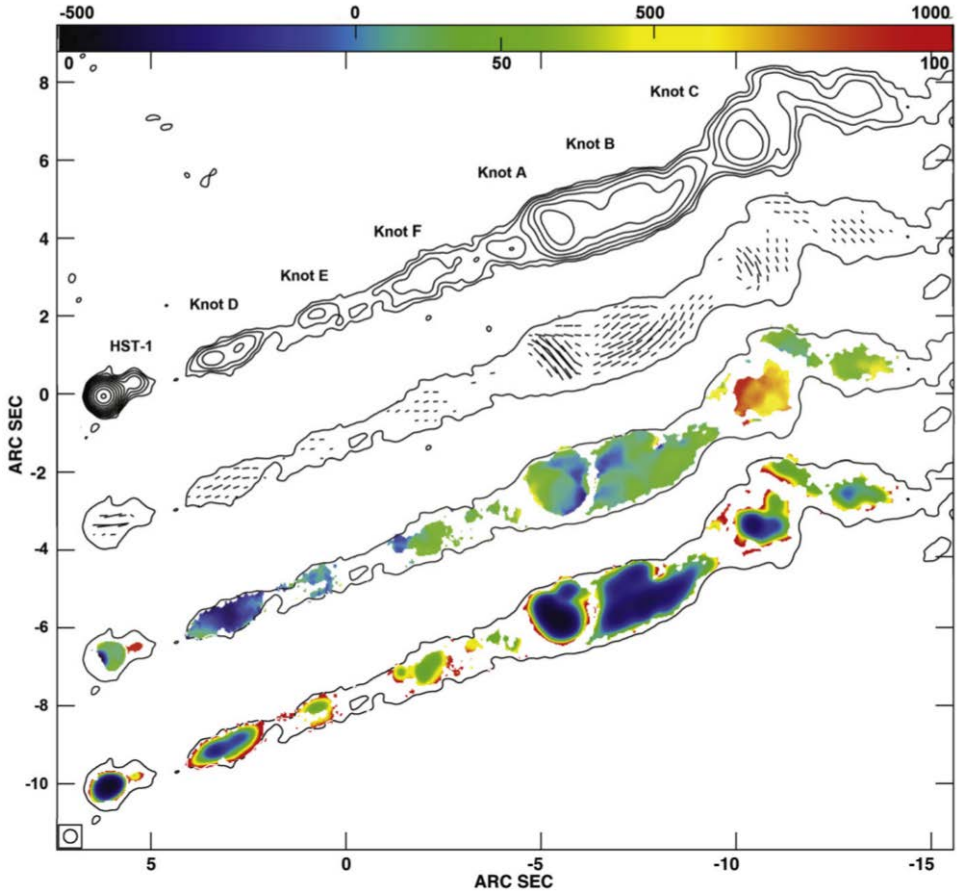

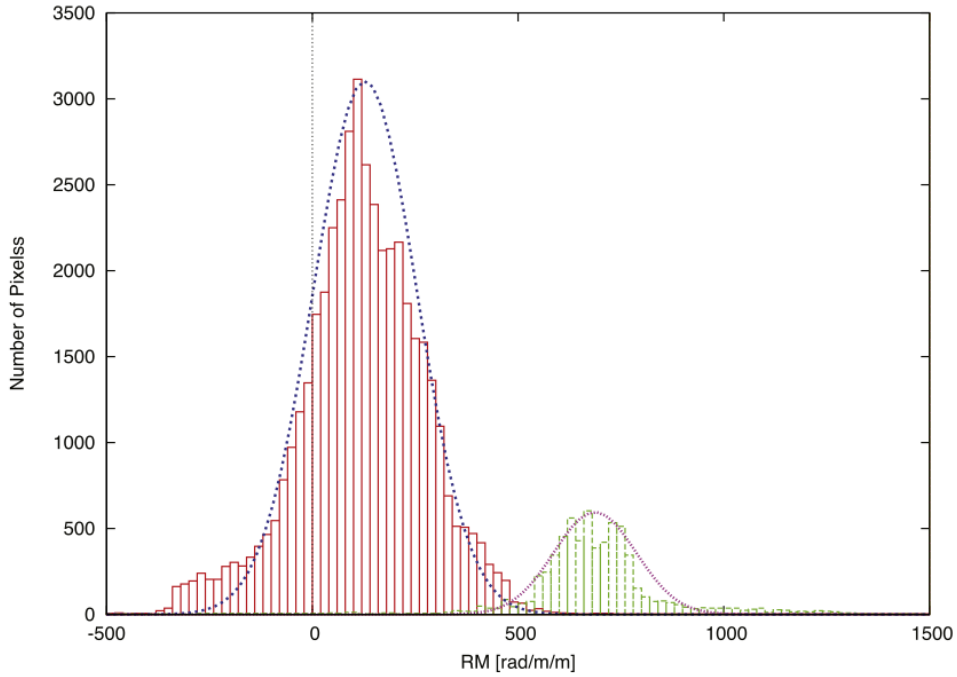

Algaba et al. (2016)

Discussion : Sudden increase of RM at HST-1

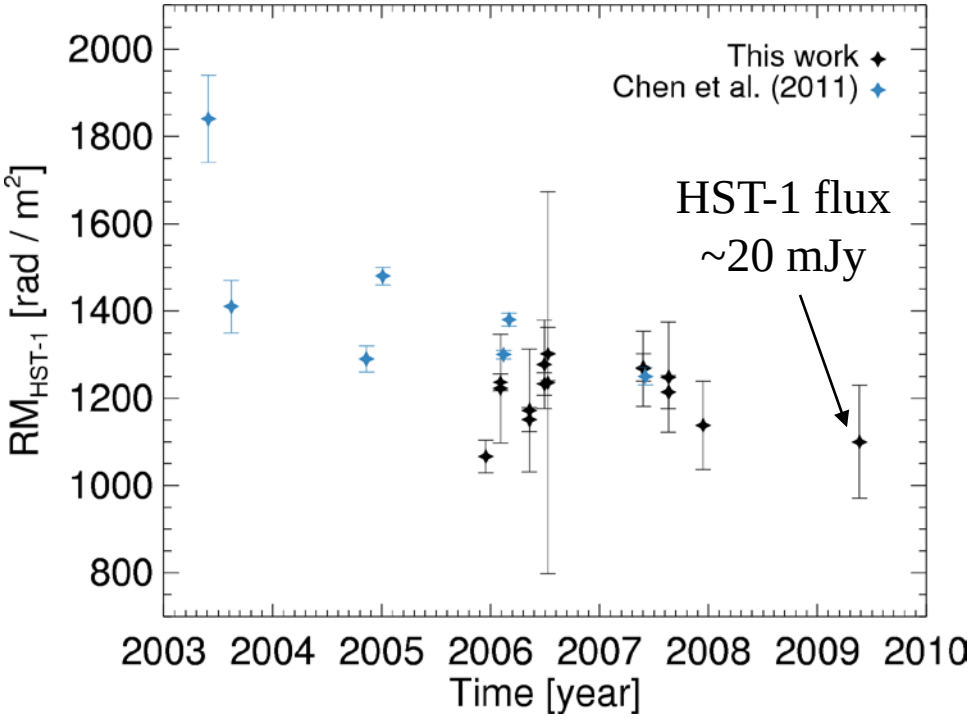

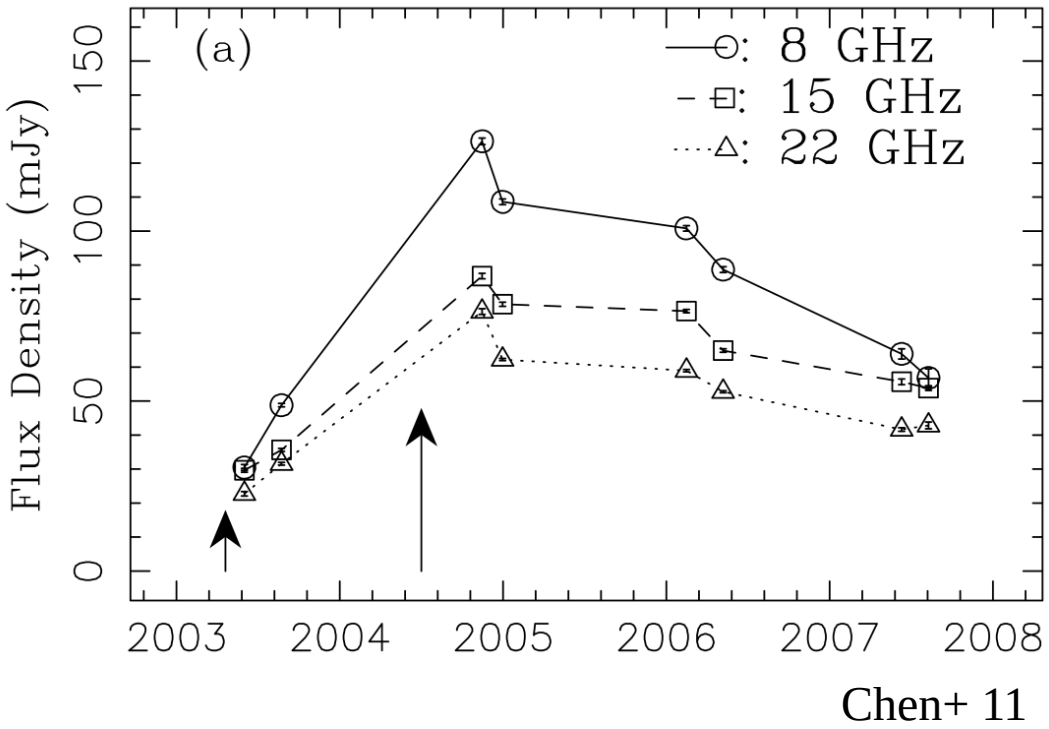

Chen+ 11

– We showed that external Faraday rotating medium is more likely also at HST-1.
– We analyzed additional epochs data and plot the RM at HST-1 together with the VLA result in Chen et al. (2011). While the flux density significantly increases in 2003 ~ 2005 and gradually decrease after then down to ~20 mJy in 2009.

The RM values are almost constant over time except the first epoch data in Chen et al. (2011).
→ Also supports an external origin of Faraday rotation at HST-1.

Discussion : Sudden increase of RM at HST-1

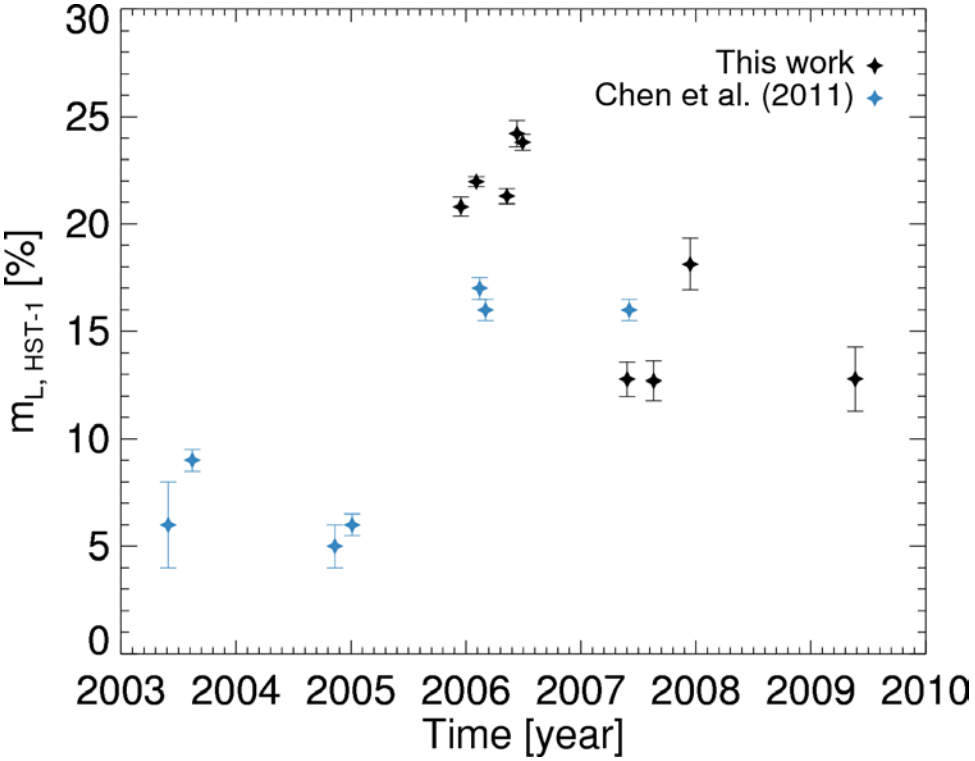

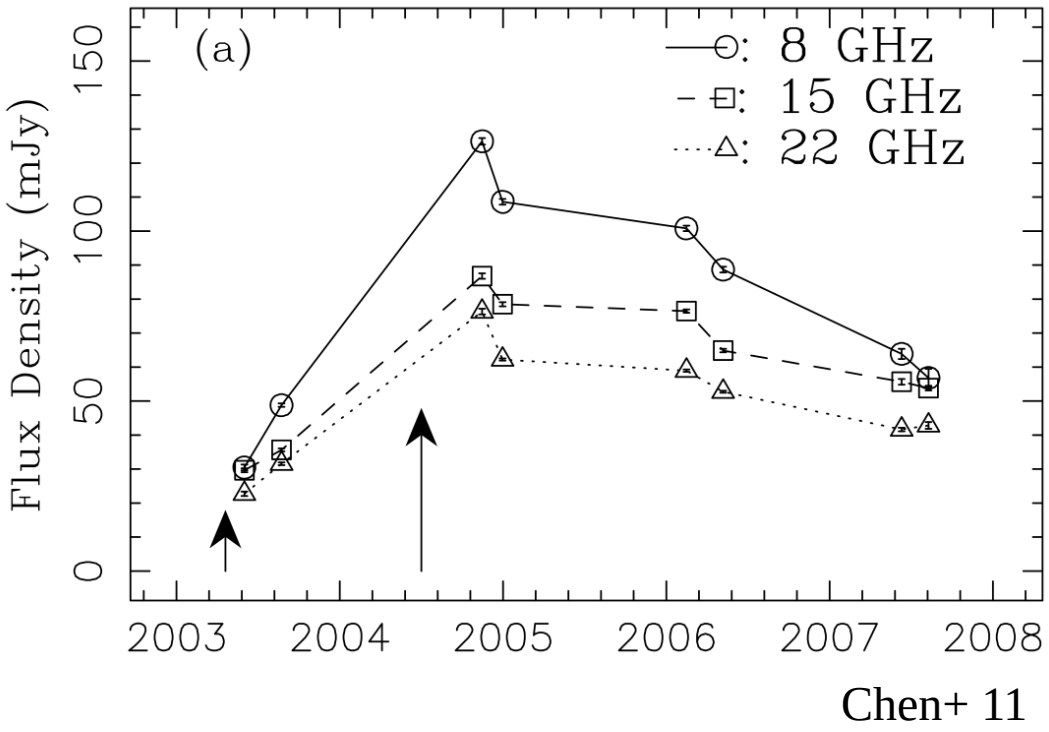

Chen+ 11

– We showed that external Faraday rotating medium is more likely also at HST-1.
– We analyzed additional epochs data and plot the RM at HST-1 together with the VLA result in Chen et al. (2011). While the flux density significantly increases in 2003 ~ 2005 and gradually decrease after then down to ~20 mJy in 2009.

The RM values are almost constant over time except the first epoch data in Chen et al. (2011).
→ Also supports an external origin of Faraday rotation at HST-1.

Discussion : Sudden increase of RM at HST-1

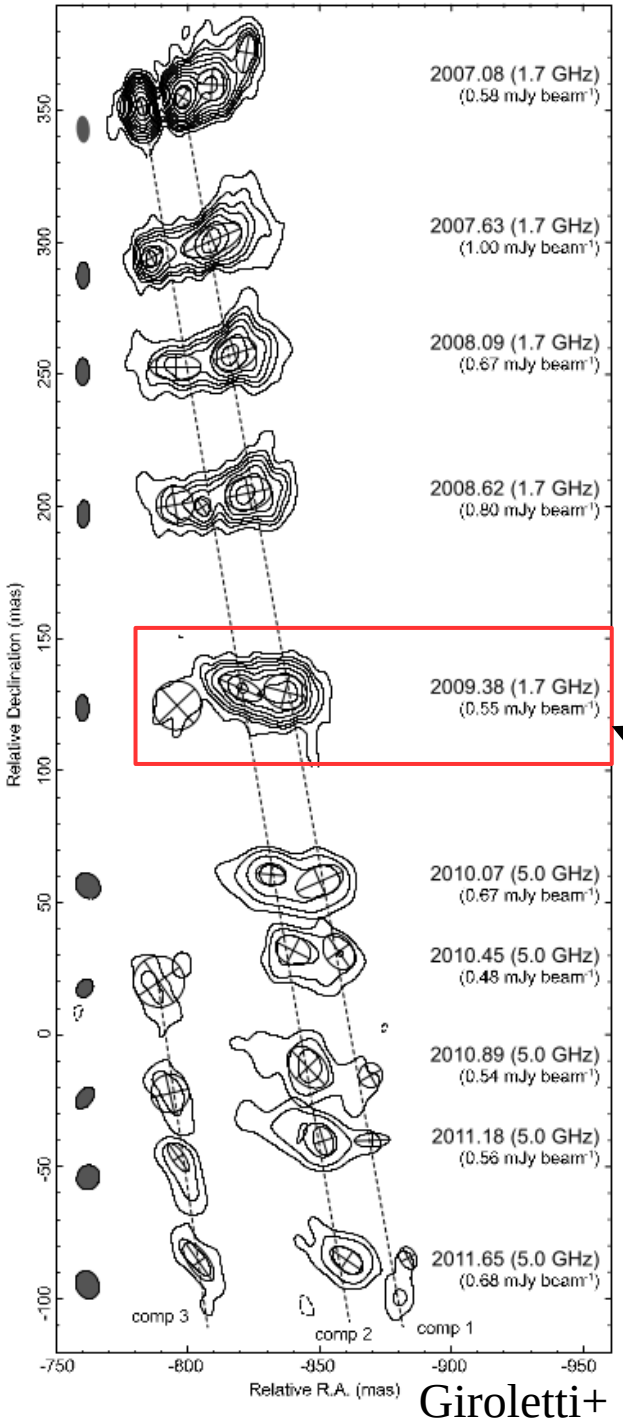

Giroletti+ 12

– Even though the jet at HST-1 moves more than ~30 mas in projected distance, RM does not change much.
→ the size of Faraday rotating medium is pretty large.

The last epoch we analysed

Discussion : Sudden increase of RM at HST-1

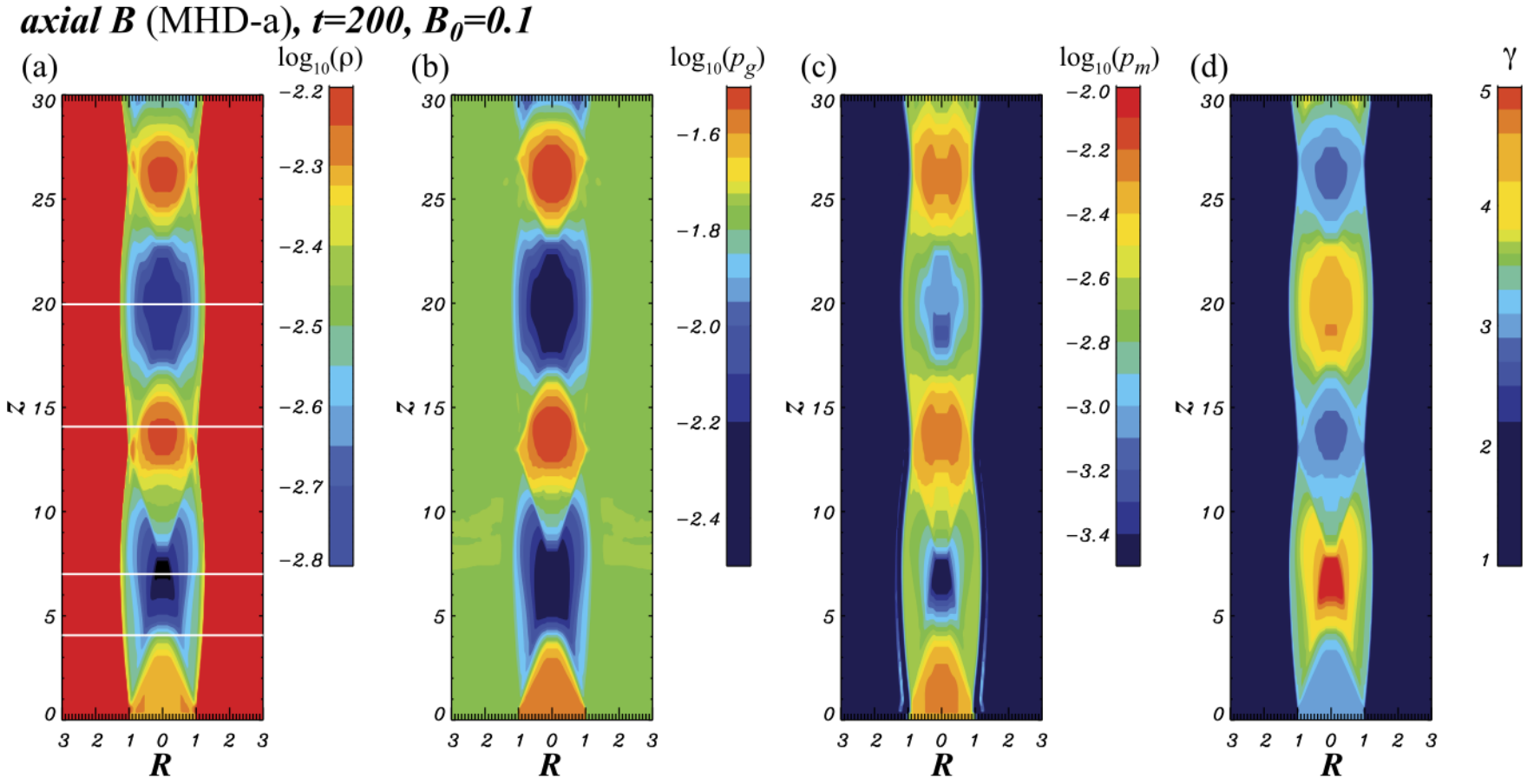

Mizuno+ 15

– At the location of recollimation shock, increase of density and pressure of the jet is expected. However, whether this might lead to density increase or B field ordering in ‘ambient medium’ is unclear.

Discussion : Sudden increase of RM at HST-1

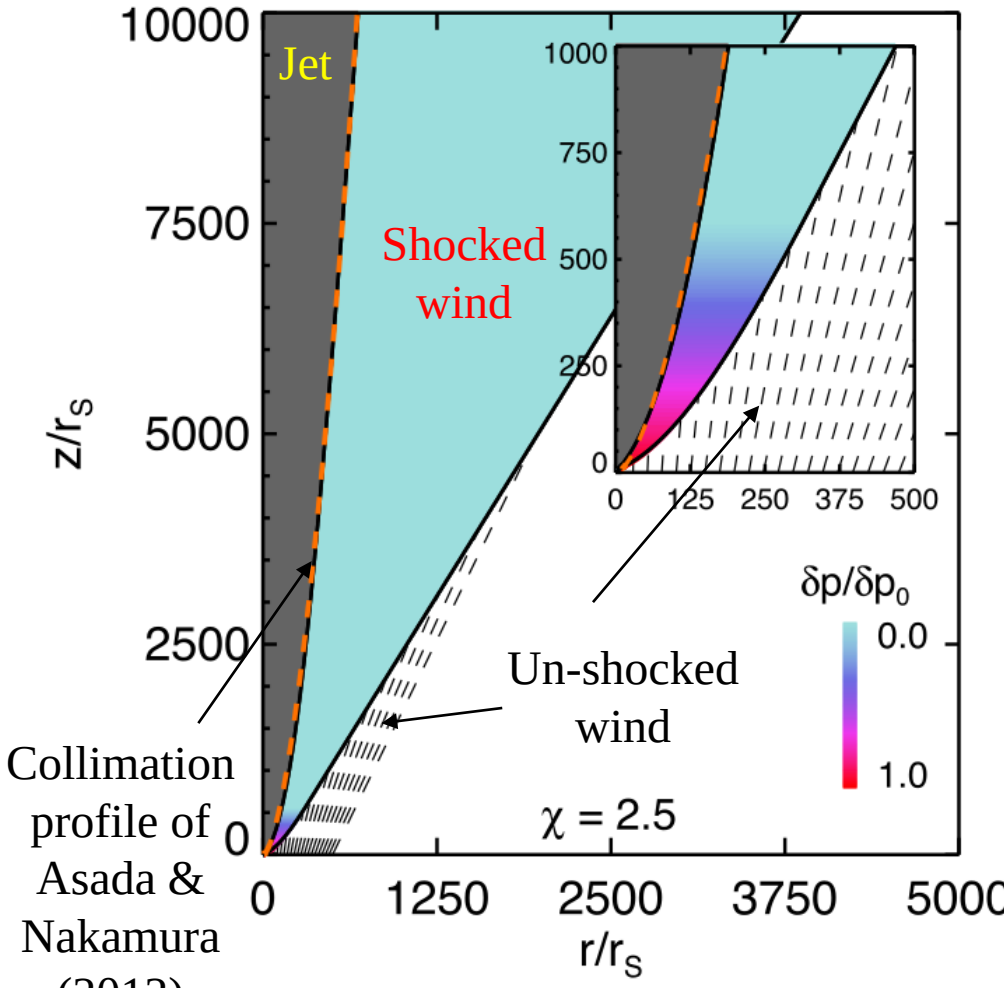

Collimation profile of Asada & Nakamura (2012)

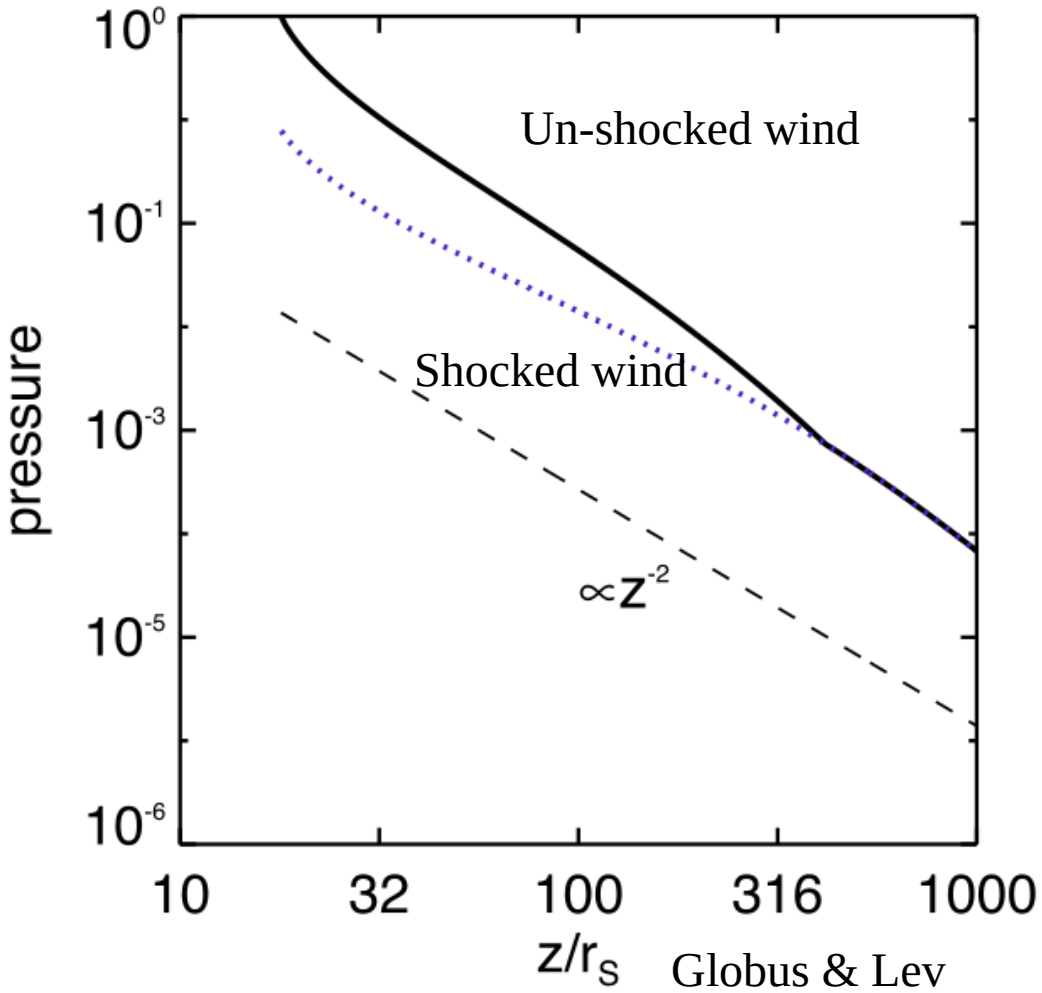

Globus & Levinson 16

– Globus & Levinson (2016) showed that injection of disk wind leads to the observed jet collimation profile, with shocks formed in the wind regions near the jet boundary.

→ We speculate that sudden change in the ISM pressure profile with a formation of recollimation shock might lead to sudden increase of RM at HST-1.

Discussion : Sudden increase of RM at HST-1

$$RM = 8.1 \times 10^5 \int n_e B dr$$

[rad/m^2] [cm^{-3}] [G] [pc]

~1200 rad/m^2

0.31 cm^{-3} (X-ray obs. in Russell+15)

?

~30 mas ~ 2.43 pc,

– We estimate ~2.03 mG for external sheath of HST-1.

→ larger than the B_{out} (2.2 μG) we obtained from the fitting of RM inside the Bondi radius by one thousand.

– Previous estimation for the HST-1 jet is ~1.1 mG from X-ray variability (Harriss et al. 2003, 2009) and ~0.7 mG from the shock jump condition (Giroletti et al. 2012).

→ Despite large uncertainty, similar degree of magnetization of the ‘jet’ and the ‘sheath’ is expected at HST-1.

VLBA archive data analysis : BJ020A, 8 GHz

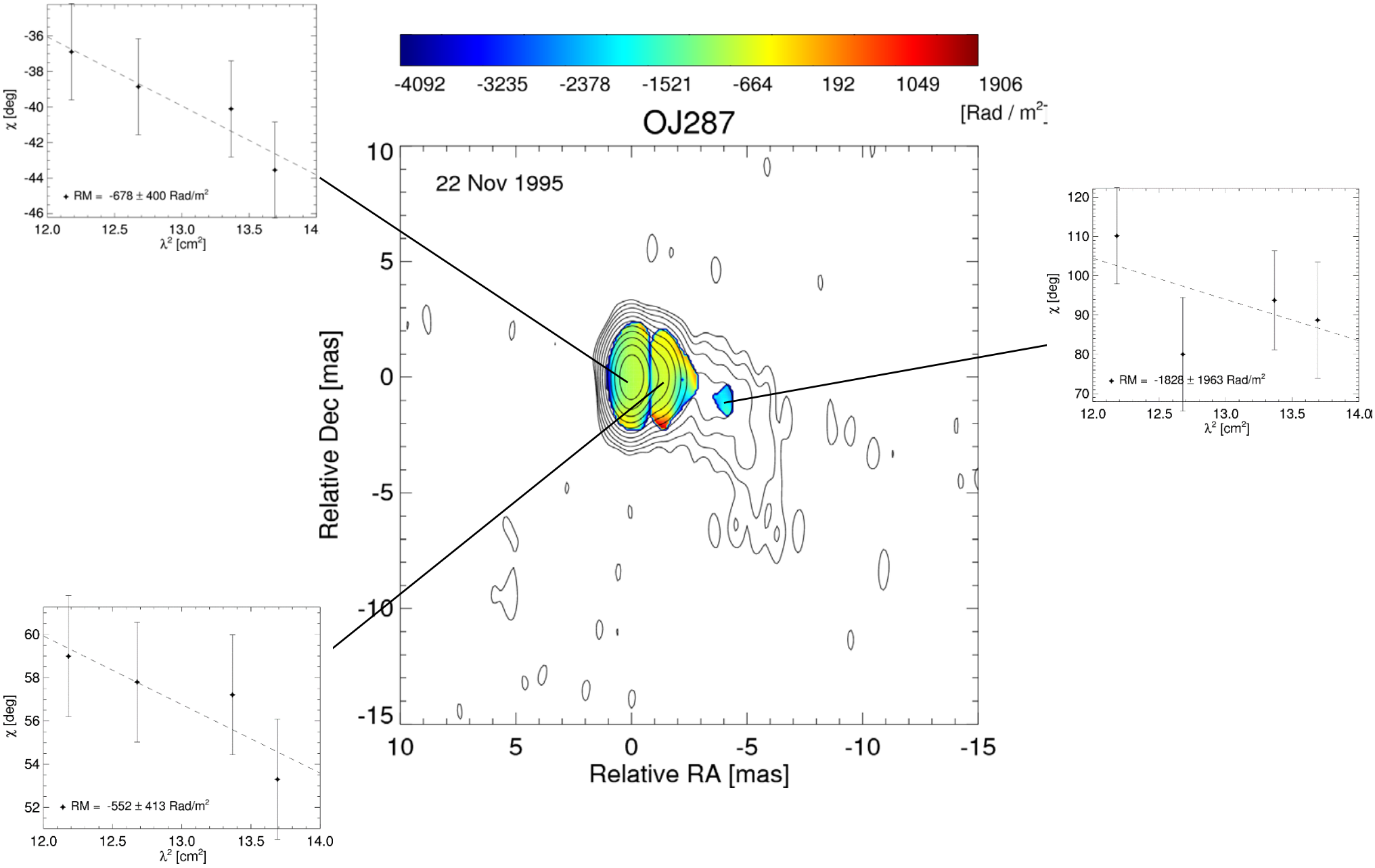

Discussion : What is the source of Faraday rotating medium?

$$m_{\rm obs}(\%) = m_{\rm max}\left|\frac{\sin(2\lambda^2{\rm RM})}{2\lambda^2{\rm RM}}\right|, \quad \text{Burn (1966)}$$

– If internal Faraday rotation is dominant, then there must be significant depolarization depending on observing frequency and RM.

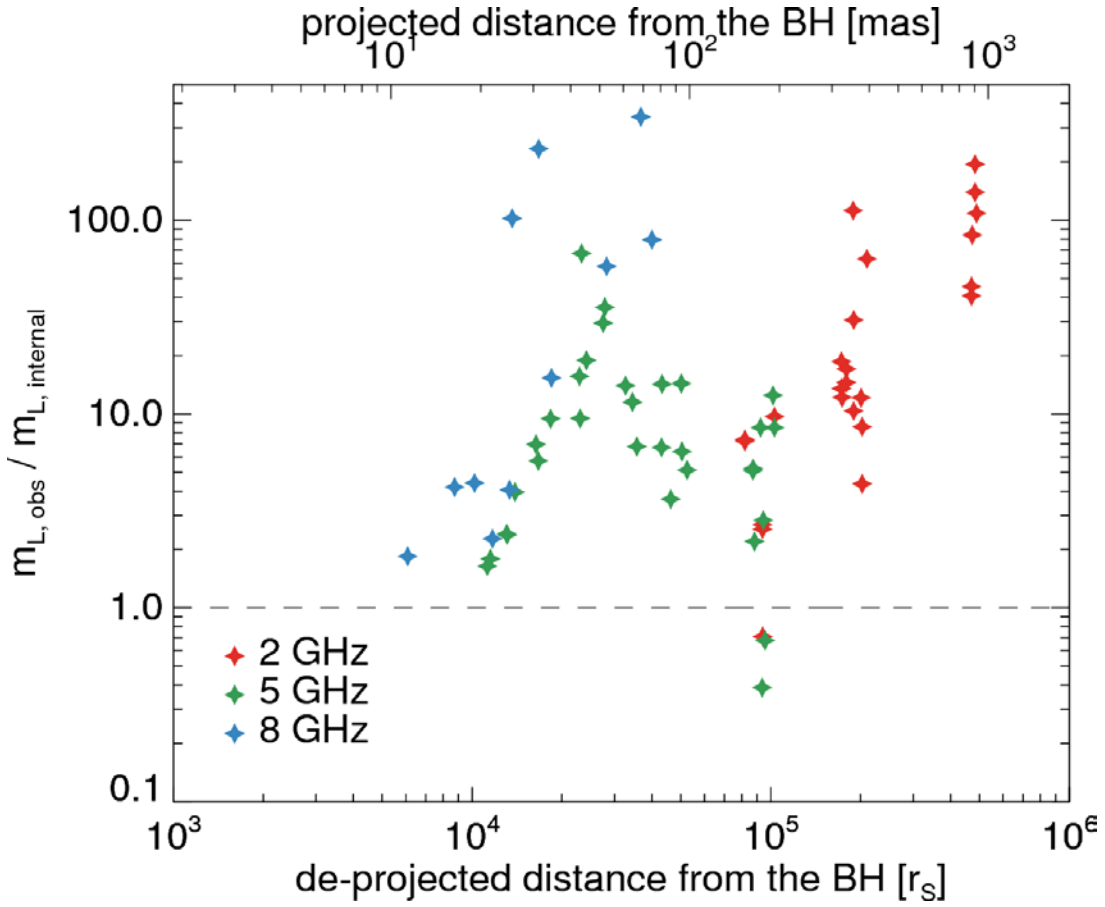

– The observed fractional polarization is almost always larger than the Burn-model.

→ the observed Faraday rotation originates from the magnetized medium external to the jet.

RM distribution as a function of distance

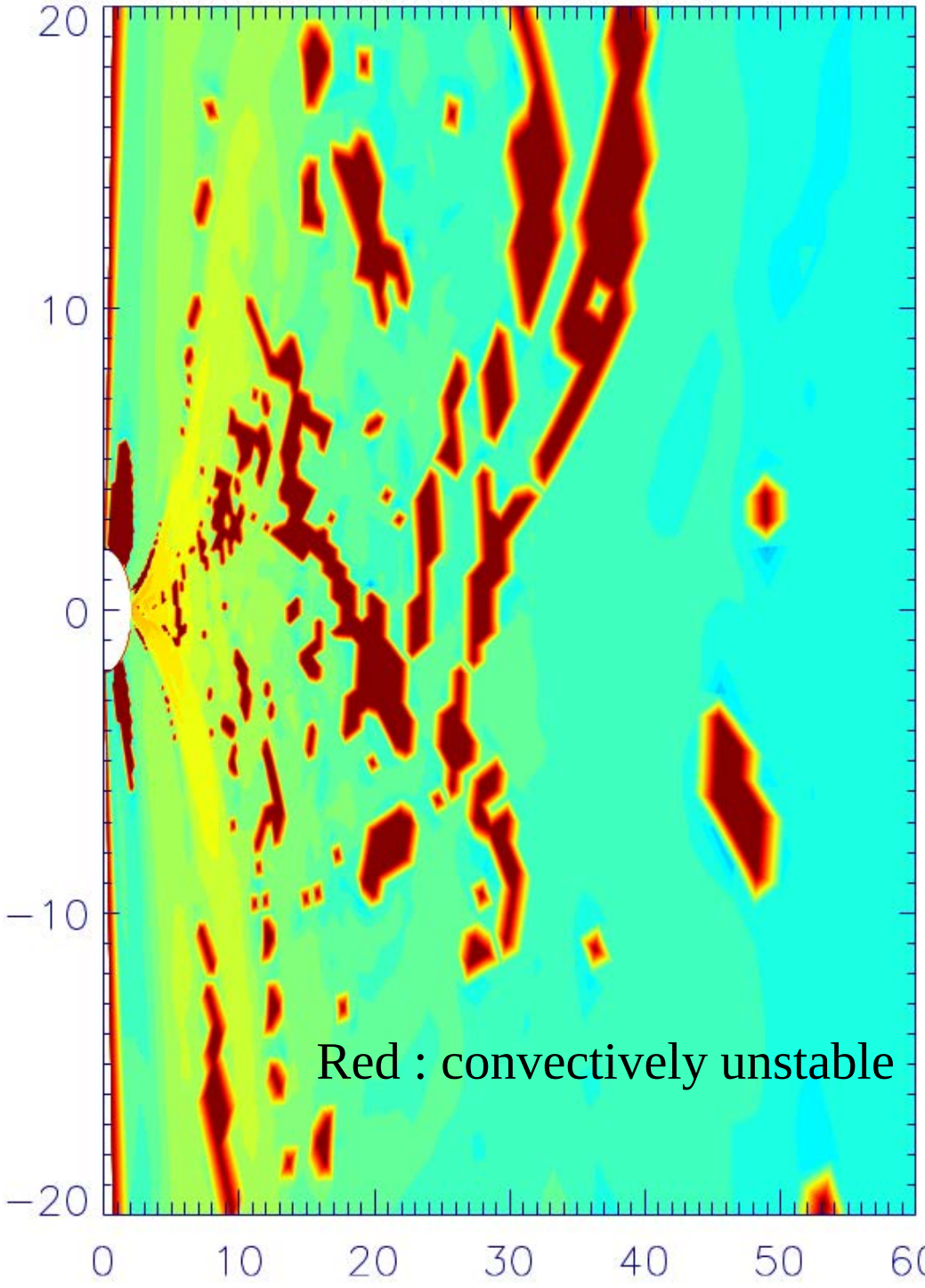

– Indeed, Yuan et al. (2012b) showed that hot accretion flows are convectively stable.

Yuan et al. (2012)

Obtaining representative value of RM and corresponding error for each region

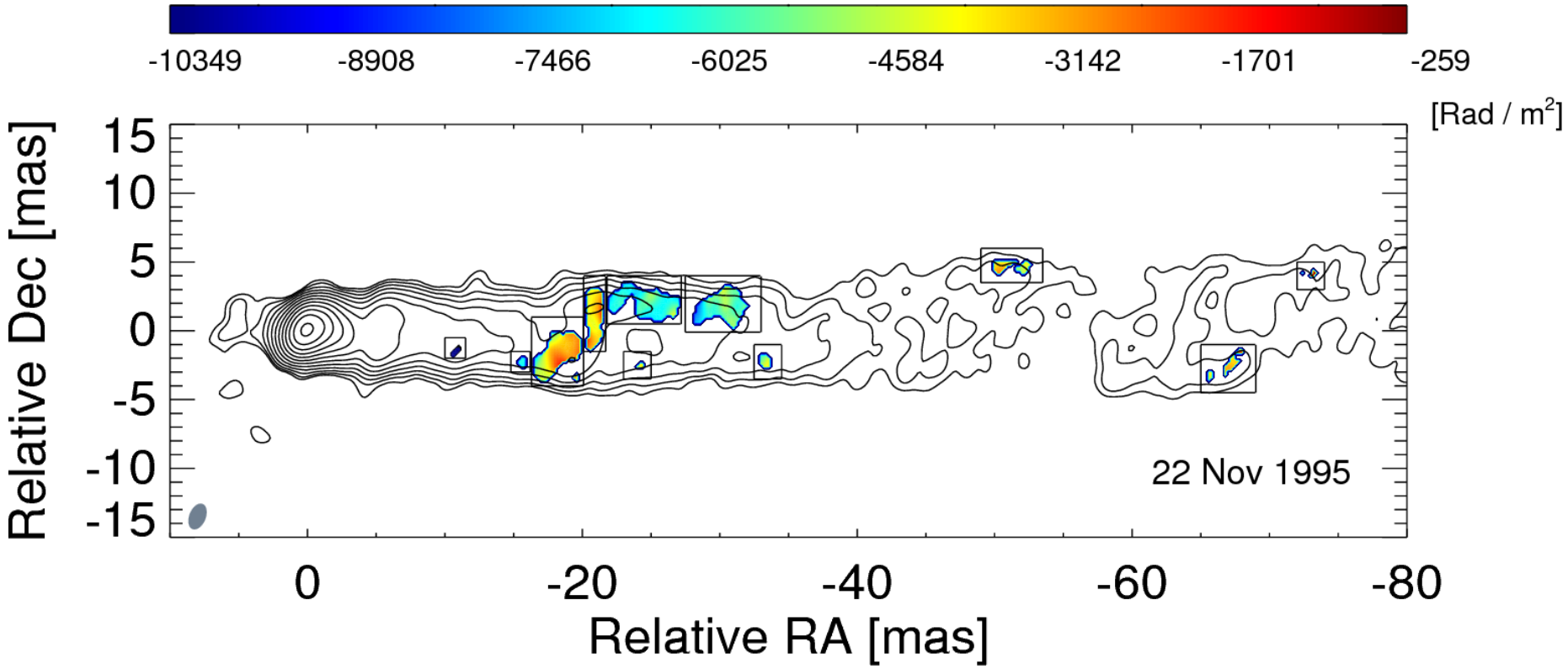

- We binned the RM values in each ‘box’ and extracted the representative value.
- We obtained ‘weighted mean’ and corresponding errors for each region.

$$\bar{x} = \frac{\sum_{i=1}^{n} \left(x_i \sigma_i^{-2} \right)}{\sum_{i=1}^{n} \sigma_i^{-2}} \qquad \sigma_{\bar{x}} = \sqrt{\frac{1}{\sum_{i=1}^{n} \sigma_i^{-2}}}$$

- However, the obtained error is very small because it assumes that all different pixels are independent on each other, which is not true. Therefore, we used

$$\sigma_{\mathrm{RM,bin}} = \sigma_{\bar{x}} \times \sqrt{n \frac{\Sigma_{\mathrm{FWHM}}}{\Sigma_{\mathrm{RM}}}}$$